SF 298 MASTER COPY KEEP THIS COPY FOR REPRODUCTION PURPOSES

REPORT DOCUMENTATION PAGE

Form Approved OMB NO. 0704-0188

1. AGENCY USE ONLY *(Leave blank)*	2. REPORT DATE	3. REPORT TYPE AND DATES COVERED
	December 22, 1999	Final, 6/01/96 - 8/31/99

4. TITLE AND SUBTITLE

Large Eddy Simulations of Diesel Combustion Chambers

5. FUNDING NUMBERS

DAAH04-96-1-0196

6. AUTHOR(S)

I.B. Celik, W.S. Lewellen, J.M. Kuhlman, E. Amin, A. Gel, D.C. Lewellen, A. Smirnov, J. Smith, I. Yavuz

7. PERFORMING ORGANIZATION NAMES(S) AND ADDRESS(ES)

Mechanical and Aerospace Engineering Department
West Virginia University

8. PERFORMING ORGANIZATION REPORT NUMBER

MAE-ARO-99-IC1

9. SPONSORING / MONITORING AGENCY NAME(S) AND ADDRESS(ES)

U.S. Army Research Office
P.O. Box 12211
Research Triangle Park, NC 27709-2211

10. SPONSORING / MONITORING AGENCY REPORT NUMBER

11. SUPPLEMENTARY NOTES

The views, opinions and/or findings contained in this report are those of the author(s) and should not be construed as an official Department of the Army position, policy or decision, unless so designated by other documentation.

12a. DISTRIBUTION / AVAILABILITY STATEMENT

Approved for public release; distribution unlimited.

20000707 152

13. ABSTRACT *(Maximum 200 words)*

This report presents findings of a systematic study of turbulence predictions for diesel combustion chambers. Particular topics covered include (i) turbulence models for Reynolds averaged Navier-Stokes solutions, (ii) turbulence scale analysis, (iii) efficiency and accuracy improvements of the KIVA codes, (iv) large eddy simulations(LES) of in-cylinder turbulence with and without combustion, (v) sub-grid scale models for LES, and (vi) combustion models for diffusion flames. The generation of the turbulence during the intake stroke and its subsequent decay during the compression stroke was predicted successfully. The turbulence induced by the piston-bowl geometry alone was investigated. It was found that significant turbulence can be generated during the compression stroke from the re-entry flow in the squish area. Simulations with spray combustion indicated an augmentation of the turbulence intensity corresponding to start of ignition. These findings are in good qualitative agreement with experimental observation. A quantitative analysis of the results in comparison with experiments will require simulations of many cycles to account for cycle-to-cycle variations. This could be possible with use of computers with parallel processors. To this end a successful attempt was made to transform KIVA to run on several parallel platforms including a locally built Beowulf Workstation cluster. Initial runs with fixed grids could handle up to four million nodes. This holds promising prospects for future LES of in-cylinder combustion/turbulence in internal combustion engines.

14. SUBJECT TERMS	15. NUMBER IF PAGES
Internal Combustion Engines, KIVA Code, Rotational Effects, Swirling Jet Flow, Dopler Global Velocimeter, Large Eddy Simulation, Turbulence, Energy Spectra, Combustion Models	16. PRICE CODE

17. SECURITY CLASSIFICATION OR REPORT	18. SECURITY CLASSIFICATION OF THIS PAGE	19. SECURITY CLASSIFICATION OF ABSTRACT	20. LIMITATION OF ABSTRACT
UNCLASSIFIED	UNCLASSIFIED	UNCLASSIFIED	UL

NSN 7540-01-280-5500

 Enclosure 1

Standard Form 298 (Rev. 2-89)
Prescribed by ANSI Std. 239-18
298-102

LARGE EDDY SIMULATION OF DIESEL COMBUSTION CHAMBERS

FINAL REPORT

I. B. CELIK, W. S. LEWELLEN, J. M. KUHLMAN
E. AMIN, A. GEL, D. LEWELLEN, A. SMIRNOV
J. SMITH, I. YAVUZ

DECEMBER 22, 1999

U.S. ARMY RESEARCH OFFICE

GRANT NO.: DAAH04-96-1-0196

MECHANICAL AND AEROSPACE ENGINEERING DEPARTMENT
WEST VIRGINIA UNIVERSITY

SUMMARY

Accurate prediction of turbulence inside diesel engine combustion chambers is one of the outstanding obstacles in realistically simulating and predicting the mixing and combustion phenomena relevant to diesel engines. As it is also demonstrated in this work that the shortcomings of the classical turbulence models, particularly the two-equation models, is the primary factor for poor predictions. This study has been performed with the premise that at least some of these turbulence modeling issues can be addressed by employing the large eddy simulation (LES) technique to predict in-cylinder flow dynamics. In the LES approach the most important (energetic), large turbulent scales are resolved, while only the effect of unresolved small scales are modeled. For the present simulations a combination of the existing KIVA family (versions 2, 3, and 3V) of codes originated from Los Alamos National Labs and a WVU/LES code developed for modeling atmospheric turbulence were utilized. The 3-D, unsteady KIVA codes, which were designed specifically for internal combustion engines, have been modified for LES of turbulent combustion. The WVU/LES code is used both as an aid in understanding the effects of swirling/rotation on turbulence as well as an initial benchmark code to compare how well KIVA/LES is behaving on relatively simple flow configurations.

First, to identify possible problems that would be encountered when running KIVA in LES mode a series of tests were performed for a swirling jet flow. This flow has many of the characteristics of the swirling flow induced during the intake stroke to aid in turbulent mixing and combustion inside the engine cylinder. The problem was simulated using KIVA-3 and the results compared favorably to those obtained from the well-validated WVU/LES code. Considering the differences in grid resolution, the sub-grid scale (SGS) model, and far-field boundary conditions, reasonable agreement between the two results was observed. Further, a new SGS model applicable to strongly rotational, swirling flows was developed using the WVU/LES code, which has significant potential for IC engine modeling.

Another goal of this research was to improve existing RANS (Reynolds Averaged Navier Stokes) models when applied to IC-engines. To achieve this a parallel study was performed on a benchmark flow, which resembles that of a motored IC-engine to assess the performance of various turbulence models. As expected the models do not perform uniformly well over all flow regimes. Significant differences were observed among various models as the engine speed increased. A new hybrid model has been proposed which tends to RANS calculations with an eddy viscosity model and to LES with a Smagorinsky SGS model, in the limit of coarse and fine girds, respectively. This is especially suitable for engine simulations because most engine simulations are inherently three-dimensional and transient as in LES. RANS simulations have also revealed that the turbulence length scale indicated by the k-E model provide a good base line for deciding on the degree of resolution needed for LES simulations.

As a first step, LES of the compression and expansion strokes under motored engine conditions were considered. Much work has focused on the compression and expansion strokes, due to the complications introduced by the valve dynamics during the intake stroke. A comparison of the results using different (SGS) models showed that the simulations with a SGS model produced an energy cascade,

derived from a spectral analysis of the fluctuating data, that qualitatively resembled experimental trends. To achieve this, the numerical errors needed to be carefully controlled using small time steps with second order convection schemes. The predicted turbulence intensity was low but showed the same trend (roughly a linear relationship with mean piston speed) as experiments. This lower intensity can be partly attributed to approximations of the unknown initial conditions inside the cylinder which may be influenced significantly by the intake stroke.

During the compression and expansion strokes, turbulence is induced primarily by the geometry of the piston-cylinder assembly, in particular the piston-bowl. Most of the turbulence in a real engine is induced during the intake stroke. For the next level of realism, simulations of the intake and subsequent expansion and compression strokes were performed for a typical two-valve cylinder assembly using the code KIVA-3V. A multi block structured mesh was set up in agreement with the experiments of Catania et al. (1996). Two sets of runs were performed on grids with different resolution: 220,000 and 440,000 nodes. Here too a study was performed using different sub-grid scale and RANS turbulence models including k-ε model, no turbulence model, and a Smagorinsky model. The study showed that the growth and the subsequent decay of turbulence during the intake phase predicted with the Smagorinsky subgrid-scale model agreed well with experiments. The power density spectra of the fluctuating velocity components were compared with those obtained from the measurements. This comparison showed that at least some of the inertial range dynamics is captured in the simulations

Throughout the studies outlined above it was found that the KIVA codes were deficient in several areas with respect to performing LES. Improvements to both the efficiency and accuracy of the KIVA code were implemented. The time accuracy of the code was made fully second-order by implementing a combination of two-stage Runge-Kutta and Adams-Bashforth schemes into the advection phase. Spatial accuracy was improved by introducing an advection scheme where central differencing is used in the momentum equations and quasi-second order upwinding is used in the scalar equations. Efficiency of the single processor version of KIVA was improved by up to 20% by implementing a more sophisticated preconditioning scheme in the pressure solver. The overall computational performance of the code was improved significantly with the distributed-memory implementation of KIVA-3 (KIVA-3/MPI) based on one-dimensional domain decomposition for parallel execution. This current version is capable of handling fixed grids on any given number of processors. KIVA-3/MPI has been tested on several hardware platforms including SGI Origin 2000, Cray T3E, and Windows NT based Intel platforms. The code also has been ported to the 20-node Beowulf type DEC Alpha Linux cluster developed for this project at WVU. With KIVA-3/MPI it was possible to attain reasonable turn-around times for up to four million grid nodes for simple flows such as the swirling jet.

With the groundwork being laid for performing LES of motored diesel engine cylinders, a parallel study has been performed focusing on development of combustion models appropriate for LES. The first such study involved implementing a modified form of an Eddy Breakup (EBU) turbulent combustion model. The modification allows the EBU model constant to be dynamically linked to the reaction surface. This link is achieved through the use of a conditional Probability Density Function (PDF) which is evaluated at the flame sheet. This model should be applicable as a subgrid scale

turbulence/chemistry-interaction model for LES of turbulent combustion in diesel engines. The application of the modified EBU model to a D. I. diesel engine using KIVA III has shown the importance of this modification to the modeling of chemistry/turbulence interaction in engines. Furthermore, a validation study of the conserved scalar/assumed pdf turbulent mixing model has been performed. This model was then applied to an experimentally studied diesel engine with combustion. The computations indicate that this approach can be used as the SGS combustion model to the modeling of turbulent mixing being a compromise between accuracy and computational expense. Given the importance of turbulence mixing on the diffusion phase of the diesel engine combustion process an additional study was performed to investigate the influence of the finite-rate chemistry in a bluff-body stabilized diffusion flame. The computations showed that both constrained equilibrium and flamelet models could reproduce the macro features of the flame. However, higher order correlations were under-predicted at the jet boundary. Also, a strained laminar flamelet library is built and used in conjunction with CFD simulation of a turbulent H2/Air diffusion flame to investigate the finite rate chemistry effects on the thermal NO_X formation. The simulations show that NO is a species that is highly sensitive to the scalar dissipation rate.

Finally spray combustion of n-Tedradecane is modeled using a 7-reaction Arrhenius mechanism and Magnussen eddy-dissipation combustion model. One set of simulations was performed for the continuation of the intake flow turbulence with valves through the compression stroke, and another set was for the compression and expansion strokes. These three-dimensional calculations can be considered as under-resolved LES, since no attempt was made to capture thin flamelets via a rigorous SGS combustion model. Nevertheless, both sets of calculations showed that the turbulence intensity increased significantly with the onset of combustion. Though, there is peripheral experimental evidence for such a phenomenon, it needs to be investigated further. It should be mentioned that extreme difficulties were encountered during spray diffusion computations. With LES the spray penetration seems to be too deep on to the wall, which results in great stability problems even with time steps as low as 1.0E-09 seconds.

On another front, a two-channel Doppler Global Velocimetry (DGV) and a point Doppler velocimetry (PDV) system have been developed, partially funded by this project, and have been used to measure the mean velocity in a plane for a rotating wheel, a fully-developed pipe flow, and an axi-symmetric turbulent jet flow. It was shown that mean pipe and jet DGV data compared well with other experimental data. However, RMS velocity fluctuations did not compare well. With minor improvements both systems can be used to obtain accurate turbulence data for validation of large eddy simulations.

As a result of this study a total of 37 papers were published in national and international conference proceedings and journals. The project involved three post doctoral fellows, five graduate students, and two undergraduate students. In addition, the research team has actively participated in dissemination of information by attending conferences and organizing symposia and publishing news letter articles. The team members were particularly active in ASME Internal Engine Combustion Division, and in Multi-dimensional Engine Modeling Sessions organized as part of the annual SAE Congress and Exposition.

TABLE OF CONTENTS

LIST OF FIGURES

LIST OF TABLES

NOMENCLATURE

CD	*Central differencing*
C_S	*Smagorinsky constant*
D	*Diffusion coefficient*
D_a	*Damkohler number*
g	*SGS mixture fraction fluctuations*
J	*Diffusion flux*
k	*Reaction rate, SGS kinetic energy of turbulence*
k	*Turbulent kinetic energy*
L	*Integral length scale of turbulence, differential operator*
l	*Turbulent length scale*
L_e	*Lewis number*
L_{SGS}	*Subgrid length scale*
p	*Probability density function; Pressure*
R_e	*Reynolds number*
S_0	*Swirl number*
$\bar{\bar{S}}_{ij}$	*Mean strain rate tensor*
u,v,w	*Velocity components in x,y,z directions*
u_{ref}	*Reference velocity*
u_i'	*Fluctuating velocity in the ith direction*
w_i	*Net formation/destruction rate of species i*
W_i	*Molecular weight of species i*
x	*Axial co-ordinate*
X	*Mole fraction*
Y	*Mass fraction*
y	*Transverse co-ordinate*
Z	*Element mass fraction*

Greeks

α	*Co-ordinate index, collision efficiency, exponent*
ρ	*Density*
μ	*Dynamic viscosity*
ϕ	*Equivalence ratio, a general variable*
β	*Exponent in beta function expression*
γ	*Intermittency*
υ	*Kinematic viscosity*
ω	*Mixing frequency*

ξ	*Mixture fraction*
χ	*Scalar dissipation rate*
σ	*Schmidt number*
ε	*SGS Energy dissipation rate*
λ_k	*Kolmogorov length scale*
δ	*Jet half width*
κ	*Von Karman constant*
τ	*Turbulent time scale; Viscous stress tensor*
ν_T	*Turbulent eddy viscosity (kinematic)*
$\Delta_X, \Delta_Y, \Delta_Z$	*Discretization in the X, Y, and Z directions*

Subscripts

c	*Chemical*
F	*Fuel*
i,j	*Species index*
i,j,k	*Cartesian co-ordinate components*
j	*Jet*
k	*Kolmogrov*
m	*Mixing*
O	*Oxidant*
P	*Product*
st	*Stoichiometric*
t	*Turbulent*

Superscripts

—	*Filtered quantity*
~	*Favre filtering average*
$'$	*Fluctuations from ensemble mean, sometimes r.m.s. value*
$''$	*Fluctuations from Favre mean*

Abbreviations

pdf	*Probability density function*
LEMF	*Large eddy mass fraction.*
LERR	*Large eddy reaction rate.*
LES	*large Eddy Simulation*
QSOU	*Quasi-Second-Order-Upwinding*
RANS	*Reynolds Averaged Navier Stokes*

INTRODUCTION

Turbulence generated during the intake stroke followed by the turbulence induced by the geometry of cylinder-piston assembly of an internal combustion (I.C.) engine during the compression-expansion stroke greatly influences the combustion process hence fuel efficiency and pollutant formation (see e.g. Heywood, 1987). The classical multidimensional modeling approach is to use some semi-empirical turbulence model (e.g. the well-known k-ε model) to close Reynolds/Favre Averaged Navier-Stokes (RANS) equations of motion. These models have serious shortcomings in that they introduce crude assumptions, which are not always validated by experiments. One such assumption is the local isotropy of turbulence inherent to most eddy viscosity models. For example, in the standard k-ε model the eddy viscosity is isotropic, and the equation for the turbulence energy dissipation rate, ε, is modeled using the local isotropy assumption (see e.g. Hossain and Rodi, 1982; Speziale, 1998). This model uses only one length scale and a time scale to represent a whole spectrum of turbulence length and time scales ranging from the large eddies (proportional to the size of the combustion chamber) down to the Kolmogorov scales. Moreover, most of these models require that the turbulent stress tensor be aligned with the mean rate-of-strain tensor, which is not valid for many complex flows such as those observed in IC-engines. They do not respond to rapid rate of strain, because the history effects on the transport of Reynolds stresses are not accounted for. An important drawback of the k-ε model is that it gives a completely unrealistic representation of the normal stresses, failing to reproduce the strong normal stress anisotropy observed essentially in all shear flows.

Most of the earlier multi-dimensional models applied to I.C. engines have used RANS models (see e.g. Amsden et al., 1985; Ramos, 1989; Burgess and O'Rourke, 1993). In this approach the equations governing the instantaneous field variables are averaged over a time interval which is relatively short so as not to render total elimination of the time variation of important unsteady flow events but still long to filter high frequency components of fluctuations. These averaged quantities are then assumed to be equivalent to ensemble-averaged quantities at the same point in space. Extensive testing and validation studies in the past (Reitz and Rutland, 1991; Celik et al., 1992; Han et al., 1996; Smith et al., 1997; Bo et al., 1997; Yang et al., 1998) have shown that the turbulence models introduced semi-empirically for computation of higher

order correlation of fluctuating quantities did not prove universality, and the success of these models (not to be underestimated) is case specific. In Chapter 5, as an example, we present our RANS calculations using various turbulence models (Yavuz and Celik, 1999a,b) with some computations performed by Yang et al. (1998) using two different turbulence models, namely, the standard k-ε model and a Reynolds stress model. The drastic differences between the results of these two models is alarming; particularly in temperature distribution. A natural question is which of these results is closer to reality? We believe that such outstanding turbulence modeling issues can be resolved by making use of the Large Eddy Simulation (LES) technique.

LES has proven to be a very promising methodology in other fields of applications for prediction of turbulent flow quantities, both in the mean and instantaneously, including major statistical properties of turbulence (see e.g. (Reynolds, 1989; Galperin and Orszag, 1993; Ragab and Piomelli, 1993, Rodi et al., 1997; Piomelli, 1993 and 1998), but it has not yet found its due role in applications to in-cylinder flows for I.C. engines (ICE). Many of the shortcomings and assumptions made in RANS simulations can be eliminated by employing the LES technique which has been widely tested for simple flows, and was recently extended to predict complex turbulent flows encountered in realistic engineering applications. This technique solves the three dimensional, transient Navier-Stokes equations after applying a spatial filtering similar to time averaging. Depending on the filter width, which is usually a function of the numerical mesh size, LES can capture the most important large-scale fluctuations in the flow quantities, leaving only relatively small scales to be modeled empirically. The finer the grids size, the better is the resolution of turbulence scales, and the less important are the modeling assumptions. At the sub-grid level, the small-scale structures in turbulence are believed to be more isotropic, hence the usual eddy-viscosity type models are more appropriate. If LES can be successfully applied to engine flows, it should provide insight into the above mentioned controversies related to turbulence models and enhance our understanding of in-cylinder turbulence generation and control. In particular, it will help to resolve the outstanding questions relevant to integral length and time scales, heat and mass transfer rates, reaction rates, and cycle-to-cycle variations. It will also provide data that can be used to refine the classical turbulence models.

As mentioned above, in the last decade a substantial effort has been put into advancing the prediction of turbulence in non-reacting flows by application of LES. It has also been applied

with considerable success to turbulent reacting flows (see e.g. Garrick, 1995; Erlebacher and Hussaini, 1993; Menon and Jou, 1991; Sykes et al., 1990, 1994). Reynolds (1980) suggested that LES was probably the best way to model combustion in reciprocating engines. The application of LES to in cylinder turbulence for I.C. engines is rare because of complications introduced by compressibility, complex cylinder and valve geometries with moving boundaries, and particularly the complication due to turbulence-combustion interaction. One of the early attempts of LES for engine flows was presented by Naitoh et al. (1992). This study even with a relatively coarse grid, and first order Euler time marching scheme has shown the great potential of LES for ICE applications. In another study, Haworth (1998) reported encouraging results using a finite volume based computer code for predicting the ensemble averaged trends for an experimental axisymmetric engine cylinder motored at 200 rpm. A comparative study by Yavuz and Celik (1999) indicates that classical two-equation turbulence models performed well for this case in predicting the mean flow quantities but failed to predict the turbulence quantities.

This report presents results from our work where predictions of turbulent fluctuations and the statistics of turbulence quantities inside IC engine cylinders were attempted. For this purpose, the well known engine simulation code KIVA (a widely used engine simulation code, see e.g. Amsden, 1993,1997) is used with a special precaution to keep the numerical accuracy at a higher level than usual as elucidated in section 2.3. The capabilities of the KIVA code when used for LES are tested against benchmark cases such as lid-driven cavity flow, swirling and non-swirling free jet flows. The code is then applied to a typical engine geometry under motored conditions with or without combustion. The predictions are qualitatively compared to experiments primarily to investigate trends and implications of certain physical mechanisms in turbulence generation. A thorough quantitative comparison with experimental data would require a resolution of such issues as comparison of predicted cycle-resolved Favre averaged quantities with the ensemble averaged quantities (which are usually presented in experimental works) in the absence of ergodicity. The ensemble averages contain cycle-to-cycle variations, which could contribute up to 30-40% of cycle-resolved turbulence (see Valentino et al., 1998; Catania et al., 1996,1997). But simulations are possible at this time for only a couple of cycles.

In the course of this study it was necessary to investigate the numerical accuracy and the efficiency of the computer code used. A formally second order time marching scheme was devised and implemented into the KIVA code. Preliminary results with the second order time

scheme compared well with the first order scheme provided that the time step used in the latter was sufficiently small. Also, a parallel version of the same code was developed using domain decomposition with MPI (message passing interface) for non-reacting flows with fixed boundaries. The scalability of the parallel version has been shown.

As for sub-grid scale (SGS) models, a Smagorinsky model, and a one-equation model were used for the flow field. For combustion the well known eddy break-up model was used as a SGS model but also an attempt was made to formulate a PDF (Probability Distribution Function) based combustion model. Preliminary results from the application of this PDF model as a SGS combustion model are presented.

Chapter 1: Computational Procedure

1.1 About the Computer Code

The calculations were performed using a readily available computer codes, KIVA-3 and -3V (Amsden, 1993,1997; see also Amsden et al., 1985 and 1989) with modifications. KIVA-3 is a transient, multiphase, multidimensional, arbitrary-mesh, finite volume computational fluid dynamics (CFD) program widely used for internal combustion engine simulations. It is based on the Arbitrary Lagrangian Eulerian (ALE) method (Margolin, 1997). The numerical representation of the convective/advective terms in Eulerian approach lead to both diffusion and dispersion errors, which create difficulties in resolving sharp interfaces in flow variables. The ALE method seems to remedy some of those deficiencies. The concept of the ALE is to allow some displacement of grid nodes during one time-step interval. A more detailed discussion on the ALE method is presented in Chapter 3. The method is typically implemented in three phases. The first phase is an explicit Lagrangian update of the equations of motion. The second phase is an optional implicit phase when the sound waves are allowed to move many computational cells per time step if the material velocities are smaller than the speed of sound. This leads to a greater computational efficiency. The third phase is the remapping (or rezoning) where the solution from the end of phase two is mapped back onto an Eulerian grid. This mapping is essentially one step of a conservative advection algorithm (Margolin, 1997). The special case of non-moving boundaries where the cells are always mapped back to the original grid is the Eulerian limit. The reader is referred to Amsden et al., (1993) and Hirt et al., (1997) for more details regarding the ALE method and the KIVA family of codes.

1.2 Sub-grid Scale Models

Favre averaging of the Navier-Stokes equations produces turbulence stresses of the form

$$\tau_{ij} = -\rho\overline{u_i' u_j'} \tag{1.1}$$

Here and after the standard tensor notation is used where repeated indices denote summation.

A similar expression is obtained when the governing equations are filtered in the large eddy simulation (LES) approach especially when a box filter is used. The Boussinesq eddy viscosity approximation is applied to determine the sub-grid scale (SGS) stresses, which in this study are expressed as

$$\left(\tau_{ij}\right)_{SGS} = -\left(\overline{\rho u_i u_j} - \bar{\rho}\,\bar{u}_i\bar{u}_j\right) = 2\mu_t \bar{S}_{ij} - \frac{2}{3}\rho k\delta_{ij} - \frac{2}{3}\mu_t \nabla\cdot\underline{u}\delta_{ij} \tag{1.2}$$

where $\bar{S}_{ij}$ is the mean strain rate tensor, and δ_{ij} is the Kronecker delta function. The extra SGS stresses arising from the non-linearity of viscous stresses (see Piomelli, 1998) are neglected.

The standard k-ε model that is implemented in KIVA-3 consists of the following equations

$$\frac{\partial \rho k}{\partial t} + \nabla\cdot\left(\rho\underline{u}k\right) = -\frac{2}{3}\rho k\nabla\cdot\underline{u} + \underline{\underline{\sigma}}:\nabla\underline{u} + \nabla\cdot\left[\left(\frac{\mu}{Pr_k}\right)\nabla k\right] - \rho\varepsilon \tag{1.3}$$

$$\frac{\partial \rho \varepsilon}{\partial t} + \nabla\cdot\left(\rho\underline{u}\varepsilon\right) = -\left(\frac{2}{3}C_{\varepsilon_1} - C_{\varepsilon_3}\right)\rho\varepsilon\nabla\cdot\underline{u} + \nabla\cdot\left[\left(\frac{\mu}{Pr_\varepsilon}\right)\nabla\varepsilon\right] + \frac{\varepsilon}{k}\left[C_{\varepsilon_1}\underline{\underline{\sigma}}:\nabla\underline{u} - C_{\varepsilon_2}\rho\varepsilon\right] \tag{1.4}$$

with the model constants $C_{\varepsilon_1} = 1.44$, $C_{\varepsilon_2} = 0.92$, $C_{\varepsilon_3} = -1.0$, $Pr_k = 1.0$ and $Pr_\varepsilon = 1.3$. The SGS heat flux vector is calculated from SGS stresses by using a constant turbulent Prandtl number, Pr_t =0.74. KIVA-3 includes a SGS model, which utilizes the k-equation given above along with constraining the ε values to satisfy the following inequality:

$$\varepsilon \geq \left[\frac{C_\mu}{Pr_\varepsilon\left(C_{\varepsilon_2} - C_{\varepsilon_1}\right)}\right]^{\frac{1}{2}} \frac{k^{\frac{3}{2}}}{L_{SGS}} \tag{1.5}$$

L_{SGS} is an input length scale whose value is typically some measure of the computational cell dimension. In this study L_{SGS} was taken to be equal to the grid related length scale, $L_G = (\Delta x\Delta y\Delta z)^{1/3}$, and used either as a variable length scale or as a constant with a typical cell size. This model will be referred to as the $k\text{-}\varepsilon\,|_{SGS}$ model.

Modifications were made to the KIVA code to allow a classical Smagorinsky model where the eddy viscosity is calculated from

$$\nu_t = (C_s L_{SGS})^2 (\bar{S}_{ij} \bar{S}_{ij})^{1/2} \tag{1.6}$$

The model constant C_s was set equal to 0.2, a typical value used in the literature (see e.g. Rodi et al., 1997). The sub-grid length-scale was estimated as an average computational cell dimension (see Smith et al., 1998).

In some of the cases presented "no SGS turbulence model" was used. This requires, in most instances, some numerical diffusion for stability, which is accomplished via the use of QSOU (Quasi Second Order Upwind) scheme, described below, instead of the central differencing (CD) which has no diffusion error, or by using a combination of CD and upwind differencing heavily biased towards CD. It should be noted that there had been other successful LES studies reported in the literature (see e.g. Kamamura et al., and Tamura et al., as referenced in the review by Rodi et al., 1997) without using any SGS model. As such, the SGS contribution to the eddy viscosity is determined by the numerical diffusion inherent to the numerical scheme used.

The above turbulence models were employed in conjunction with the commonly used law-of-the-wall boundary condition which is implemented in KIVA-3. The basic assumption here is that the interaction between the modeled near wall region and the outer region is weak as observed experimentally by Brooke and Hanratty (1993) for a range of flows.

1.3 Numerical Schemes

Convective terms are advanced explicitly in time, and the diffusion terms are advanced explicitly, implicitly, or semi-implicitly. The degree to which the diffusion terms are implicitly discretized is based on a combination of stability and efficiency considerations. Sub-time steps (referred to as sub-cycles) are taken to advance the convective terms. The time step in each sub-cycle is based on Courant stability considerations. The convective terms are advanced with time steps that are the same or smaller than what is used for the diffusion terms. Though the overall time accuracy for convection terms is only of the first-order, the global time step is based on several considerations including stability and several accuracy constraints. To increase the time accuracy even further the time step was confined to the interval [1.5e-7 - 5.e-7 sec] far below the Kolmogorov time scale, which is in the order of 10^{-4} -10^{-5} seconds for a typical automotive size

engine ranging at speeds 1000-2000 RPM (Celik and Yavuz, 1997). This precaution compensates for the first order time accuracy of convective terms and guarantees the time resolution required for LES. For these reasons, the authors strongly believe that the time accuracy is adequate for LES despite the formal order of accuracy, as it is demonstrated below. The dominating errors in the present calculations with an average grid resolution of ~1.0 mm are due to spatial discretization.

All spatial derivatives other than the convective terms are approximated with central differencing. Spatial accuracy of the convective terms is limited to several choices including first-order upwinding (FOUP), not used in this study, central differencing (CD), a user defined scheme that combines the previous two choices, and a flux-limiting scheme known as Quasi-Second-Order Upwinding (QSOU). Both the first-order upwinding and the QSOU schemes are monotonic. In this study either QSOU or CD schemes is used. More details about the numerical issues can be found in Chapter 3.

Further justification to the numerical scheme can be provided by an order of magnitude analysis of the truncation error. It can be shown that in our case the normalized truncation error is given by

$$\text{T.E.} = \underbrace{C_1 \frac{\overline{V}_p \Delta t}{d_v}}_{\text{I}} + \underbrace{C_2 \frac{\Delta x^2}{d_v^2}}_{\text{II}} + \vartheta\left(\Delta t^2, \Delta x^3\right)$$

where a typical mean piston speed is $\overline{V}_p \cong 500$ cm/sec, $d_v \cong 3$ cm is the valve diameter and C_1, C_2 are assumed to be well behaving functions of space and time and $\vartheta(C_1) \cong \vartheta(C_2)$. Then, for $\Delta t = 1.0 \times 10^{-7}$ sec, and $\Delta x = 0.1$ cm,

$$\frac{\text{Term I}}{\text{Term II}} \approx \frac{\overline{V}_p d_v \Delta t}{\Delta x^2} \approx 10^{-2}$$

which shows that spatial error will still be the dominating factor, and there is no need for further refinement of the time scheme. It should be noted that there are other successful LES studies in the literature which use first order time scheme (see the work of Tamara et al., and Onera et al. as reported by Rodi et al., 1997 in an LES Workshop; see also Naitoh et al., 1992).

Chapter 2: Rotational Effects in an LES Model

Swirl is often an important part of the flow in a diesel cylinder, either as a byproduct of how air or fuel is introduced into the chamber, or by special arrangement to enhance mixing for combustion. The WVU/LES code, which can not be used directly to simulate flow in a realistic cylinder due to its lack of sufficient flexibility in boundary conditions, was used for two sub tasks during this project. One was to simulate swirling jet flow, which was then used as a benchmark for intercomparison between WVU/LES and KIVA. The second was to derive an LES subgrid model capable of including some rotational damping effects. This later task was completed in coordination with two other grants dealing with large eddy simulations of swirling flows (a NSF grant on modeling Tornado dynamics and a NASA grant on modeling aircraft trailing vortices). Results of these two tasks are described briefly in this chapter. More complete details may be found for the swirling jet in Lewellen et al. 1998, and for the subgrid rotational damping in the appendix to Lewellen et al. 1999.

In an LES one explicitly simulates turbulent eddies large enough to be resolved on the computational grid, and models the effects of eddies which are smaller. If, in a given problem, one can resolve the scales of eddies most important for turbulent transport, then the most important role of the subgrid model is simply to provide an energy sink so that energy does not pile up on the grid scale. In such cases the simulation results should be insensitive to the details of the subgrid model. Sometimes, however, there are regions in a simulation where the larger scale turbulence is suppressed for some physical reason, and the subgrid contribution becomes relatively more important. A familiar example is near a wall, where the scale of the most important eddies is limited by the distance to the wall. One must insure in such cases that the subgrid model is not overly dissipative, i.e., that any physics suppressing the resolved turbulence also suppresses the turbulence represented by the subgrid model. In the appendix to Lewellen et al. 1999, we detail how the most important effects of rotational damping were included within our subgrid model, in analogy with how damping in a stratified flow has been treated in previous LES studies of the planetary boundary layer (e.g., Lewellen et al. 1996).

The subgrid model used in WVU/LES is based on a subgrid turbulent kinetic energy equation, and a diagnostic variable Λ, representative of the characteristic size of eddies

comprising the subgrid scale turbulence. A rotational damping term was added to the determination of the subgrid turbulence length scale, Λ, allowing rotation to have the same limiting influence on the scale as that represented by the stratification damping term in previous atmospheric versions of the code. The new algorithm is:

$$\Lambda = \text{Min}[\, 0.65z,\ c\ \text{Max}[\Delta x, \Delta y, \Delta z],\ q/(2N),\ q/(2\xi)] \tag{2.1}$$

where q is equal to the square root of twice the subgrid turbulent kinetic energy, N is the Brunt - Vaisala frequency determined by stratification, and ξ is a measure of the rotational radial oscillation frequency. In a pure axisymmetric, rotating flow

$$\xi^2 = 2\Gamma\Gamma'/r^3 \tag{2.2}$$

where Γ is the product of the tangential velocity times the radius, r, and the prime represents the derivative with respect to r. An energy balance argument shows that ξ^2 satisfies the analogous criterion for axisymmetric disturbances in a pure axisymmetric, rotating flow, as N^2 satisfies in stratified planar flow.

Of course, in a general 3-D flow it is difficult to measure the local value of $\Gamma\Gamma'/r^3$ about it's local center of rotation. The problem was to find a function to approximate this in the general case where the local center of rotation is unknown and may be moving. Such a desired function in Cartesian coordinates was found to be:

$$\xi^2 = 2(\nabla p \cdot \mathbf{V}_{,i})(\nabla p \cdot \mathbf{V}_{,i} - \nabla p \cdot \nabla \mathbf{V}_i)/(\nabla p \cdot \nabla p) \tag{2.3}$$

Where **V** is the velocity vector and p is the pressure. In the pure axisymmetric, rotating flow Eq. 2.3 reduces exactly to Eq. 2.2. We note in passing that the stabilizing effects of strong radial temperature gradients within a rotating flow can be included in the same level of approximation by adding the term $(-\nabla p \cdot \nabla \mathbf{T}/\mathbf{T}_o)$ to the right hand side of Eq. (2.3).

The implementation of this term in the LES code appears to work well. Its primary influence is to reduce the small-scale turbulent diffusion in any coherent vortex cores. This would have no effect as long as one has the luxury of resolution much finer than any local vortex core size, but this is not likely to be the case in any diesel chamber simulation, particularly when wall effects are dominant.

Results of high resolution, fully 3-dimensional, unsteady simulations (utilizing WVU/LES) of a strongly swirling annular jet are presented in Lewellen et al. 1998. The goal was to provide high enough resolution to permit the dominant turbulent eddies to be examined. Near the nozzle the jet spread is approximately axisymmetric and driven by small scale (relative to the jet radius) turbulence; further downstream the spread rate increases as the turbulence becomes characterized by a small number (~ 2 - 4) of localized parcels of concentrated angular momentum spiraling radially outwards. Mean velocities, turbulent variances, and joint probability distributions are compared with laboratory experimental data previously obtained by Holzapfel (1996). The simulated jet dynamics is found to be quite sensitive to low-wave number perturbations of the velocity distributions issuing from the nozzle with differences between laboratory and numerical data easily masked by the uncertainty in this boundary condition. Definitive comparisons between simulations and laboratory results would require quite detailed specification of the fluctuations within the flow from the nozzle. This inherent sensitivity of the swirling jet to details of the inlet conditions suggests that it should not be used as a standard for fine-tuning closure model parameterizations. However, qualitative conclusions can be drawn by comparison of these results with the KIVA predictions (see Chapter 3).

Figure 2.1 shows an instantaneous view of the jet vertical velocity in a plane cutting through the center of the annular swirling jet utilizing 1.5×10^6 grid points distributed over a grid stretched in all three directions. The axisymmetric average over a few flow through times is superimposed as contours over the instantaneous view. It is these averages which are compared to the laboratory data. Comparison tests (Chapter 3) with KIVA utilize both these averages and instantaneous distributions for a qualitative comparison of the turbulent fluctuations.

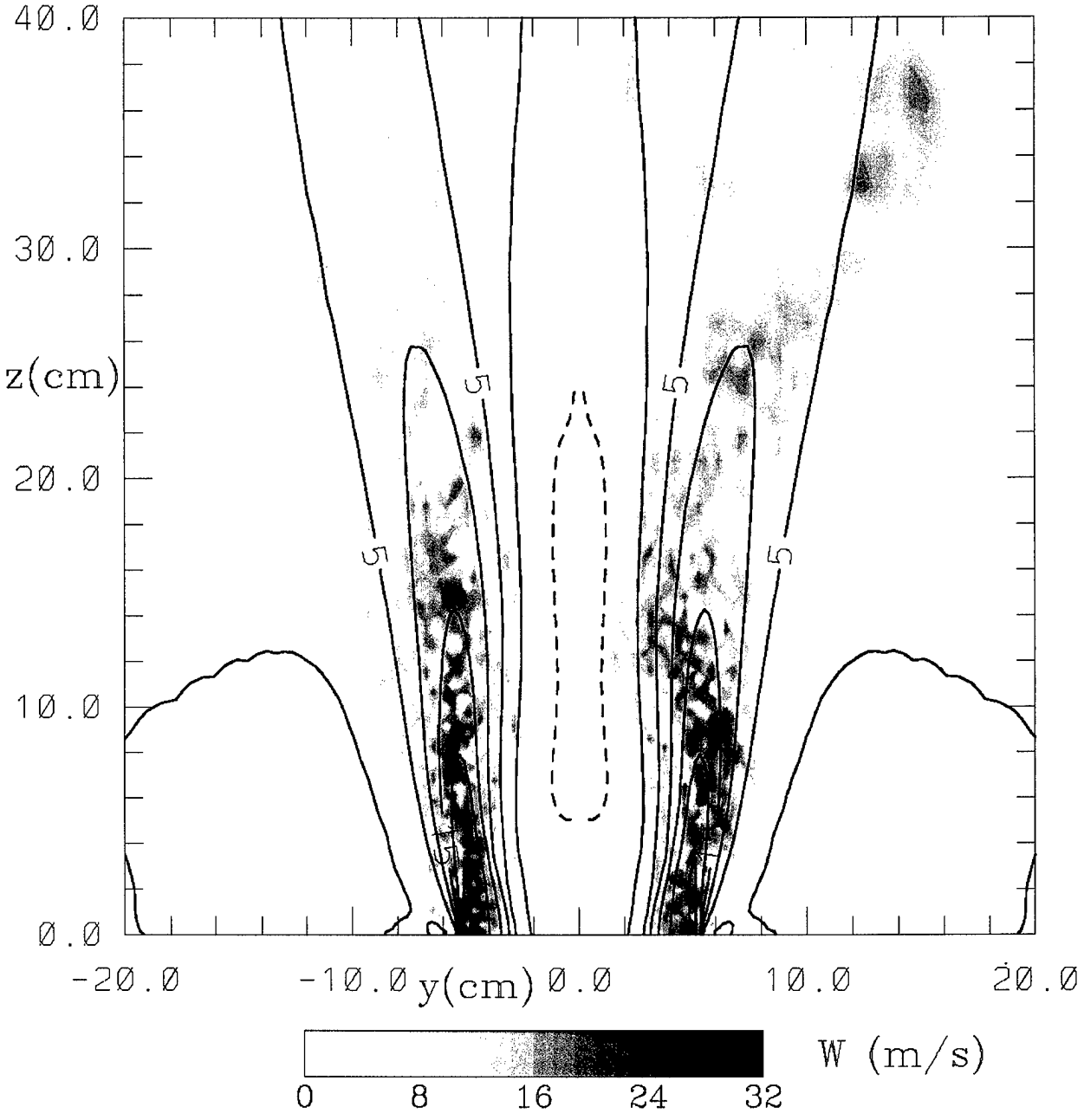

Figure 2.1 Vertical velocity distribution obtained from WVU/LES simulation of an annular swirling jet. Time averaged contours at intervals of 5 m/sec are superimposed over an instantaneous view represented by shading.

Chapter 3: Validation of KIVA and the ALE Method for LES Application

3.1 Background

There are several popular solution strategies that are employed in performing LES. The most effective appear to be spectral methods. This is due to the high accuracy and energy conserving properties associated with these methods. However, spectral methods are not as flexible as traditional finite volume methods due to difficulties in applying them to non-uniform grids, a necessity for representing complex geometries. Finite volume methods are easily applied to non-uniform grids, and as a result can represent complex geometries. The most severe drawback to using finite volume methods to perform LES is related to accuracy, a problem made worse when non-uniform grids are used. When finite volume based codes are applied in the LES approach accurate non-diffusive convective differencing schemes are required. Fine grid resolution is also necessary. The later problem requires that a relatively more efficient implementation has to be used. The ALE (Arbitrary Lagrangian-Eulerian) method may be computationally more efficient than other finite volume implementations, especially those based on variants of the SIMPLE algorithm (Patankar, 1980). In addition, there is a possibility that the convective modeling procedure utilized in the ALE method may be more accurate than traditional approaches. This will be discussed in more detail in the next section.

Swirling flows are of great interest to the engineering community due to their widespread application in engineering systems. They are of particular interest to both the gas turbine and the internal combustion engine communities. In the later example significant vorticity is induced during the intake stroke to aid in turbulent mixing and combustion inside the engine cylinder. One of the keys to the successful simulation of internal combustion engine flows is the accurate modeling of the effects of rotation on the mean flow field. However, the simulation of the intake stroke of an IC engine is too complicated of a problem to use as a test case. It is desired to simulate a flow that has similar swirling properties to that of flows commonly encountered in engineering systems, yet is simple enough such that detailed experimental data exists for comparison. A good choice is the case of an annular swirling jet such as that recently studied by Holzapfel (1996).

The main objective of this study is to assess the LES capabilities of the ALE method. In addition, the same assessment is desired of the commonly used computer code KIVA-3 (Amsden et al, 1989,1993) which is based on the ALE method. This assessment will be performed by simulating a free three-dimensional swirling jet. This problem is complicated mainly due to the presence of rotation. It is well known that many traditional turbulence models (e.g. standard k-ε model) fail in the presence of rotation due to the isotropic Boussinesq eddy viscosity approximation. Many add-hoc modifications have been made to the k-ε equations, specifically to the ε equation, to capture the effects of rotation in the traditional Reynolds Averaged Navier-Stokes (RANS) models (Bardina et al, 1985; Launder et al, 1977; Sloan et al, 1986). However, when similar models are applied as sub-grid scale (SGS) models in conjunction with Large Eddy Simulation (LES), there is some discrepancy in the literature as to whether there is a need for such modifications. Some researchers believe that extra rates of strain such as rotation, streamline curvature, and stratification affect the large scales much more than the small scales (Ferziger, 1993). If this is true, then it should be possible to use SGS models without major modifications for flows where these extra rates of strain are significant. Previous investigations (Smith et al., 1997, 1998) have shown promise in capturing a swirling flow field with relatively simple SGS turbulence models when sufficient grid resolution is used.

In this study, a simple Smagorinsky SGS model is used in addition to relatively fine grid resolution. The flow field obtained from the simulations is compared to experimental data for the same flow (Holzapfel, F., 1996). The turbulence quantities are compared to assess the LES capabilities of the ALE method. Previous work on this particular flow situation has been performed using a widely tested LES code (Lewellen et al., 1996, 1998), hereafter referred to as the WVU-LES code. The results and experience gained from applying the WVU-LES code to this particular problem were used as a guide for this work. In addition to comparing to the experimental data, the results obtained in this work are compared to those obtained with the WVU-LES code. Qualitative duplication of the WVU-LES results using KIVA is desired and would be further validation of the KIVA code for use in LES.

The swirling jet test case will also be used as validation of a newly implemented second-order Runge-Kutta time integration scheme.

3.2 Computational Issues

The KIVA-3 code is based on the Arbitrary Lagrangian Eulerian (ALE) method. The ALE algorithm combines features of Lagrangian and Eulerian representations. In a Lagrangian simulation, the mesh moves with the local velocity of the fluid. An advantage of the Lagrangian representation is that in this reference frame convective/advective terms vanish. However, Lagrangian meshes tend to tangle and in general can not represent large deformations that result from shear and vorticity. In an Eulerian simulation the mesh is fixed in space and fluid moves from one cell to another. The Eulerian methodology does not lead to tangled meshes. However, the numerical representation of the convective/advective terms leads to both diffusion and dispersion errors that create difficulties in resolving sharp interfaces. It is these errors, especially numerical diffusion, which make finite difference applications in LES difficult.

The Lagrangian and Eulerian methodologies are two special cases of mesh motion. The concept of the ALE method is that mesh motion can be chosen arbitrarily. The method is typically implemented in three phases. The first phase is an explicit Lagrangian update of the equations of motion. The second phase is an optional implicit phase that allows sound waves to move many computational cells per time step if the material velocities are smaller than the fluid sound speed. This allows for greater computational efficiency. The third and final phase is the remap (or rezone) phase where the solution from the end of phase two is mapped back onto an Eulerian grid. This mapping is essentially one step of a conservative advection algorithm (Margolin, 1997). The special case of no boundary motion where the cells are always mapped back to the original grid is the Eulerian limit. The reader is referred to Amsden et al. (1989, 1993) and Hirt et al. (1997) for more details regarding the ALE method and the KIVA family of codes.

The underlying computational methodology of the ALE method differs considerably from more popular methods. However, from the user's point of view the ALE methodology is not that different. Time advancement is similar to many codes that utilize the LES methodology where the convective terms are advanced explicitly and the diffusion terms are advanced explicitly, implicitly, or semi-implicitly. The degree to which the diffusion terms are implicitly discretized is based on a combination of stability and efficiency considerations. It should be noted that the user can set the implicitness factor. Sub-time steps (referred to as sub-cycles) are

taken to advance the convective terms. The size of the time step for each sub-cycle is based on stability considerations. Although the overall time accuracy is only first-order accurate, the global time step is based on several considerations including stability and several accuracy constraints. The convective terms are advanced with time steps that are the same or smaller than what is used for the diffusion terms. Due to these reasons, the present authors believe that the time accuracy is quite good despite the formal order of accuracy. To further insure time accuracy, the diffusion terms were advanced in a second-order Crank-Nicolson approach with an implicitness factor of 0.5. The minimum number of subcycles taken for the convective terms was set at 10. This reduces the leading temporal error by an order of magnitude. It should be mentioned that second-order time accuracy is still not achieved. However, the implementation outlined above should yield time accuracy that is adequate for this problem given the accuracy restraints on the time step. Also, the size of the time step that was used for each sub-cycle was much smaller than dictated by the accuracy constraints. In addition, a fully second-order time accurate Runge-Kutta time marching scheme is implemented and tested. It should be noted that even with second-order accuracy, small time steps need to be taken to resolve the turbulence spectra (Choi and Moin, 1994).

The QSOU scheme used in the KIVA code approaches second-order accuracy in the absence of steep gradients. However, when it is desired to resolve turbulence in combination with subgrid-scale models CD is typically used (Piomelli, 1998; Mittal and Moin, 1997) to prevent numerical diffusion from entering the calculation. Special care must be taken in applying CD in a compressible code. Small dispersion errors can be catastrophic to a compressible code such as KIVA. For a LES application the added turbulent eddy viscosity is usually enough to ensure that the effective Peclet numbers are small. Thus the dispersive errors are small in the momentum equations. However, even small dispersion errors lead to problems when the advective schemes are applied to scalar transport equations. For example, the internal energy equation is particularly sensitive to dispersion errors and can lead to non-physical density and temperature values. These quantities are always solved for in the presently used ALE approach regardless of whether the code is applied to a compressible or incompressible situation. Small oscillations in these variables can grow and lead to divergence of the solution. For the problem studied here variation in temperature and density should be small and have little or no effect on the flow field. To ensure that this is the case a modification was made to the code. Whenever

CD is used for the convective terms in the momentum equation, QSOU is used for all scalar variables. This appears to have negligible effect on the simulations since both temperature and density remain relatively constant (less than 2% variation). This is an excellent result for what is normally a compressible code.

By combining the Lagrangian and Eulerian approaches in the ALE method it is hoped that some of the discretization errors associated with the approximation of the convective terms will be eliminated. This would make the ALE approach attractive as a LES methodology since the major problem facing standard finite difference approaches is the error resulting from the convective discretization.

For the present test case a standard Smagorinsky model was implemented as described in Section 1.2.

C_s was taken as 0.2, a typical value used in the literature for isotropic turbulence. L_{SGS} is an input length scale whose value is typically some measure of the computational cell dimension. Here it was calculated from

$$L_{SGS} = (\Delta x \Delta y \Delta z)^{1/3} \tag{3.1}$$

3.3 Application

The geometry of the free annular jet was defined to be the same as that experimentally studied by Holzapfel (1996). Laboratory conditions were duplicated as close as possible in formulating the numerical simulation. The computational domain was defined as a three-dimensional prism, with the jet inlet at the bottom, and the outlet at the top. The jet inlet was defined by an annulus that ranged from R=2.7-5.3 cm on the xy-plane at the bottom of the domain. The width of the domain was defined at 100 cm. The axial length was set at 100 cm, which translates into 40 annulus widths. The far field boundary on the left, right, front and derriere sides of the domain consisted of setting the radial entrainment velocity. This was obtained from extrapolating the values from the experimental data while at the same time satisfying global continuity. It is believed that the domain width is of sufficient size such that any errors in the far-field boundary condition will have little effect on the jet. The axial, radial, and swirl velocities at the inlet are given by Holzapfel (1996). The same profiles were measured

at different axial locations through the use of a hot-wire technique. The simulation was performed by assigning the velocity profiles at x=0.0, and then letting the jet develop as it propagated downstream. The inlet plane itself consisted of a flat plate, the sole purpose of which was to guarantee radial entrainment near the inlet. The log-law boundary layer approximation was used for this boundary. This approximation should be adequate given the fact that the turbulence in this flow field is generated at the inlet. The Reynolds number for the jet based on the average axial velocity at the inlet and the width of the jet annulus is approximately 20,000.

The radial plane was discretized using a 78x78 non-uniform grid as is shown in Figure 3.1. The axial (z) direction was discretized using 82 vertices. The computational grid thus formed consisted of approximately 500,000 nodes. Since the computational domain was defined as a prism, a Cartesian grid system could be used. This allowed more control over the numerical errors due to the discretization. Though the choice of a Cartesian-type grid helps to minimize discretization errors, it introduces errors in approximating circular shapes, in this case the annular inlet. To better resolve the annular jet at the inlet, the grid was contracted near the center of the xy-plane. The contraction was kept at slightly less than 3%. It has been found that when CD is used grid stretching in excess of 3% introduces grid to grid de-coupling that is manifested by oscillations (Mittal and Moin, 1997). This constraint was relaxed in the far field since this region should have little effect on the flow field. Even with grid clustering the annulus was not perfectly defined. However, this error helps in introducing small-scale perturbations in the flow field. These perturbations are a result of the combination of strong shear zones that exist near the inlet and the asymmetries that exist in the grid. This helps initialize the turbulent jet. Introducing random perturbations (10%) to all three components of the inlet velocity further initializes the turbulent field. It should be noted that the turbulence intensities reported by the experiments were much higher than this.

The axial direction was also defined with a non-uniform grid (Figure 3.2) and consisted of 82 vertices. The vertices were placed uniformly for the first 10-cm of the jet at an interval of 0.5-cm. This allowed for good resolution for the first jet diameter where the jet is particularly sensitive to the inlet conditions. The grid was allowed to expand at 1.7% from z = 10 cm to z = 20 cm. The grid was expanded at a rate of 2.7% from z = 20 cm to z = 52 cm. The region of interest is confined to $z \leq$ 40-cm since this is where experimental data is available. With this in

mind the expansion was increased to 10% for the remaining 48-cm. It is this last region where the effects of the outflow boundary conditions are expected to be nullified. It should be noted that the Smagorinsky model introduces enough eddy viscosity such that the effective cell Peclet numbers are small. This helps prevent the grid-to-grid decoupling that occurs when CD is used.

Two different outflow boundary conditions are available in KIVA-3. The first is a zero slope condition for the velocity gradients. The second involves specifying the pressure at the outflow. Since this flow is highly convectively dominated, the outflow boundary condition should not have significant effect on the upstream velocity. In fact previous work on the same problem using the WVU-LES code (Lewellen et al., 1998) has confirmed this. Also, it is believed that the domain is long enough so as to eliminate the influence of the outflow boundary condition on the flow region of interest. The zero slope boundary condition was used as is commonly employed for this type of flow (Lewellen et al. 1998; Xia et al., 1997).

The swirl strength is characterized by the jet inlet swirl number S_0 . S_0 is defined as the ratio of angular to axial momentum flux in the nozzle divided by the outside nozzle radius. In the experiments an approximate swirl number was calculated based on the swirl generator geometry. The free jet case that was simulated in this work had a swirl ratio (S_0) equal to 0.95 as reported by Holzapfel (1996).

3.4 Results

3.4.1 Numerical Data Acquisition

The jet was allowed to develop from an initial state of zero velocity. This consisted of simulating the jet for approximately five flow-through times using relatively large time steps. A flow-through time is defined as a time scale representing the average length of time required for flow to get from the inflow boundary to the outflow boundary based on the average inlet velocity. After the jet had developed, the simulation was continued for an additional 5000 time steps (approximately five flow-through times). KIVA automatically adjusts the size of the time step by the criteria previously outlined. However, for the last 5000 time steps it was not allowed to exceed 5.0e-5 seconds.

The instantaneous flow fields at two different times are shown in Figures 3.4 and 3.5. These two flow fields are from an axial plane of 40x40-cm cut from the center of the domain at two different instances in time 0.01 seconds apart. As can be seen the flow is highly unsteady and is certainly turbulent. However, to compare the numerical results obtained in this study with the experimental data requires that average velocity profiles be calculated. Calculating meaningful averaged velocity profiles for different axial locations is not a trivial task. This is due to the fact that the jet varies significantly in the radial direction. However, the most difficult problem is associated with the fact that the jet is non-stationary in that it fluctuates about the centerline. This is demonstrated in Figure 3 where the axial velocity at the centerline is shown to vary significantly over time. This is an indication that the large-scale coherent structures of the jet are highly unsteady, and as a result the jet is rarely positioned about the center of the domain. To obtain an accurate time average many more time steps would need to be taken which is not feasible at this time. However, it is believed that a sufficient number of time steps have been taken such that a qualitative comparison to the experimental data can be made. Despite oscillatory nature of the jet, temporal and partially spatial averaged velocity profiles were calculated at two different axial locations (z = 20-cm and z = 40-cm). The spatial averaging was performed by averaging the velocity profiles at four circumferential locations ($\theta = 0$, $\theta = \pi/2$, $\theta = \pi$, $\theta = 3\pi/2$). The spatially averaged profiles that resulted from this procedure were then used to obtain a time average.

An important side note to this investigation involves the computational performance of the ALE method and particularly the KIVA code. To perform the 5000 time steps discussed above required approximately eight days using a dedicated 533 MHZ DEC ALPHA NT workstation. It has been demonstrated that the CPU time required to perform large simulations using KIVA scales either linearly, or close to linear (Gel et al., 1998). This appears to be more of a feature of the ALE method than of the KIVA code, and can be considered a very good feature. The KIVA code itself is not particularly efficient. The code needs to be revised so that it can take advantage of modern computer architecture, which would include parallelization. One of the major drawbacks of the ALE method is the memory requirement. On minimum settings KIVA requires approximately 0.8 kb/node. However, the KIVA code was not written with LES in mind. It is suspected that a code based on the ALE methodology could be written that is more efficient with respect to memory usage.

3.4.2 Comparison to Experimental Data

The velocity profiles obtained from averaging the numerical results are compared to the experimental profiles in Figures 3.9-3.20. From the outset of this investigation it was known that the swirling jet problem was particularly sensitive to initial conditions. This has been demonstrated by Lewellen et al. (1998). As a result achieving very close agreement with the experimental data should not be expected. However, as can be seen the overall the mean velocity profiles (Figures 3.9 – 3.14) compare fairly well. In particular the extent of the radial spreading of the jet is predicted. The simulated jet exhibits a behavior that more closely resembles circular jet farther downstream (Figure 3.10). However, the time average given here is somewhat misleading due to the oscillatory nature of the jet discussed above. The radial velocity is a measure of the jet entrainment. The average radial velocity is given in Figures 3.11 and 3.12 for z = 20-cm and z=40-cm, respectively. It is seen that the radial velocity is over-predicted at z=20-cm, and this trend seems to have been reversed at z=40-cm. It is possible that more grid resolution in the radial plane may improve this situation. The improvement would be due to better resolution of the shear region. More grid resolution in the radial plane may also improve the axial velocity agreement since the inflow velocity profiles and the resulting flow rate would be better approximated. It is likely that the simulations would then more resemble the experimental situation. The swirl velocity agrees fairly well at both axial locations (Figures 3.13 and 3.14).

The averaging process previously described was used to obtain statistics of resolved turbulence. These are compared to the experimental profiles shown in Figures 3.15-3.20. In general the turbulent statistics are under-predicted. This indicates that the subgrid contributions at this grid resolution are significantly large. However, given the fact that it is not possible to initialize the inlet turbulence such that it is identical to the experiments, then the agreement can be considered quite good. Also, the initialized turbulence was steady as opposed to the real situation where it is unsteady. To create a more realistic simulation, the initialized turbulence should be both spatially and temporally correlated. Another problem, which has been previously discussed, is related to the averaging process and non-stationary nature of the jet. The RMS fluctuating axial velocity is shown in Figures 3.15 and 3.16 for the two different axial positions.

The levels are under-predicted in some regions. Similar results were obtained for the other RMS fluctuating velocity components (Figures 3.17-3.20).

3.4.3 Comparison to WVU LES Results

As was mentioned previously, work on this particular flow situation has been performed using the WVU-LES code. However, both the grid and the subgrid scale model used were different. Given these differences exact duplication of the WVU-LES results using KIVA is not possible. However, qualitative duplication of the WVU-LES results using KIVA is desired and would yield further validation of the KIVA code.

Figures 3.6 and 3.7 show the instantaneous pressure contours on the radial plane at two different axial locations (z = 10-cm and z = 40-cm, respectively). Again the flow field appears turbulent and is not centered about the center of the domain. Figure 6 shows that the eddies are relatively symmetric about the center of the domain at z = 10-cm. Further downstream at z = 40-cm radial diffusion of the vorticity has occurred (Figure 3.7). In addition the structure of the flow field is tri-modal. A similar structure is observed at z = 40 cm using the WVU-LES code (Figure 3.8). In addition, the order of the variances between the experimental data and the simulations reported by Lewellen et al. (1998) are quite similar to the present results.

Due to the similarity between the results obtained with KIVA and those obtained with the WVU-LES code it is believed that some success has been achieved in capturing the turbulent nature of this flow field despite the comparatively low grid resolution.

3.4.4 Validation of the Second-Order Time Integration Scheme

The jet was simulated for an additional 5000 time steps using the newly implemented Adams Bashforth/Runge Kutta time integration scheme (see Chapter 4 for details). Averaged profiles were obtained in the same manner as those obtained with the first-order scheme. Since it is the nature of the unsteadiness that is of interest, only the fluctuating quantities obtained from both schemes are compared. Also, since the flow field is more turbulent closer to the jet annulus, the closer of the two axial locations will be considered (i.e. Z=20 cm). The three fluctuating components of velocity obtained using the two different time integration schemes are shown in Figures 3.15 to 3.18. As can be seen the profiles are nearly the same, with small differences

being attributed to the unsteadiness of the flow field, not the numerics. This result can be justified by an order of magnitude analysis the purpose of which is to determine whether the temporal or spatial discretization errors are dominating the overall error. The error assessment technique known as Richardson extrapolation will be used for this purpose. The dominating error for the temporal and spatial errors using the first order backward Euler time integration scheme (i.e. the default in KIVA) and central differencing for the convective terms is $O(\Delta t, \Delta x^2)$.

$$U = C_\tau \Delta t + C_x \Delta x^2 \approx \frac{u_{ref}}{\tau} \Delta t + \frac{u_{ref}}{l^2} \Delta x^2 \tag{3.2}$$

Where u_{ref} is the reference velocity, τ is the reference time scale, and l is the reference spatial scale. The reference time is determined from

$$\tau = l / u_{ref} \tag{3.3}$$

which can be substituted into the Equation 3.2 above to yield

$$U = \frac{u_{ref}}{l/u_{ref}} \Delta t + \frac{u_{ref}}{l^2} \Delta x^2 \tag{3.4}$$

The ratio of the errors then becomes

$$\frac{temporal\ error}{spatial\ error} \approx \frac{C_t}{C_x} = \frac{u_{ref}\, l\, \Delta t}{\Delta x^2}$$

The reference velocity is related to the turbulent kinetic energy, k, as

$$u_{ref} = k^{1/2} \tag{3.5}$$

The reference length scale for a round jet is given by Wilcox (1993) as

$$l = 0.1\ \delta \tag{3.6}$$

where δ is the jet half width (jet radius). The time step size and spatial discretization as well as other parameters are listed in Table 3.1 for different axial locations.

Using the experimental values for k and δ, $C_t/C_x = 0.13$ at Z = 20 cm and $C_t/C_x = 0.04$ at Z = 40 cm. When it is considered that the sub-cycling time step size is 1/10 that of the global

time step given above these numbers drop by a factor of ten. Thus this analysis shows that for the chosen grid and time step size the spatial error is dominant.

Table 3.1: Parameters needed for error analysis.

Parameter	Z = 20 cm (2 jet diameters downstream)	Z = 40 cm (4 jet diameters downstream)
k_{max} (m^2/s^2)		
experimental	27.90	7.52
numerical	8.50	2.57
δ(m) (experimental)	0.25	0.30
Δt (s) (numerical)	$5.0x10^{-5}$	$5.0x10^{-5}$
Δx (m) (numerical)	0.007	0.01

3.5 Discussions

This work outlines the preliminary attempt at LES of a swirling jet using an ALE approach in conjunction with the KIVA-3 code. The goals were to capture some of the non-linearity and hence some of the larger coherent turbulent structures and unsteady effects. If successful then some proof of the LES capabilities of both the ALE method and the KIVA code will have been obtained. This is especially the case given the relatively coarse grid used in this study.

The preliminary results show that the mean velocity profiles were fairly well predicted. Also, the simulation captures the unsteady nature of the jet, and predicts some of the turbulent statistics well. This was achieved despite the fact that the chosen problem is extremely sensitive to initial conditions, and duplicating the experiments exactly is nearly impossible. This is certainly evidence that the both the ALE method and the KIVA code in particular are accurate enough to be used for LES given proper selection of convective differencing scheme and grid.

Also, the method does have the potential for good scaling with respect to grid resolution. This later point makes the ALE approach attractive compared to other finite volume methods.

In addition to validating the LES potential of the KIVA code, a new time integration scheme has been tested. Time accuracy has been shown to be relatively unimportant for this particular flow situation and in particular with the grid and time step size used. However, time accuracy will be important for other problems and even this problem when the grid is refined. It was demonstrated that the new second-order scheme that has been implemented into KIVA is working.

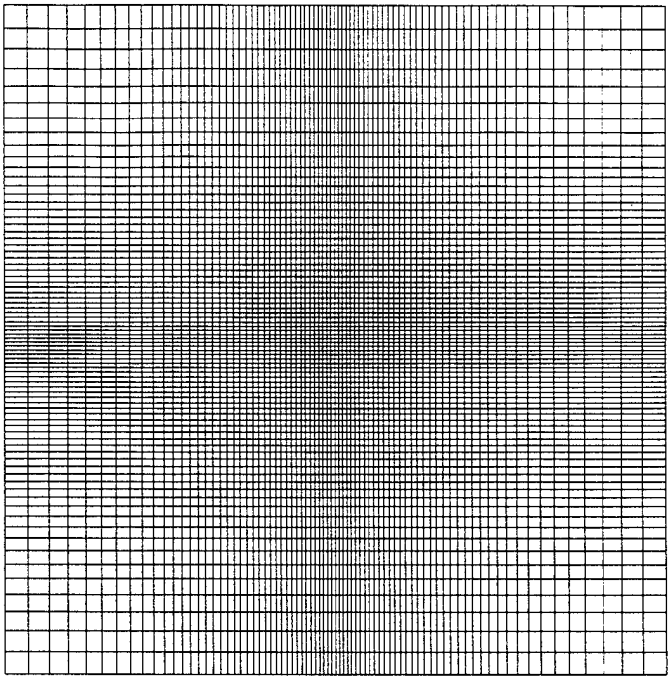

Figure 3.1 Grid in the radial plane.

Outflow boundary

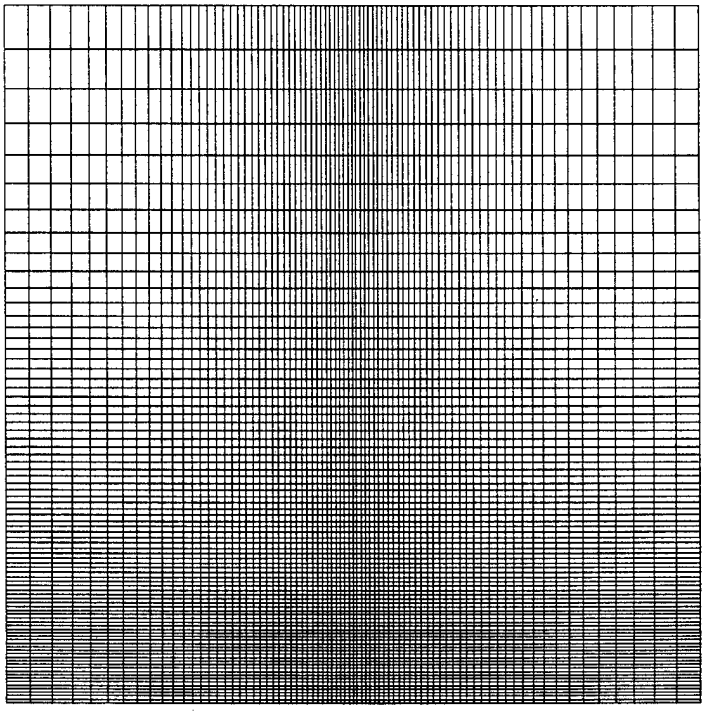

Inflow boundary

Figure 3.2 Grid in the axial plane.

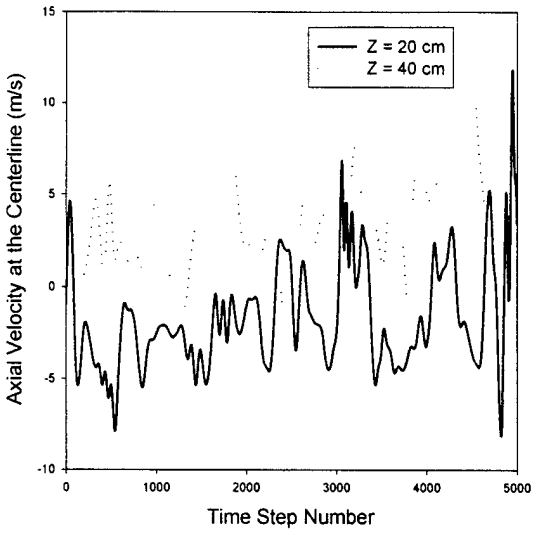

Figure 3.3 Variation of axial velocity at the centerline with time.

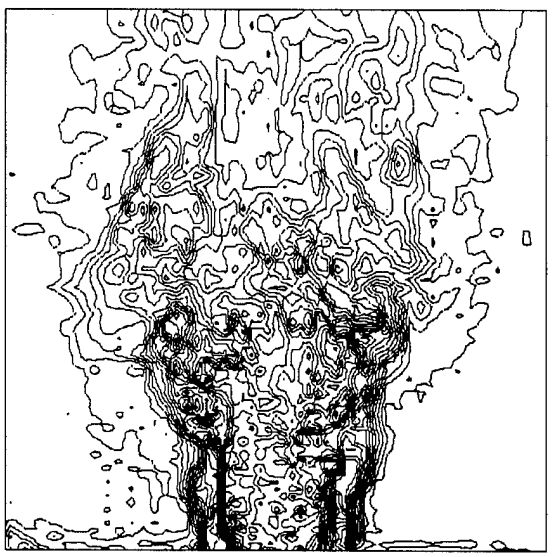

Figure 3.4 Instantaneous velocity at time = 0.645 seconds.

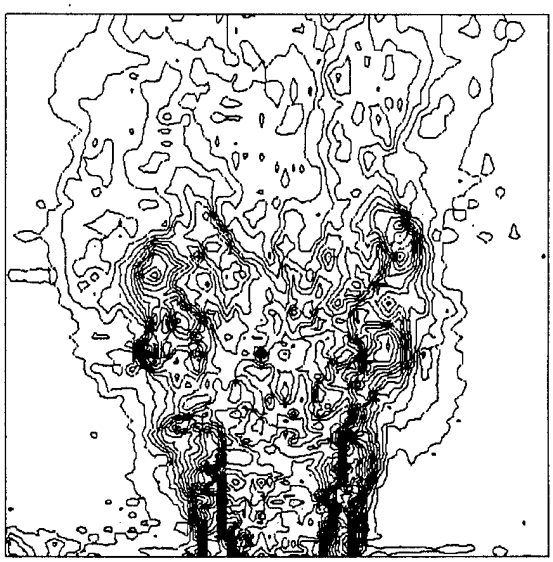

Figure 3.5 Instantaneous velocity at time = 0.655 seconds.

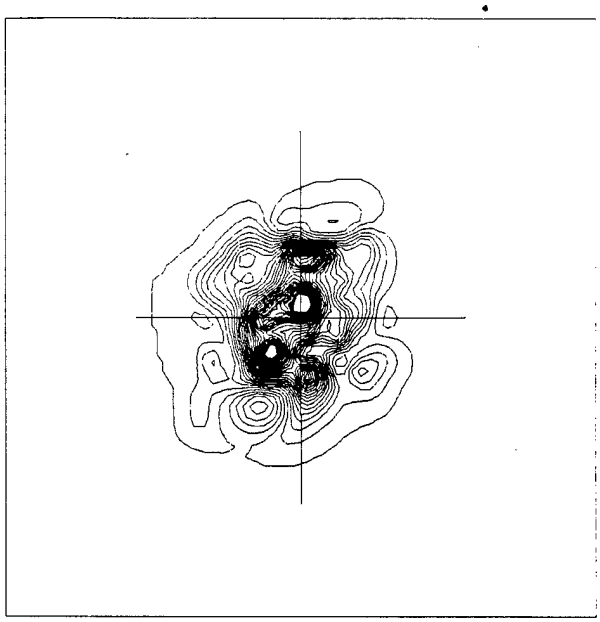

Figure 3.6 Instantaneous pressure contours at z = 10-cm.

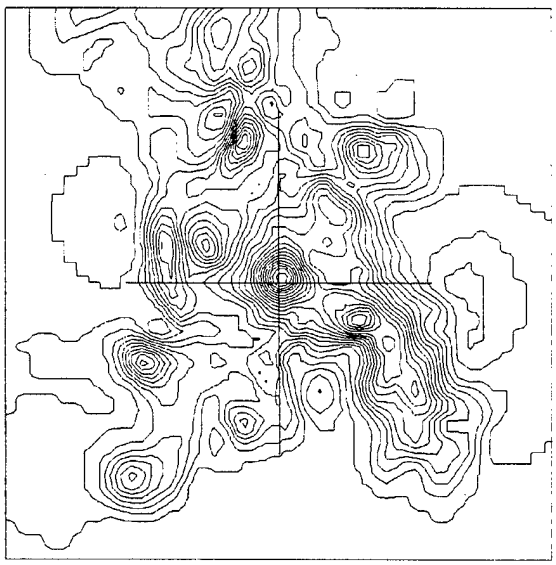

Figure 3.7 Instantaneous pressure contours at z = 40-cm.

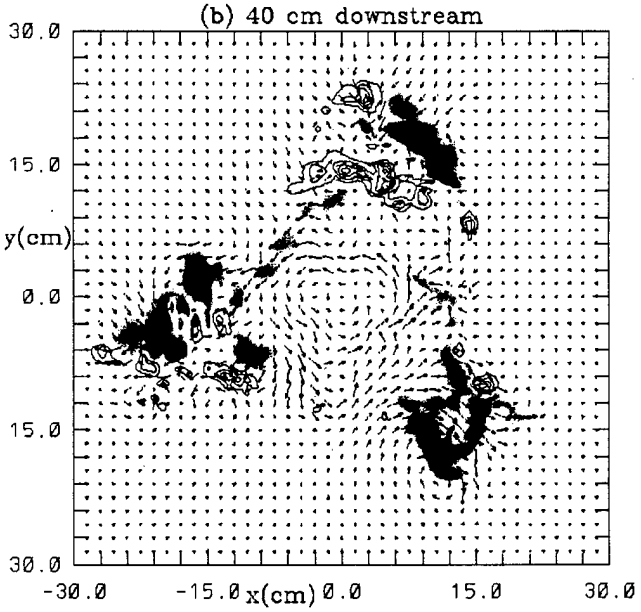

Figure 3.8 Instantaneous angular momentum showing tri-modal structure (z = 40-cm, WVU-LES).

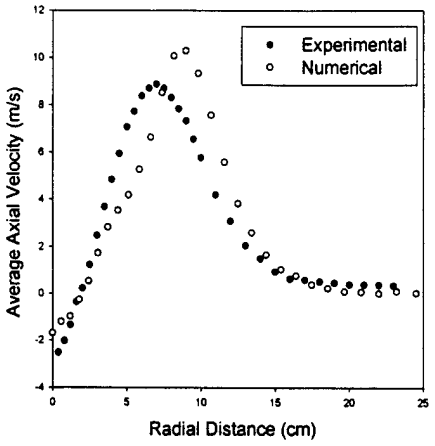

Figure 3.9 Average axial velocity at z=20 cm.

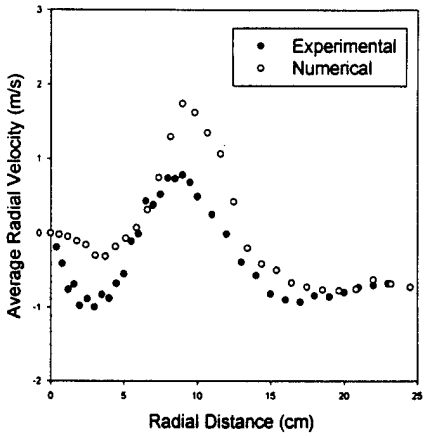

Figure 3.11 Average radial velocity at Z=20 cm

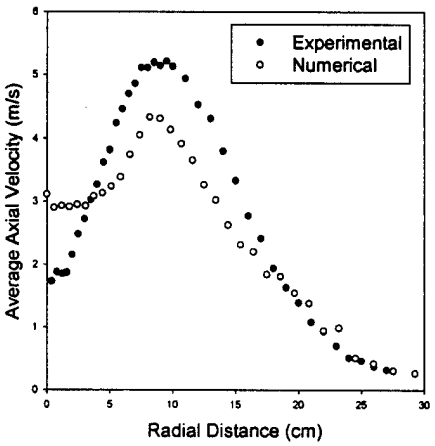

Figure 3.10 Average axial velocity at z=40 cm.

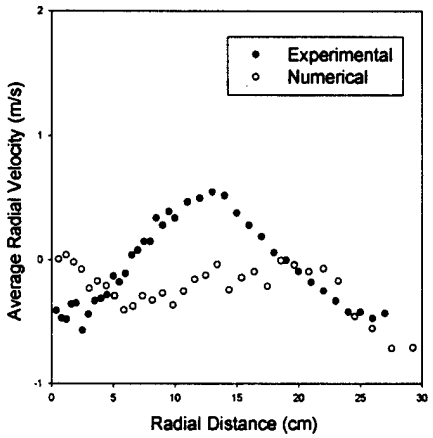

Figure 3.12 Average radial velocity at z=40 cm.

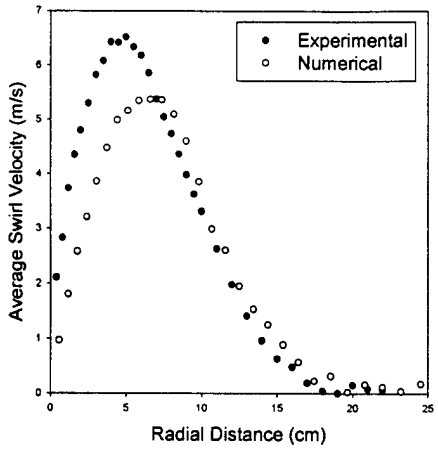

Figure 3.13 Average swirl velocity at z=20 cm.

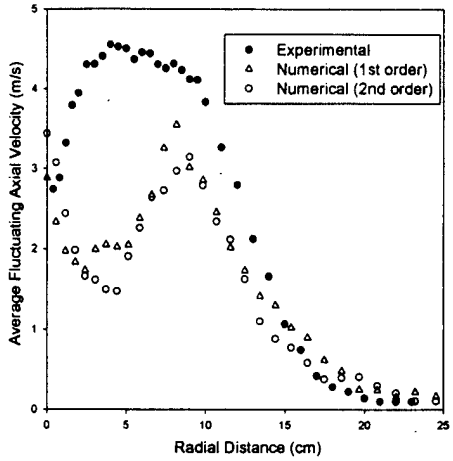

Figure 3.15 $\overline{U_z'}$ at z = 20 cm.

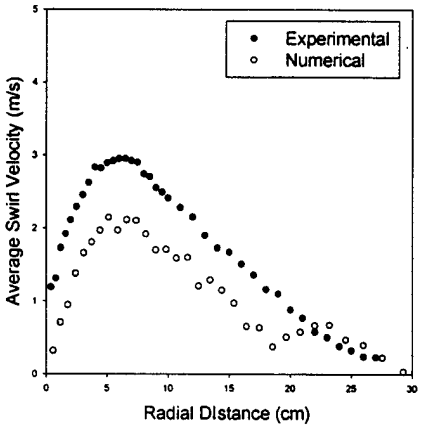

Figure 3.14 Average swirl velocity at z=40 cm.

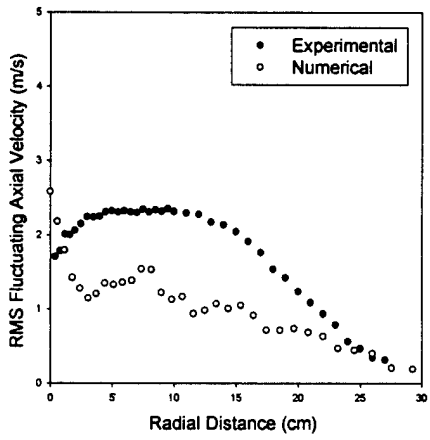

Figure 3.16 $\overline{U_z}$ at z = 40 cm.

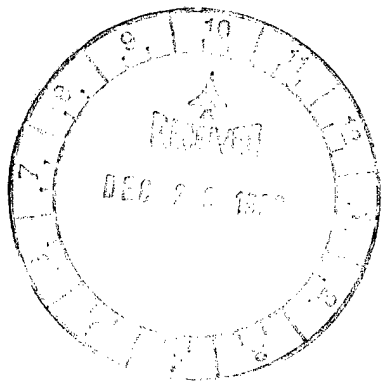

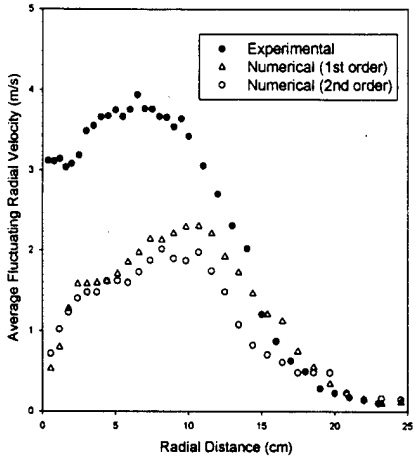

Figure 3.17 $\overline{U_r'}$ at z = 20 cm.

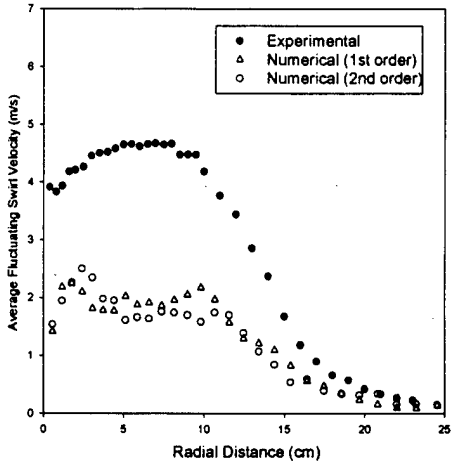

Figure 3.19 $\overline{U_\theta'}$ at z = 20 cm.

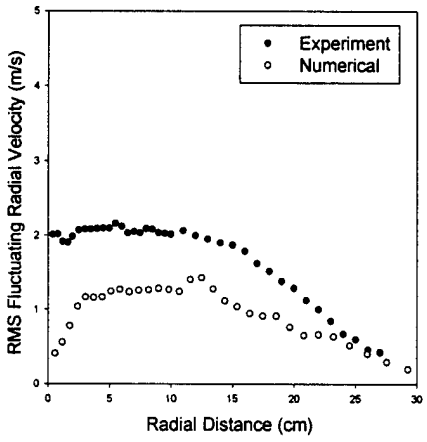

Figure 3.18 $\overline{U_r'}$ at z = 40 cm.

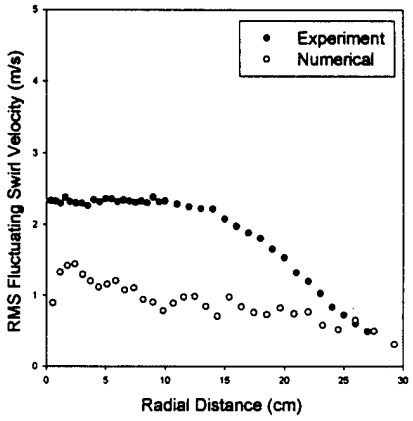

Figure 3.20 $\overline{U_\theta'}$ at z = 40 cm.

Chapter 4 Accuracy and Efficiency Improvements in KIVA

4.1 Accuracy Improvements

The numerical scheme in the original KIVA-3 was kept simple and robust as much as possible in order to incorporate all the capability to model complex flows and make KIVA-3 a general purpose code (i.e., laminar/turbulent flows, single-phase or multiphase with fuel spray dynamics, combustion chemical reactions, etc.). This was done by introducing a numerical scheme that is first order accurate in time and approximately second order accurate in space. However, today's challenging problems demand more accurate schemes with higher resolution and faster convergence. Particularly for LES higher accuracy of at least second order is necessary.

In this section the improvements to enhance the spatial and temporal accuracy of the KIVA code are discussed. First, time integration scheme improvements are presented. These improvements were as a result of joint effort with Mr. M. Prinkey (1999). The second part is dedicated to the spatial accuracy improvements in the code. A new flag has been introduced to run the code with central difference scheme for the convective terms in the momentum equations while applying Quasi-Second Order Upwind (QSOU) scheme for the density, energy and other scalar equations. Both of these implementations are verified by comparing the results with the two-dimensional lid driven cavity flow calculations of Ghia et al. (1982). Furthermore to assess the overall spatial accuracy of the code, the simulation of a three-dimensional lid-driven cavity was performed and compared with benchmark results. The details of these results can be found in Gel et al. (1998).

4.1.1 Time Integration Improvements

Time advancement in KIVA-3 is performed essentially in three phases (i.e., Phase A, B, and C). In Phase A, spray droplet collision and oscillation/breakup terms are calculated and explicit source terms due to chemical reactions, fuel spray etc. are integrated in the mass and energy equations. Phase B calculates, in a coupled, implicit fashion, the acoustic mode terms (namely the pressure gradient in the momentum equation and velocity dilatation terms in mass &

energy equations), the spray momentum source term, the source terms in the turbulence-model equations, and the terms due to diffusion of mass, momentum and energy. Phase C is the rezone phase, in which the convective transport associated with the moving mesh relative to the fluid is calculated by freezing the flow field and then rezoning (remapping) it onto a new computational mesh (in Lagrangian phase) or onto the same computational mesh (in Eulerian phase). All these phases apply to the same time interval but one at a time built on top of each other. The advective terms of Phase C are advanced explicitly in consecutive sub-cycle timesteps (Δt_c) which is simply an integral submultiple of the global computational timestep (Δt). However, the diffusion terms of Phase B can be integrated explicitly, implicitly, or semi-implicitly. In certain problems, when timesteps are small enough, KIVA-3 automatically uses a stable explicit scheme for which no costly iterative solution is required. When timesteps are not suitable for explicit marching, a semi-implicit time advancement option is employed. The degree to which the diffusion terms are implicitly discretized is based on a combination of stability and efficiency considerations. The implicitness parameter (ϕ) enables some sort of weighting of the old- and new-time values of the solution variable.

Numerical experiments have shown that this approach improves the computational efficiency without degrading the numerical stability when possible. Two separate implicitness factors are calculated in KIVA-3. The first one is ϕ_d which is associated with the diffusion terms. The second one is ϕ_p which is associated with the pressure wave propagation.

During Phase C, sub-cycle timesteps are taken to advance the convective terms explicitly. The convective terms are advanced with time steps that are the same size or smaller than what is used for the diffusion terms. The time step size of the each sub-cycle is based on stability considerations. Though the overall time accuracy is only first-order accurate, the global time step is based on several considerations including stability and accuracy constraints which restricts the time step to fairly small values hence assuring accuracy.

Further details on the time integration scheme and the implicitness parameters can be found in Appendix H of the KIVA-II manual (Amsden et al. (1989)).

The new second order accurate time scheme

For the problems without any spray/droplet and chemical reactions, the source term contributions due to these terms can be omitted. Also if we consider that there are no source terms in Phase B this yields the semi-implicit formulation for the diffusion terms. Following the suggestion in Appendix H of KIVA-II manual (Amsden et al. (1989)), setting the implicitness factor for diffusion, ϕ_d , equal to 0.5 throughout the simulation yields to second order accurate Crank-Nicolson scheme which may have overshoots and lead to inaccurate results for large values of C_d (= $\nu\Delta t$ / Δx^2). Hence it follows that by selecting an appropriate valued for ϕ_d, the KIVA-3 code can be made second order accurate in time except only the time integration steps in Phase C.

For this purpose a scheme consisting of a two stage Runge-Kutta and Adams-Bashforth method was proposed and implemented for the advected quantities (e.g internal energy, ρE and momentum, ρU) in Phase C. Further details of the implementation of the new time scheme can be found in Gel (1999).

4.1.2 Spatial Accuracy Improvements

All derivatives other than the convective terms are approximated with central differences. Spatial accuracy of the convective terms is limited to several choices including first-order upwinding, central differencing, a user defined scheme that combines the previous two choices (PDC), and a flux-limited higher-order scheme known as Quasi-Second-Order Upwinding (QSOU). Both the first-order upwinding and the QSOU schemes are monotonic. It is important to note that KIVA-3 is a compressible flow code. Oscillations from non-monotonic schemes can be catastrophic for compressible codes where scalar variables such as density and temperature are involved. This can lead to code instability and/or largely inaccurate solutions. As a result, monotonic schemes are the preferred choice in KIVA-3. The trade-off for monotonacity is the loss of accuracy near steep gradients. This is true for all monotonic schemes, including what is probably the most accurate of these type of schemes known as the Piecewise Parabolic Method (PPM) (Colella and Woodward, 1984). On a uniform grid in the absence of steep gradients, PPM is formally fourth-order accurate whereas the QSOU method is second-order accurate. In the

presence of steep gradients PPM reduces to second-order accuracy whereas QSOU reduces nominally to a kind of first-order upwind scheme.

Another convective scheme option included in the Partial Donor Cell (PDC) formulation in KIVA-3 is the central differencing (CD). Applying CD is difficult due to the well-known dispersive error that results when this scheme is applied to a situation where the cell Peclet number is greater than 2.0. This constraint imposes prohibitively fine grids. When CD is used special care needs to be taken to prevent numerical dispersion from dominating the solution. This includes using some form of deferred correction, or explicitly letting extra diffusion enter into the calculation. In practice higher-order upwinding methods (such as the QUICK scheme) are often used to obtain grid independent results with a much smaller grid. However, no such scheme is available in KIVA-3, and for the reasons that will be discussed in the next paragraph upwinding schemes are not specifically desirable.

CD is of particular interest since it is typically used when finite volume methods are applied in the Large Eddy Simulation (LES) approach (Piomelli, 1998; Mittal and Moin, 1997). CD is used in order to prevent numerical diffusion from polluting the calculations. Truncation errors associated with numerical diffusion are more harmful to LES than those that are associated with numerical dispersion. Unfortunately, the dominating errors that result from any kind of upwinded scheme are diffusive. The fine grid resolution used in LES combined with the added diffusion provided by the subgrid-scale turbulence model causes the effective Peclet number to be smaller than it would be in the laminar case. This allows some control over the dispersion errors without the introduction of subgrid-scale damping numerical viscosity.

KIVA-3 has a fourth-order node coupler that is included as part of the base code. This routine is provided as a means of filtering oscillations that occur due to grid-to-grid de-coupling of the pressure and the velocity fields. Pressure-velocity de-coupling occurs when CD is used in the pressure solver on a non-staggered grid. The current release of KIVA-3 should not encounter the pressure de-coupling problems that existed with the older versions since a staggered grid is now used. However, the node-coupler is still included in the code. This routine appears to introduce fourth-order diffusion, which is used to filter the oscillations. It should be recognized that the oscillations that result from pressure de-coupling are similar to those that result from

applying CD to the convective terms. The use of the alternate node coupler as a filter to remove those unphysical oscillations that result from using CD is proposed as an alternative.

Several parametric studies to assess the degree to which the node-coupler needs to be employed to remove the unphysical oscillations were carried out. In order to assess the accuracy of the overall scheme, a lid-driven cavity test case was simulated with KIVA-3 after some modifications in the code.

For an LES application the added turbulent eddy viscosity is usually enough to ensure that the effective Peclet numbers are small enough to minimize the dispersive errors in the momentum equations resulting from CD.

Small oscillations in density and energy can grow and lead to non-convergence of the solution. However, for truly incompressible problems such as that studied here (i.e., lid driven cavity problem) the energy equation is de-coupled from the velocity field and both density and temperature should remain constant. To ensure that this was the case a modification was made to the code. Whenever CD is used for the convective terms in the momentum equation, QSOU is used for all scalar variables. This appears to have negligible effect on the simulations since both temperature and density remain constant, except for very small perturbations (4 % difference between maximum and minimum density for the problem studied here). This is as would be expected since these quantities should be de-coupled from the velocity field and should not change.

4.1.3 Verification

The time and spatial accuracy improvements presented mentioned above were verified in case of the well known benchmark problem of a lid driven cavity. The results of this verification work can be found in Gel (1999). A separate study to assess the overall spatial accuracy of the code with the spatial accuracy improvement was performed with the three-dimensional lid driven cavity test case. The results can be found in Gel et al. (1998).

In addition to the above test cases, the time and spatial accuracy improvements presented in this study were utilized and used in the LES of a free swirling jet in the study of Smith et al. (1999a). Although numerical accuracy improvement analysis was not conducted, the fact that the

new implementations gave very close results or sometimes better results than the original, indicates the validity of the modifications introduced.

4.2 Efficiency Improvements

In an attempt to improve the computational efficiency of KIVA-3, the bottlenecks in the single processor (i.e., original) version were investigated before proceeding with the parallel version implementation. For this purpose the two example cases provided with the KIVA-3 manual were evaluated, performance wise, at the subroutine level profiling. These particular test cases were selected due to the fact that they constitute the majority of the features of the code during the execution. As seen from the Table 4.1, implicit pressure solver (PSOLVE, RESP) is one of the most CPU intensive segments of the code which becomes more crucial in pressure dependent problems. The last column in this table shows about 13 % of the total execution time is spent on that particular subroutine.

Table 4.1 Listing of top ten routines with the highest CPU utilization during the execution of TEAPOT example case

Subroutine	Tot Time	Calls	Avg. Time	%
CCFLUX	2.58e+01	1649	1.56e-02	28.75
RESP	1.09e+01	4257	2.55e-03	12.11
MOMFLX	8.69e+00	1649	5.27e-03	9.68
REST	4.85e+00	1778	2.73e-03	5.40
PSOLVE	4.48e+00	119	3.76e-02	4.99
TSOLVE	3.35e+00	119	2.81e-02	3.73
RESUVW	2.67e+00	532	5.03e-03	2.98
EXDI	2.48e+00	110	2.25e-02	2.76
BC	2.14e+00	2981	7.19e-04	2.39
RESK	2.09e+00	1311	1.59e-03	2.32

An extensive investigation of the implicit iterative solvers in KIVA-3 was carried out due to lack of concise documentation on the implementation of Conjugate Residual (CR) method in

the code. Improving the preconditioner used in the original version was determined to have a significant impact on single processor performance.

In this section the implementation of a more sophisticated preconditioner and the consequent performance improvement without any overhead in memory allocation is discussed. The implementation was carried out in such a way that the user can simply replace the two associated subroutines with the new ones to get the new preconditioner implemented into their version of KIVA-3. The details of the improved pressure solver can be found in Smith et al. (1999b).

4.2.1 Conjugate Residual Method

KIVA-3 features a Conjugate Residual (CR) method (Amsden et al. (1985)) based algorithm for the solution of matrices iteratively. This solution approach is activated only when the value of implicitness factor is greater than zero, i.e. semi- or fully-implicit. For example for pressure , if $\phi_p = 0.0$ then the solution of the pressure field is obtained explicitly. However, if $\phi_p > 0.0$ then the solution is obtained iteratively with the CR method based solver (PSOLVE). This method falls in the class of matrix solution procedures known as "Krylov subspace" methods (see Saad (1984) and Golub et al. (1996) for further information on Krylov subspace methods). Since the initial implementation of the CR method in KIVA in 1986, significantly improved methods like Conjugate Gradient and Multigrid methods have been developed and widely used. However, CR method was not replaced with any of these newer methods due to the memory conservative approach followed in implementing it into KIVA, i.e., the coefficient matrix is not stored.

Another reason that has hindered the implementation of improved algorithms is probably the lack of detailed documentation on the solver algorithms of KIVA-3. This shortcoming has necessitated considerable effort to understand the implementation logic of the CR method in order to be able to modify the code to improve its efficiency. A detailed description of the pressure solution technique employed in KIVA-3 is given in Gel (1999) and Smith et al. (1999b).

4.2.2 Symmetric Gauss-Seidel and Successive Over-Relaxation Preconditioning (SGS-SSOR)

The traditional way of generating a precondition matrix is to find an approximate inverse of the coefficient matrix. This could be done in several ways. The simplest preconditioning method is known as "Jacobi preconditioning", which is also used in KIVA-3 but for reasons that will become apparent later, this method is more appropriately referred to as "diagonal preconditioning". In this method, the reciprocal of the center diagonal of coefficient matrix, A, is used as preconditioner. This approach is memory efficient since only one full size array needs to be saved. However, it is a primitive form of preconditioning. More advanced procedures involve calculating an incomplete LU (ILU) decomposition, or an incomplete Cholesky (IC) factorization of the original matrix. The later is a special case of ILU decomposition for symmetric matrices. The coefficient matrix is approximately factored such that only non-zero elements that exist in the original coefficient matrix are considered. Although this procedure often yields very good preconditioning, the generation of the incomplete factorization is CPU intensive and is not easily parallelizable. Furthermore, the memory allocation is increased due to fact that the factored matrix needs to be stored. For the pressure matrix in KIVA-3 this would require an additional seven full size arrays which is a significant burden for a memory bounded code. A substantially improved approach for preconditioning can be implemented by performing several sweeps of a simple iterative solution procedure such as Jacobi, Gauss Siedel (GS), or Successive Over-Relaxation (SOR) and in this approach only the original coefficient matrix need to be stored.

The advantage of the GS/SOR approach is that convergence is accelerated over the Jacobi method. Also, only one array is required for the later two methods since new values are simply substituted for the old values. However, two arrays are required for the Jacobi approach since two iteration levels must be stored.

In most cases the pressure matrix will be non-symmetric due to various reasons such as the non-uniformity of grids used. However, for some special cases the matrix will be symmetric, for which the Krylov methods converge faster. In fact, for many Krylov subspace methods, including the CR method, convergence is guaranteed only if the matrix is symmetric. This seldom causes problems in application in that the procedure rarely fails to find a solution.

Depending on how it is applied, preconditioning may destroy the symmetry of the matrix. One directional sweeps of the Jacobi method will retain symmetry. However, one directional sweeps of both GS and SOR will destroy symmetry. For those cases where the matrix is symmetric it is desirable to apply the preconditioning in such a way as to preserve symmetry. This can be done by using symmetric GS (SGS) and symmetric SOR (SSOR). Employing symmetric versions of these schemes is a simple procedure that entails making two separate sweeps; the first from the first node in the matrix to the last, then reversing the sweep direction from the last node to the first. The two opposite direction sweeps represent one iteration of the symmetric scheme. A detailed discussion on the implementation issues of this new combined approach and how the original memory allocation requirements of KIVA-3 were preserved without introducing any memory overhead can be found in Gel (1999).

4.2.3 Benchmark Problems

Four different benchmark problems were used to demonstrate the effectiveness of the new preconditioning scheme. The types of problems vary from axisymmetric (two-dimensional) to full three-dimensional simulations. The test cases also include compressible flows with combustion, which are more relevant to engine applications, and a flow situation which is mostly incompressible.

The first problem, hereafter referred to as Case 1, was the standard Baseline case that is included as an example problem with KIVA distribution. This problem is the case of a two-dimensional (axisymmetric) engine cylinder with compression and expansion strokes and including combustion. There were a total of 1,380 grid cells in this problem.

The second problem (Case 2) is the same as Case 1, except that the axisymmetric grid has been rotated 360° to make it three-dimensional. The rotation was achieved by placing 36 grid points in the tangential direction, giving approximately 16,000. As with the first problem, only the compression and expansion strokes are simulated, but combustion is still included. This problem should demonstrate how the pressure solution dominates the overall solution time as both the number of grid cells and the dimensionality of the problem increases.

The third problem (Case 3) is the same as Case 2, but 72 grid points are placed in the tangential direction. Thus the total number of grid points is twice that of Case 2 at approximately

32,000. This problem is used to test the performance of the new preconditioning scheme as the grid resolution becomes finer. It is expected that the pressure solver will dominate the overall CPU time more than it does in Case 2. As a result, the quality of preconditioning will become more important. This phenomenon is related to the fact that the matrix becomes more difficult to solve (invert) as it becomes larger.

The fourth problem (Case 4) is a different kind of problem from the first three in that it does not involve an engine cylinder. It is a three-dimensional swirling jet defined on a non-uniform rectangular grid. A total of 64,000 grid cells were used. This particular problem does not include combustion and is for the most part incompressible. It is suspected that the computational effort will be dominated by the pressure solution. The reader is referred to Smith et al. (1998) for more details on this particular problem.

Table 4.2 Performance comparison of KIVA-3 and KIVA-3/WVU for the benchmark problems

	KIVA-3		KIVA-3/WVU		
Case Number	Normalized CPU Time	Pressure Iterations	Normalized CPU Time	Pressure Iterations	Speedup
1	1.0	38	0.93	15	6.8
2	1.0	54	2 sweeps 0.81	29	18.6
			3 sweeps 0.80	24	20.4
3	1.0	75	2 sweeps 0.90	51	9.8
			3 sweeps 0.84	44	16.1
			4 sweeps 0.82	39	18.3
4	1.0	45	2 sweeps 0.80	15	20.0
			3 sweeps 0.79	12	21.3

The size of the time step in all four problems is controlled by the stability/accuracy constraints contained in the original code. The k-ε model was used for Cases 1-3. A Smagorinsky turbulence model was employed in Case 4, thus no turbulence transport equations need to be solved for this problem. All computations were performed on a DEC Alpha 533 MHz workstation running Windows NT v4.0.

4.2.4 Discussion

The subroutines DRDP and PSOLVE have been modified in such a way that the original routines in both KIVA-3 and KIVA-3V can be directly replaced to yield a more efficient code on a single processor. The improvement in the efficiency of the overall code is problem dependent. For problems that do not contain a large number of grid cells the diagonally preconditioned CR routine is robust. However, as the grid is refined and the total number of grid cells increases, the solution of the matrix becomes more difficult. Hence, the quality of the preconditioning becomes more important, and the modifications outlined in this paper may provide a significant reduction in overall CPU time. The PSOLVE routine has been re-written in such a way that the user can choose between the original preconditioning scheme and the one presented in this chapter.

Table 4.2 shows the speedup achieved after the implementation of the new preconditioner based on the number of sweeps employed. The dimensionality of the problem seems to be the most important factor in the effectiveness of the new preconditioning scheme. The overall code speedup is significantly less for the axisymmetric problem (Case 1) compared to the three-dimensional problems (Cases 2-4). This is likely due to the fact that the matrix produced is relatively small and the existing diagonal preconditioning is robust. Also, the matrix produced by an axisymmetric problem is easier to solve since there are two less diagonals. The modified pressure solver appears to have a significant impact on three-dimensional problems where the number of grid cells is large and the quality of the preconditioning becomes more important. In this work KIVA-3/WVU was observed to be up to 20 % faster than the original code on two different kinds of three-dimensional problems. It should be noted that the CR method is also used in several other routines including KESOLVE (for k and ε), TSOLVE (for T), VSOLVE (for velocities), and YSOLVE (for species densities and mass fractions). Implementing the new preconditioning method in these routines is expected to be a simpler procedure. It was observed that TSOLVE and KESOLVE are expensive for three-dimensional problems such as Cases 2 and 3. The modifications outlined in this work could provide significant CPU savings for problems where the local iterations for the scalar field variables dominate the overall solution procedure.

4.3 Performance Improvements

The KIVA family of codes have been primarily developed on Cray vector supercomputers with explicit directives to take advantage of vector processing units without stalling the pipelines. However, the gain from vector supercomputers are becoming obsolete due to the significant improvements in processor chip design and introduction of efficient parallel processing platforms. As a result of these developments, the definition of "high performance computing" has evolved and changed significantly. These changes had significant impact on the problem complexity and size to be tackled.

Since the release of it's first version in 1985, the KIVA code has been also evolving and improving in parallel to all the new developments in computational resources and CFD techniques. For example, the block-structured grid capability in KIVA-3 provides significant advantages over KIVA-II, especially for complex internal combustion engine geometries. Another example is the indirect addressing introduced in KIVA-3, which eliminates the obligation to go through the storage array elements in a particular sequence. In spite of these improvements in the metholodogy, there are certain bottlenecks, which are quite difficult to overcome. For example the ghost cells surrounding the grid still impose severe restrictions on the maximum grid resolution that can be achieved on single processor systems.

Considering today's challenging problems which require adequately fine grid resolution capability, the most economical way to achieve progress towards this goal with KIVA-3 is to acquire the capability to run this code on parallel systems, preferably on distributed-memory architectures.

A shared-memory parallel implementation of KIVA-3, which is particularly optimized for Silicon Graphics symmetric multiprocessor systems, has been available to public for some time. However, the speedup characteristic of this version is not favorable. Figure 4.1 shows the speedup plot up to eight processors for a test case based on a 180° wedge with a grid of 80 x 18 x 80. It is seen that speed-up efficiency stalls after four processors. Due to this poor scalability and parallel efficiency, a domain decomposition based approach with explicit message-passing was investigated by Yasar et al. (1992).

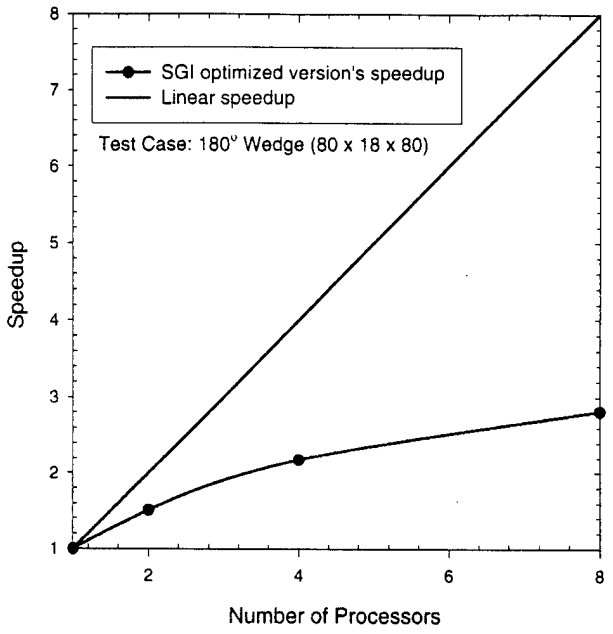

Figure 4.1 Speedup plot of SGI optimized shared-memory implementation of KIVA-3

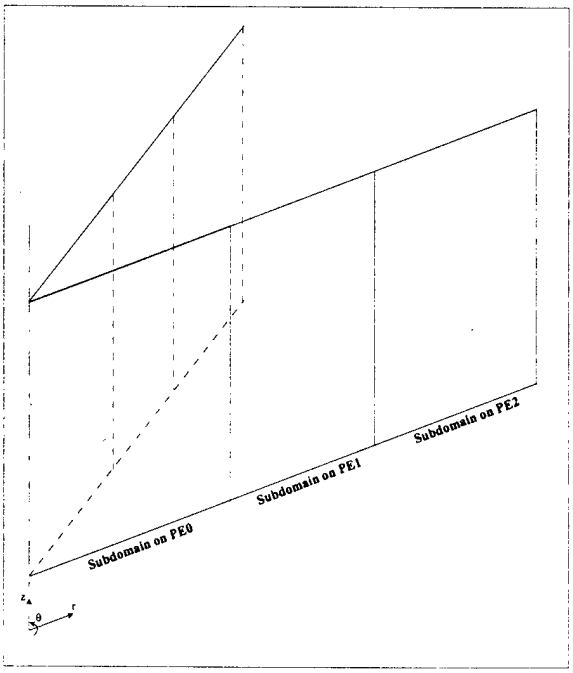

Figure 4.2 One-dimensional domain decomposition applied to a sector domain

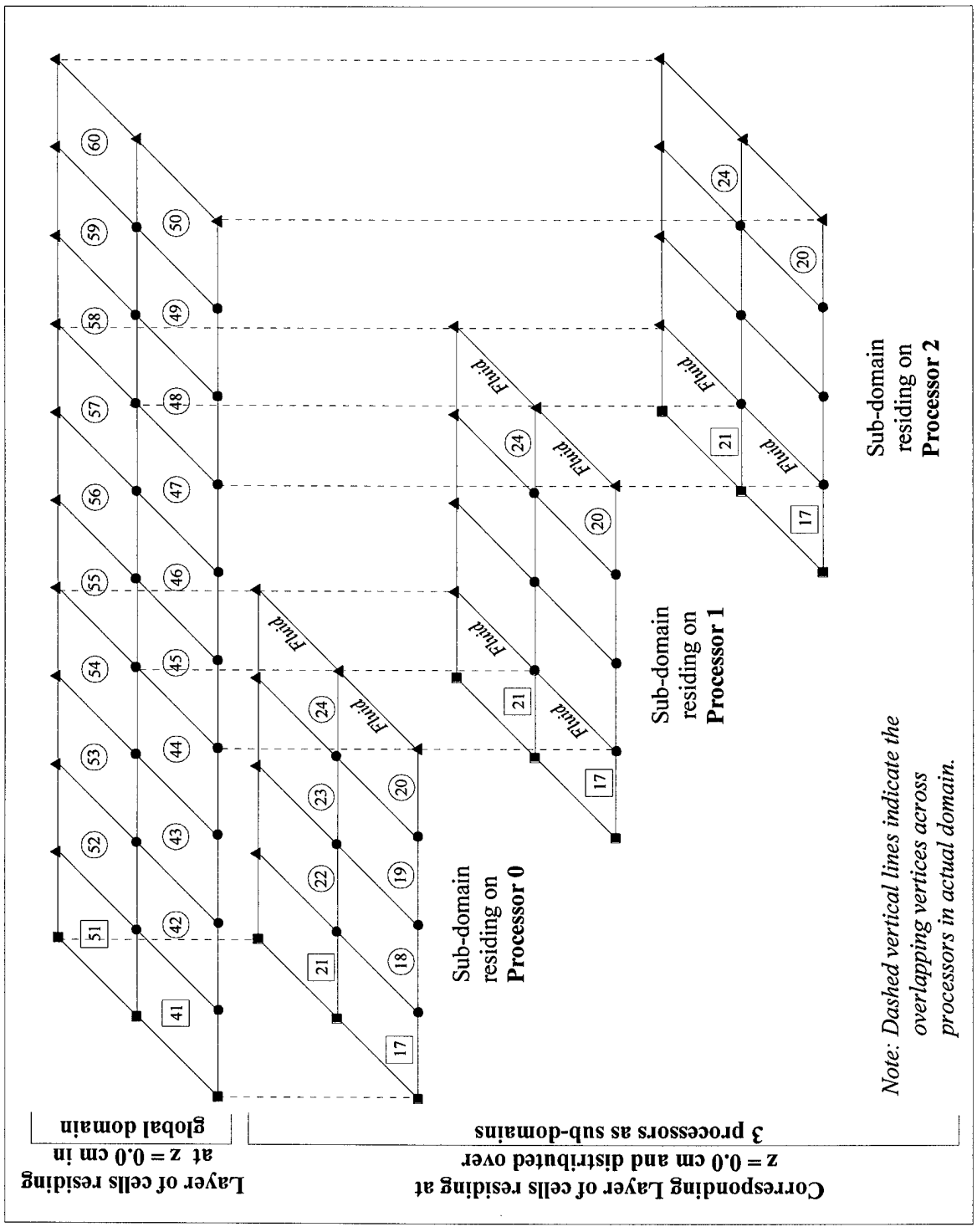

Figure 4.3 Illustration of domain decomposition over 3 processors for single layer in z-direction

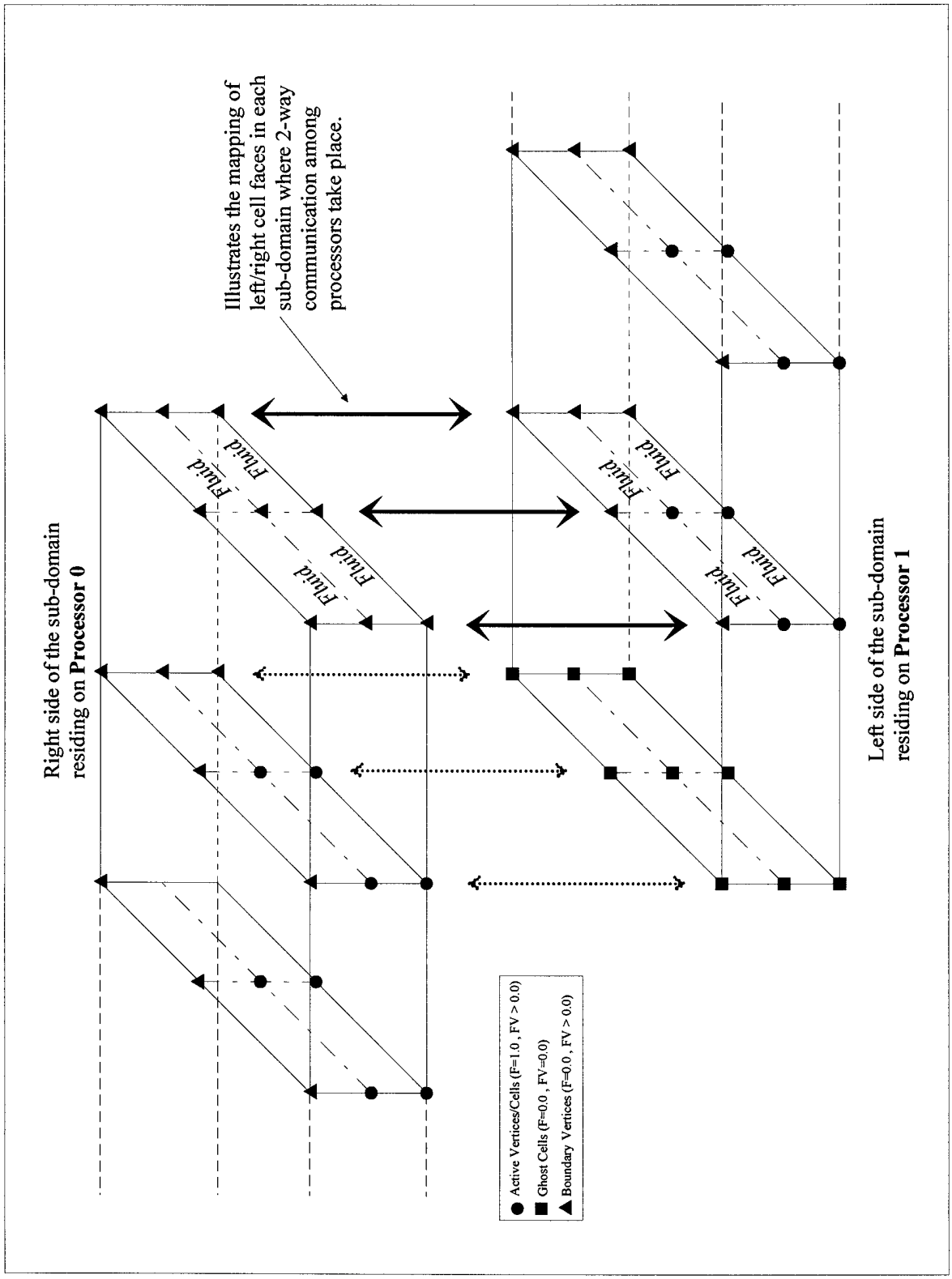

Figure 4.4 Detailed illustration of overlapping cell faces between two adjacent sub-domains on 2 processors.

In this study, a domain decomposition strategy in the x-direction (or radial direction) is based on the idea of overlapping the left & right faces of adjacent subdomains. This approach was initially proposed by Yasar (1998) who developed a preliminary implementation of KIVA-3 on Intel Paragon platform with NX message-passing libraries.

The parallel version has been ported to various distributed-memory and shared-memory parallel computer platforms with MPI message-passing library. Note that although the fundamental ideas of the current implementation are based on the previous work by Yasar et al. (1992), the current work essentially originated from scratch by building on top of the original source code of KIVA-3. The current domain decomposition approach is applicable to various geometries in engine applications ranging from full 360° mesh or a sector mesh as shown in Figure 4.2.

Figure 4.3 shows how a cartesian computational domain of 9 cells in length, 2 cells in width and height is decomposed into 3 subdomains; here in Figure 4.3, only a single z-layer is shown for brevity. Different symbols have been used to distinguish various cell types and boundary vertices available in original KIVA-3. The symbols can be interpreted as follows,

- Square symbol implies GHOST cells on the left and bottom faces of the whole domain with F = 0 and FV = 0 attributes.
- Circle symbol implies ACTIVE cells with F > 0 and FV > 0 attributes.
- Triangle symbol implies the BOUNDARY vertices (i.e., active vertices without any cell association) with F = 0 and FV > 0 attributes.

Domain decomposition is carried along the x-direction and each subdomain contains 3 x 2 x 2 cells. Each subdomain is assigned to a processor. Left and right faces of each subdomain overlap with the adjacent subdomains right and left face. Each processor has it's own grid with defined boundaries and runs the same KIVA-3 code separately. Note that, in practice when a computational domain is decomposed over several processors, grid resolution is increased as high as possible to take advantage of each processor. In this example overall grid resolution was kept low for demonstration purposes only. An enlarged view of the overlapping face between adjacent subdomains (i.e., on Processors 0 and 1) is shown in Figure 4.4. The vertical arrows between subdomains illustrate the left/right faces where two way communication between

processors take place. KIVA-3 employs staggered grids, i.e., scalar quantities are at cell centers and vectorial quantities (U, V, W) are at the vertices. This configuration obliged the necessity of two distinct communication types to be created. The first one was for the cell-center based quantities and the second for the vertex based quantities. A more detailed illustration of various communication types among different processors can be found in Gel (1999).

After completing the insertion of all communication directives into the code, a rigorous debugging of the parallel version was necessary to make sure that all of the necessary variables are communicated at the appropriate locations and all the processors were behaving in a synchronized manner without any problem.

4.3.1 Benchmarking for Speedup

An important component of effective parallel computing is determining whether the program is running efficiently (i.e., how effectively is the processor being utilized), and how well it will perform if a large number of processors are used or how well it scales up. These issues are usually quantified by two important parameters in parallel computing.

$$\text{Speedup} = \text{SerTime}(n) / \text{ParTime}(n,p)$$

$$\text{Efficiency} = \text{SerTime}(n) / (p \bullet \text{ParTime}(n,p))$$

where SerTime(n) is the time of best serial algorithm to solve instance of a problem A of the size n on one processor. ParTime(n,p) is the time needed by a given parallel algorithm and given parallel architecture to solve an instance of problem A of size n, using p processors.

Note that $\text{SerTime}(n) \leq \text{ParTime}(n,1)$ and in general, one expects to have

$$0 \leq \text{Speedup} \leq p$$

$$0 \leq \text{Efficiency} \leq 1.0$$

In order to determine the efficiency of the distributed-memory implementation of KIVA-3 developed in this study, a series of benchmark runs with different size grids and total number of processors were carried out. All the runs presented in this section were conducted on a 112 processor SGI Origin 2000 system at Department of Defense's ERDC (formerly CEWES) Major Shared Resource Center at Vicksburg, MS. The runs performed for benchmarking purposes were

conducted for a pre-determined number of timesteps where the dependency of speedup trends on the number of timesteps were also investigated. It was determined that beyond 100 timesteps no significant difference in speedup trends was observed. Due to the significant overhead in setup phase in single processor runs, speedup and parallel efficiency figures were calculated first by including and then excluding the time elapsed in setup phase. Such a distinction was necessary due to the superlinear speedup behavior observed when setup phase time was included.

The first benchmark problem is the three-dimensional laminar channel flow at a Reynolds number Re=1,000 which was tested up to 48 processors with several grid resolutions starting from 250,000 vertices to 1,500,000 vertices, referred as 250K and 1500K grid, respectively. This problem was particularly selected for debugging purposes during the development of the parallel version and utilizes nearly 80 % of the subroutines, which was expected to give an idea about the overall performance. The results show that under favorable conditions with a simple problem like laminar channel flow, a speedup factor of 38 could be achieved with 48 processors for the 1500K grid case (see Figure 4.5) which corresponds to a parallel efficiency of 0.79. Note that the ratio of computational volume to communicated subdomain face area is an important factor in determining the optimal number of processors for a given grid size.

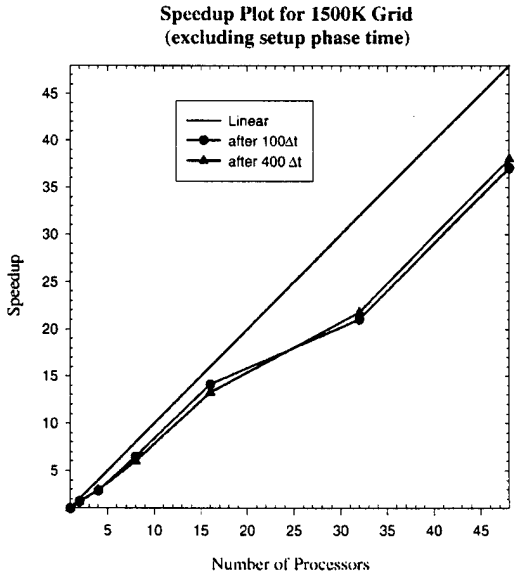

Figure 4.5 Speedup plot for 1500K cases based on excluding setup phase time.

The second problem was the turbulent round jet problem with an inlet velocity of 1500 cm/s and a diameter of 10 cm enters a three-dimensional rectangular domain through the left wall. This problem is the simplified version of the free swirling annular jet case (i.e., annular jet replaced with round jet without any swirl) studied by Smith et al. (1999a) on a single processor DEC Alpha machine with KIVA-3 up to 500,000 vertices. Benchmark tests up to 32 processors with a maximum grid resolution of 4,370,000 vertices were performed with KIVA-3/MPI (acronym for the present parallel version of KIVA-3). A Smagorinsky type subgrid-scale (SGS) model was facilitated during these simulations. Also an improved convection scheme combination was used by introducing a third option into KIVA-3 which simply selects a convection scheme based on central differencing for the convective terms in the momentum equations and Quasi-Second-order Upwind (QSOU) for the density and energy equations (Gel et al. (1998)). Up to 3 % grid stretching was employed in radial plane (y-z) to capture the core flow and maintain the second order spatial accuracy as close as possible.

Several preliminary large-scale runs over one million vertices were performed for the second and third cases at different grid resolutions. Table 4.3 shows the grid specifications, the total number of processors (PEs) employed, and the average CPU time required per each timestep of the simulation for the second case (i.e., turbulent round jet).

Table 4.3 CPU seconds per timestep for the preliminary production run

Grid Layout	Tot. Vertices	# PEs	CPU
160 x 80 x 80	1,089,288	16	32.0
160 x 80 x 80	1,089,288	32	17.0
208 x 100 x 100	2,184,840	16	62.0
288 x 122 x 122	4,370,000	32	130.0

Single processor KIVA-3 runs at these grid resolutions that are required for the calculation of the speedup and parallel efficiency for these cases could not be performed due to very long turn-around times. However, as seen from Table 4.3 for the first two cases, when the number of processors employed were doubled for the same size problem, the average CPU time per timestep nearly reduced in half which demonstrates a nearly linear speedup.

The third problem was the free swirling annular jet case studied by Smith et al. (1999a). An annular jet with an inner and outer radius of 2.7 cm and 5.3 cm, respectively, enters a three-dimensional rectangular domain from the left wall with an initial swirl velocity profile. Initial conditions were based on the measurements of Holzapfel (1996). Table 4.4 illustrates the speedup and parallel efficiency achieved for the 80 x 80 x 80 grid configuration up to 16 processors. Note that the numbers reported here are based on setup phase excluded timing. Other benchmark results can be found in Gel (1999), Gel & Celik (1999a, 1999b, 1999c).

Table 4.4 Speedup & Efficiency for 80 x 80 x 80 (500K) Grid

Number of PEs	Speedup	Efficiency
1	1.0	1.00
2	1.7	0.86
8	6.6	0.82
16	11.4	0.71

4.3.2 Hardware Improvements

As part of an effort to improve the local computational resources, a 20 node DEC Alpha cluster was built within our CFD Laboratory. Currently 12 nodes are active but the other nodes can be easily activated. Each compute node consists of 533 MHz DEC Alpha 21164 processor with 256 MB RAM, 8.3 GB harddisk, two DEC Tulip chipset based Kingston TX100 Fast Ethernet cards. The head node consists of the same configuration except that the memory is 512 MB and an additional ethernet card is installed for accessing the Beowulf cluster from outside networks to submit jobs. The operating system is the Red Hat Linux 5.2 with 2.0.35 kernel level. Each system is configured to boot standalone without the necessity of a keyboard, a mouse and a graphics card to be attached. The system configuration changes are performed through serial port where the I/O at the reboot is being forwarded. This configuration reduced the cost of each node significantly. In order to achieve a peak I/O throughput of 200 Mbit/s via channel bonding, the nodes were connected to each other through two 24 port Fast Ethernet switches.

Table 4.5 Speedup and Efficiency Comparison for 80 x 80 x 80 Grid

	No. of Processors	Speedup	Efficiency
Origin 2000	1	1.0	1.00
	2	1.7	0.86
	8	6.6	0.82
	16	11.4	0.71
Beowulf Cluster	1	1.0	1.00
	8	5.1	0.64
	10	6.0	0.60

Several benchmark runs were performed with the annular swirling jet test case using KIVA-3/MPI. Table 4.5 shows the speedup and efficiency figures this case. As seen in this table, the performance of the new Beowulf cluster is almost as good as SGI Origin 2000. Further details about the cluster configuration and the benchmark runs can be found in Gel & Celik (1999d).

Chapter 5: RANS Modeling and Turbulence Scales

As part of the objectives of this project the commonly used Reynolds averaged Navier-Stokes (RANS) turbulence models are studied and the results are assessed with regards to their performance for predicting mean flow and turbulence scales. This study has enhanced our understanding of the deficiencies of the RANS models and provided insight as to how they can be remedied. It was also important to establish the order of magnitudes of the turbulence length and time scales in relation to the engine geometry and speed to guide us in determining the minimum mesh and time resolution for LES. This section presents the important findings of our study concerning RANS models and turbulence scales as predicted by these models for IC engines. Detailed information can be found in the papers referenced.

5.1 Reynolds Averaged Navier-Stokes Models

The literature on applications of computational fluid dynamics (CFD) to internal combustion engines show that the turbulence model of choice widely utilized are of the two-equation models based on isotropic eddy viscosity concept (see Celik et al., 1999, for a review). However, there is little information in the common literature with regards to the validation and performance comparison for various models of this type. Our experience has been that these models do not give results consistent with each other when applied to realistic in-cylinder engine flows. It is found necessary to perform a comparative validation study among various models, which might benefit the CFD community involved with in-cylinder turbulent flow predictions.

The current understanding of turbulence phenomenon as it relates to combustion, engine performance, and pollutant emissions is far from being satisfactory. The combustion process, hence fuel efficiency and pollutant formation, (see e.g. Heywood, 1987) is greatly influenced by the turbulence generated during the intake stroke followed by the turbulence induced by the geometry of cylinder-piston assembly during the compression-expansion stroke. The control of the consequences of turbulence can only be possible with a well tested and validated turbulence model specifically tuned for IC engine applications.

There is an extensive amount of literature on RANS modeling for IC engines (Bo et al., 1997; Celik et al., 1992, 1997; Reitz and Rutland, 1991; Han et al., 1997; Ramos, 1989;

O'Rourke and Amsden, 1987; Bashay et al., 1986; Gosman, 1985). Most of the current computational studies utilize some version of the so-called k-ε turbulence model. Because of the multiple eddy structures and the strongly elliptic nature of the governing equations, low-order (i.e. zero-equation) models do not work well. Some studies use algebraic stress models (ASM), but the improvements over the k-ε model and its variants (e.g. low Reynolds number k-ε model; RNG k-ε, Lien and Leschziner, 1994, Han et al., 1996) are marginal and there is no consensus in the literature as to which model performs better. The isotropic eddy viscosity concept and gradient diffusion model, where the turbulent stresses are related solely to the local strain rates, are central to the k-ε model. It is well known (see e.g. Reynolds, 1980) that in most cases relevant to engine combustion chambers the above assumptions are not correct. Due to this fact, the performance of the k-ε model has not been fully successful, and the predictions are not as accurate as it is desirable; in some cases performance is very poor. The comparisons presented by Leschziner (1991), Celik et al. (1987), and Mongia et al. (1986), confirm the above arguments. The applications of second moment closure models (i.e. Reynolds stress transport-RST models) to IC-engines are scarce in the literature for the obvious reason that six additional non-linear partial differential equations must be modeled and solved. RST models were applied to engine-like geometries in a recent study by Yang et al. (1998). Although this study shows some promise it remains to be validated. This study also shows significant differences between k-ε and RST model results. Leschziner (1991) has demonstrated that while considerable improvement can be gained from second moment-closure, predictive performance is not consistently satisfactory. Hence the two-equation turbulence models remain the modelers choice in IC simulations, and their predictive capability need to be assessed.

In the present study, an isothermal, incompressible flow within a piston-cylinder arrangement (Morse et al., 1979; Haworth, 1998) motored without compression at 200 RPM is investigated (Yavuz and Celik, 1999a,b). The mean piston speed V_p was 40 cm/sec in these calculations. There was no swirl imposed. The seat angle was 60° with the horizontal axis. A time step of $1x10^{-5}$ seconds was used for time marching. A numerical mesh of 40,000 vertices was employed with a wedge angle of 0.5 degrees in the circumferential direction. The maximum cell size for the wedge calculations was 0.5x0.5 mm in the radial and axial direction inside the cylinder. The inlet pressure was atmospheric and the initial flow was at rest till the piston started

to move away from TDC (0° CA). Five models were considered, namely, (1) The standard k-ε model, the RNG-k-ε model, a low Re number k-ε model, a modified k-ε model for curvature effects (RNC-k-ε; see Yavuz and Celik, 1999a), and a new Smagorinsky based eddy viscosity (SEV; see Yavuz and Celik, 1999b) model. All of these were implemented into the KIVA code.

The predicted streamlines from the intake flow case are shown in Figure 5.1 as compared to the measurements of Morse et al., (1979). The results from all models compare well with the measurements in the overall sense. The RNG k-ε model solutions deviate more from the measurements in capturing the size of the lower wall recirculation zone. The Low-Re k-ε model performs slightly better in this regard, which is supported by the fact that the turbulent Reynolds number is low in such a flow.

In Figure 5.2 the axial velocity profiles are compared at various stations inside the cylinder. The standard k-ε model and the Low-Re model results are essentially the same and compare well with the measurements. The Low-Re model seems to improve the results near the wall (as expected) as well as in the vicinity of the reattachment point at the wall.

Then the flow field inside a typical piston-cylinder assembly (Catania et al., 1995) was simulated under motored conditions at 600 RPM, which implies a mean piston speed V_p =150 cm/sec. A numerical mesh of 20,000 vertices was used with a wedge angle of 0.5 degrees in the circumferential direction. The maximum cell size for the wedge calculations was 0.6x0.9 mm in the radial and axial direction. As reported by Celik and Yavuz (1997), the minimum integral length scale occurs at the end of the compression stroke in the order of squish clearance height. To investigate grid dependency another mesh with 70000 vertices was used for the same case, which provided approximately the same results in the mean flow for the standard k-ε model.

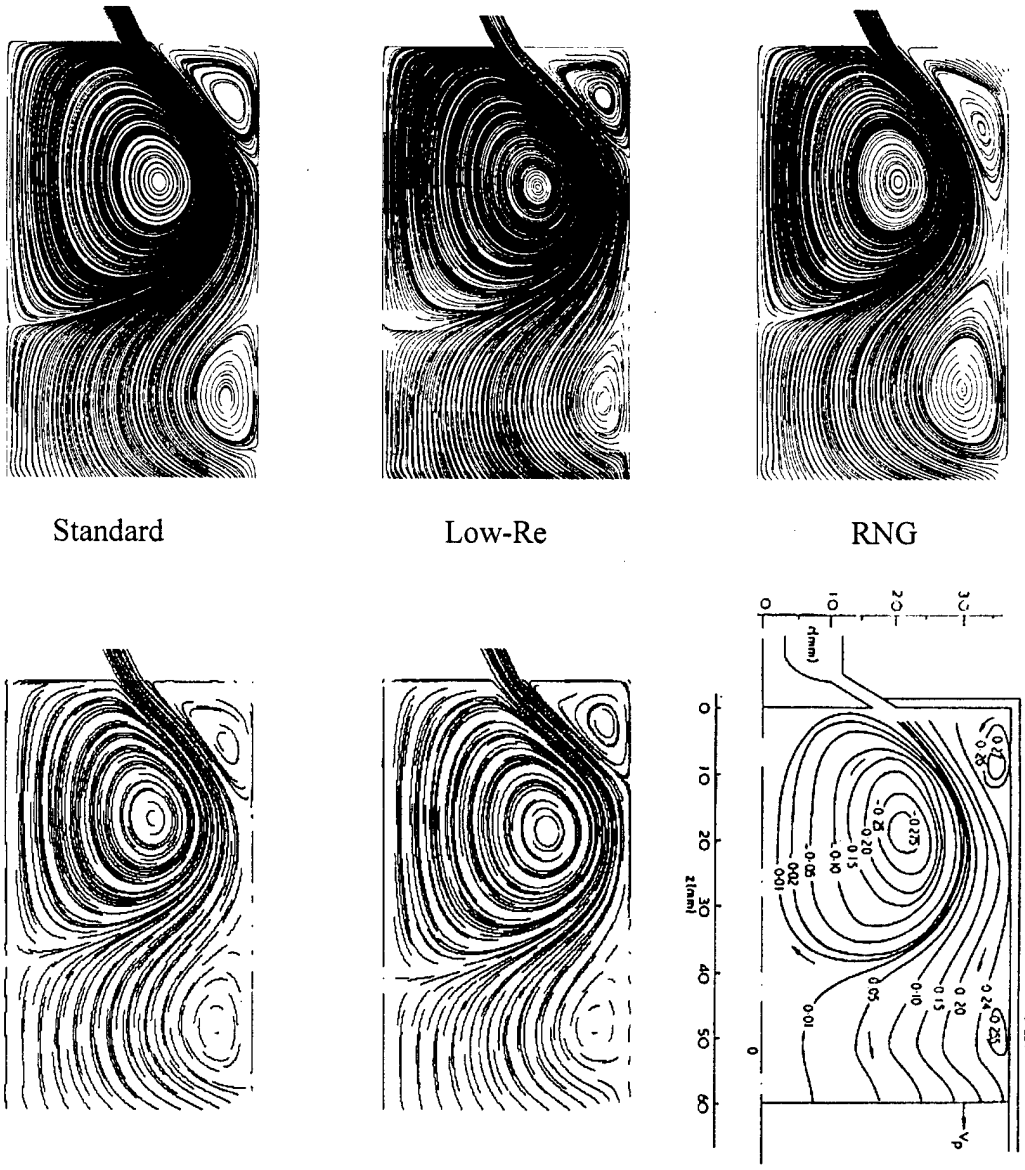

Figure 5.1 Streamlines of the intake case at 90° CA (Yavuz and Celik, 1999a, 1999b)

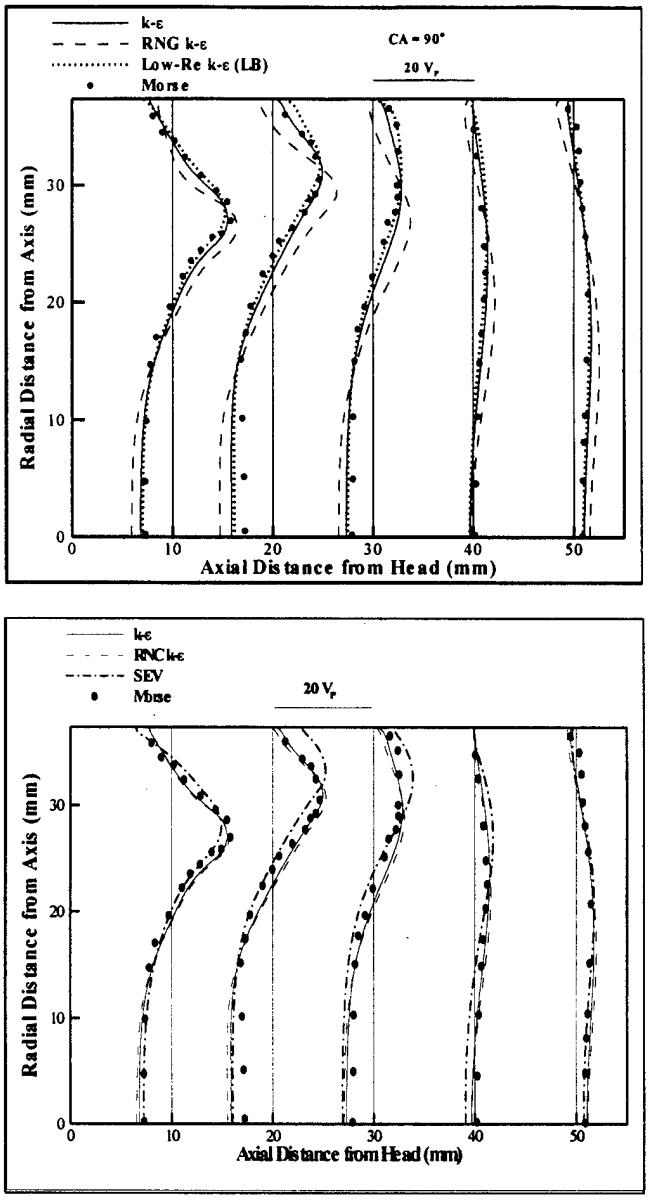

Figure 5.2 Profiles of axial velocity at 90° CA (Yavuz and Celik, 1999a, 1999b)

The results of the standard k-ε and RNG k-ε models are compared the piston-bowl assembly (Figure 5.3). While no significant differences were observed in the intake flow case, solutions for the piston-bowl assembly are drastically different at some crank angles. That again raises the question, if these models are applicable to IC-engine flows at all speeds and operating conditions? Even if they both predict good results for one case, they could predict significantly different results for other cases, which immediately challenges the validity of the solution.

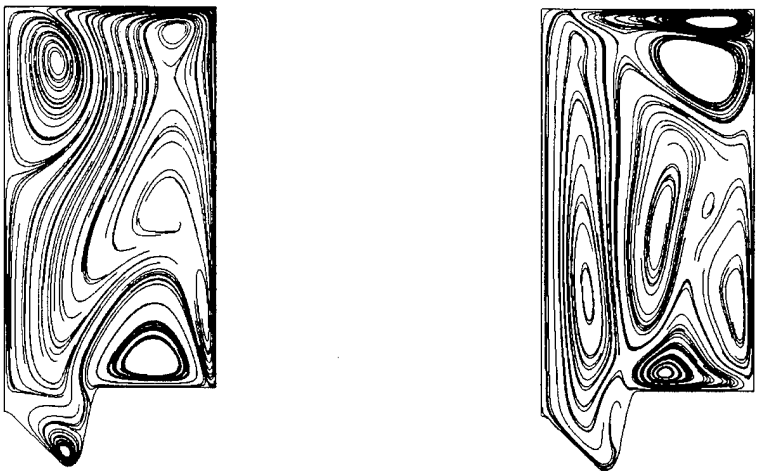

Figure 5.3 Streamlines for the piston-bowl case at 90° CA (Yavuz and Celik, 1999a, 1999b)

In general all of these models do a reasonably good job in predicting the main features of the mean flow during the intake stroke when the valve is not moving and the piston speed is low. Detailed quantitative comparisons revealed that the Low-Re model and the RNC k-ε (with curvature correction) model seems to perform the best, with an appreciable improvement near the walls for the case where the relatively low turbulence Reynolds numbers were observed. In this case the RNG k-ε model performs worse than the standard k-ε model contrary to our expectation. Perhaps a low Reynolds number version of this model would perform better. The SEV model has the potential to predict the physics of this flow better, provided that the characteristic length scale is calculated dynamically, including all the relevant scales of the engine, and the distance from the wall. Such a model is currently under investigation by the authors. However, although the mean flow predictions are reasonably good, the turbulence intensity predictions do not compare well with the experimental data, which would show the real performance of a turbulence model. An improved version of this model is being developed as a hybrid Smagorinsky turbulence model, which is used for flow predictions ranging from RANS to LES automatically depending on the grid size. Further information can be found in Yavuz (2000).

As for the case of the piston-bowl assembly with closed valves (i.e. compression and expansion stroke) the two models (standard k-ε and RNG k-ε) produce drastically different results, even though their performance was very similar in the case with intake flow. Unfortunately, the resolution of this unexpected behavior requires more validation studies at

higher engine speeds and analysis of the results from several engine cycles against a reliable set of experimental data. It seems that for IC flows transient effects are very important and the turbulence models need to be tested against a good time-dependent (in the mean) benchmark case.

5.2 Turbulence Scales

There is extensive amount of information available in the literature concerning turbulence intensity, length scales and turbulence in general. However this information which come from discrete experiments which are engine or problem specific, have rarely been assessed together under the realm of theory and engine simulations using turbulence models. We have reviewed only the most relevant literature (see Celik and Yavuz, 1997). Here we present a summary of our findings.

The relevant length and time scales pertaining to both the geometry and to turbulence are reviewed by Reynolds (1980) and Heywood (1987), and computed by Shah and Markatos (1986). The length scales exhibit a wide spectrum of sizes from the size of the combustion chamber down to the Kolmogorov microscale. In between are the thickness of the wall boundary layers, the width of the intake jet, the integral length scale of turbulence, and the Taylor microscale as relevant length scales which must be considered. The important time scales include the integral time scale of turbulence, large eddy turnover time, the flow-pass time (a measure of time required for a fast moving fluid eddy to travel the length of the shear layer), and development time (time required for a boundary layer to reach equilibrium). Since burning occurs at the smallest scales, it is desirable that these scales are either resolved or modeled (e.g. via sub-grid scale models) to accurately predict the flame structure and propagation. The time scale associated with the smallest eddies is the Kolmogorov time scale ($=(\nu/\varepsilon)^{1/2}$, ν being the kinematic viscosity, and ε the dissipation rate of turbulent kinetic energy, k).

Heywood (1987) presents a review of the turbulence length and time scales in IC engines which is summarized in Table 5.1. An important information pertaining to the length scales in engines is that the maximum wall boundary layer thickness on the cylinder head and piston surfaces could be as high as 5 mm at moderate engine speeds. The flow regimes inside the boundary layer as well as the main vortex motion inside the cylinder can be characterized by a

Reynolds number defined as $Re = V_p L/\nu$; where V_p is the mean piston speed, L is the stroke, and ν is the kinematic viscosity.

Table 5.1 Estimated length and time scales for an automotive size engine at 1000 RPM

	Estimated Value	Process, location	Comments
l_I	10.0 mm	During intake	scales with valve lift
l_I (min)	2.0-5.0 mm	end of compression	scales with clearance height, varies little with engine speed
l_T	1.0 mm	end of compression	varies little with engine speed
l_K	0.01 mm	end of compression	
τ_I	1.0 ms	end of compression	decreases with engine speed
τ_T	0.1 ms	end of compression	decreases with engine speed

Notation: l_I = Integral length scale ; l_T = Taylor micro length-scale; l_K = Kolmogorov length scale; $\tau\backslash_I$ = Integral time scale; τ_T = Taylor micro time-scale

Fraser et al. (1986) presents direct measurements of lateral integral length scale (Figure 5.4) using laser Doppler velocimetry (LDV). This length scale ranges between 2 to 3.5 mm for crank angles between 320 to 380 degrees ATDC with a local minimum at the TDC. When the same data is normalized by the instantaneous clearance height the non-dimensional value increases from 0.1 to 0.2 at TDC and remains approximately fixed after that. Lancaster's measurements agree with those by various other authors within a factor of two. The previous work reviewed by Lancaster along with his work seem to indicate that the relative integral length scale of turbulence should be function of the engine speed, swirl ratio, and compression ratio. He also points out that the longitudinal and lateral length scales could be significantly different; for homogeneous, isotropic turbulence.

Recently, Corcione et al. (1990) presented results from direct measurements of lateral length scale inside the combustion chamber of a diesel engine during the compression stroke at 600 and 1000 RPM. They calculate indirectly the lateral length scale using Taylor's hypothesis, however due to the uncertainty involved in this analysis we only consider the direct measurements. Their correlation coefficients are also of the form of Equation (1). The measured

lateral length scales were in the order of 1 to 2.5 mm and decreases during the compression stroke (330 to 370 degree crank angles). These authors showed that the cylinder geometry had a significant influence on turbulence length scales.

Detailed measurements of root mean square (rms) turbulent velocity fluctuations using a state-of-the-art LDV system are reported by Arcoumanis et al. (1994) for a 1.9 liter direct injection (DI) diesel engine. The rms values of the swirl velocity fluctuations are very high (about 4Vp, Vp being the mean piston speed) during the intake due to counter-rotating jets, they decay to about 1Vp near the BDC. The rms axial velocity fluctuations attain peak values of about 4Vp during early induction. Both swirl and axial velocity fluctuations show as much as three fold spatial variation with radial position at a dimensionless distance x/S = 0.1 (here x is the axial distance and S is the stroke) from the cylinder head indicating that the turbulence is strongly non-homogeneous.

Figure 5.4 compares some results from our own computations (Celik and Yavuz, 1997) for an axisymmetric flow during the compression and expansion stroke of a typical IC engine. The results indicate that the standard k-ε model does seem to give the right orders of magnitude and even the right trends for the turbulence velocity and length scales. Needless to say that this model assumes local isotropy, hence it can not predict the usually observed non-isotropic distribution of turbulence, especially during the intake and exhaust strokes. The flow during compression and expansion strokes is known to be nearly isotropic.

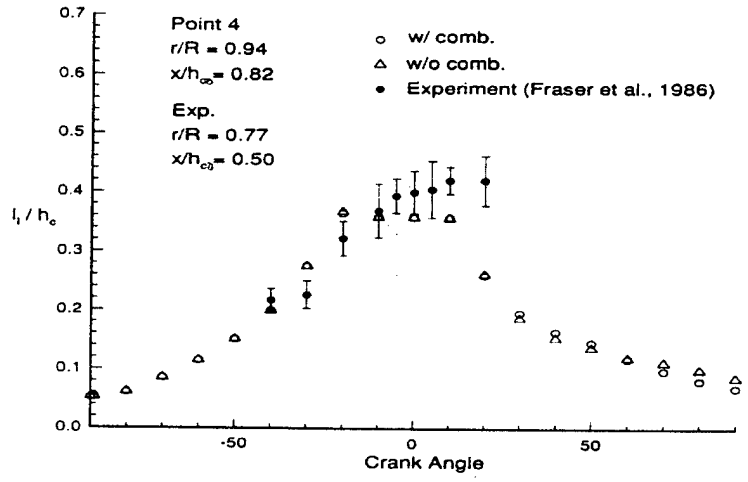

Figure 5.4 Comparison of calculated (Celik and Yavuz, 1997) dimensionless integral length scale with experiment (Fraser et al., 1986)

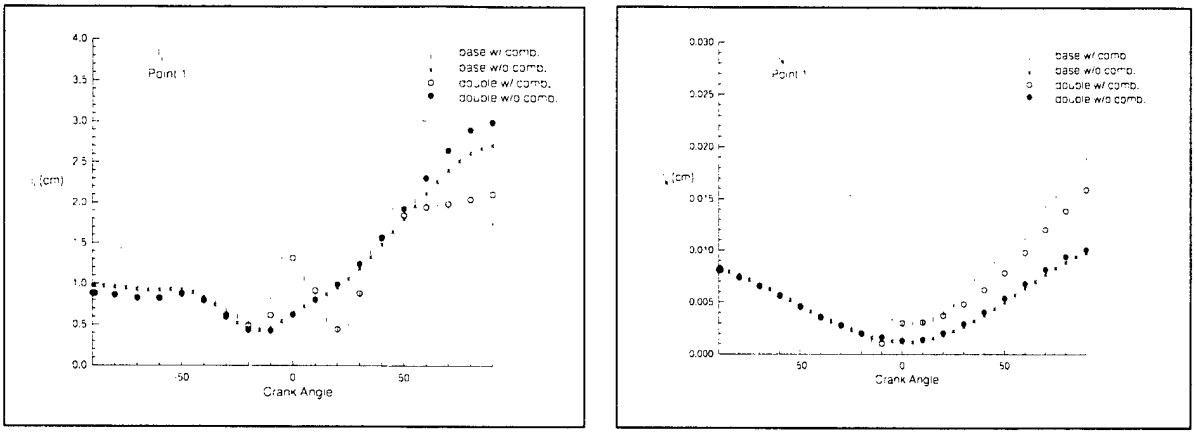

Figure 5.5 Integral and Kolmogorov length scales inside an IC-Engine (Celik and Yavuz, 1997) with and without combustion.

The computational results further indicate (Figure 5.5.) that the turbulence intensity is very sensitive, but the integral length scale is not as much sensitive to combustion. Interestingly, the Taylor and Kolmogorov length scales are sensitive to combustion, and this influence manifests itself with a considerable lag with respect to the increase in temperature.

The minimum length scales (integral, Taylor, and Kolmogorov) are predicted near the TDC, and are 1 to 5 mm, 0.05 mm, and 0.01 mm, respectively, which are in good agreement with experimental observations. In this regard the k-ε can be used as a guide to determine computational strategies for fine grid LES simulations. It seems that it would be logical to isolate the zone near top dead center and use many more spatial grid nodes in this zone as compared to other zones with accurate interpolation and/or extrapolation to continue the computations elsewhere.

Chapter 6: Development and Application of A Subgrid-Scale PDF Combustion Model

6.1 Background

In this chapter the development and application of a subgrid scale combustion model to be used for Large Eddy Simulation studies is presented. The theoretical basis of the model is described first. Then, the model capabilities are demonstrated by comparing the combustion predictions to some available experimental benchmark cases. Because most of the experimental measurements are available as time averaged or as Favre averaged quantities direct validation of instantaneous computations is not possible. However, predictions of instantaneous temperature in a two-dimensional model will be presented to demonstrate the capabilities of the proposed model. Before going into the explanation of the model development, we will present first the development of some auxiliary studies and computations that were initially conducted to investigate the capabilities of Kiva-3 code to be used in Large Eddy Simulation studies.

6.2 Large Eddy Simulation of a Round Turbulent Free Jet

This investigation is aimed at research in the large eddy simulation (LES) of a passive scalar mixing problem using Kiva-3 code. The preliminary simulation performed here is for a free round turbulent jet of methane. The jet is at Reynolds number, Re = 2000 and it is discharging into stagnant air. This small Re is chosen in order to be able to resolve the basic features of free jet turbulence using the available workstation computer power. The computations are started from the near orifice field with uniform initial turbulence intensity and length scales. No subgrid eddy viscosity models has been used as the subgrid dissipation is achieved through numerical truncation errors. The convection terms are discretized by a hybrid scheme with 10% upwinding (i.e. first order) and 90% central differencing. The second order (Crank Niclson) temporal discretization scheme is used for the pressure gradient and diffusion terms. The convection terms are discretized by a first order accurate scheme in time.

The all-Mach number formulation employed in Kiva-3 allows the use of this compressible flow code to simulate the weakly compressible conditions by employing the proper

pressure gradient scaling. The time step is limited by courant stability requirements and it is in the order of 10^{-6} seconds. The computational domain in radial and azimuthal directions is five orifice diameter (d) while in axial direction it is 20d. Outlet flow boundary conditions with allowance for flow reversal are assigned to the surrounding of the jet. This choice for the boundary conditions is based on the code limitations rather than representing the actual situation. The initial instability was introduced into the computations by perturbing the axial velocity randomly by 20% to simulate fluctuations due to turbulence in the nozzle. In the latter stages of the computations this artificial forcing is removed to see whether the computed flow instabilities could be self-sustained.

The computations are continued several flow-through times which is defined as $t_f = L/U_0$, where L is the length of the domain and U_0 is the mean flow bulk velocity. Figure 6.1 shows the transition from the inviscid potential core to the chaotic turbulent structure to occur at approximately 3-4d downstream of the jet inlet. At the early stages in the computations ($t < t_f$) this location is strongly affected by the development of the large-scale structures in downstream locations (Grinsten, et al., 1987). It is known that the near-field of the free jet is also affected by the large-scale structures which form in the annular region between the jet and the surroundings as a result of the shear layer instability (Gladnick, et al., 1990). This feedback process from organized large eddies affects the shear layer ahead of the nozzle for times less than the flow-through time and continues to do so after several flow-through times. This feedback is also reflected in the decrease of the time step, which is computed dynamically from Courant number limitations during computations. In the computations, for reason of numerical accuracy (and stability) the Courant number is set to 0.1 of its maximum value. The details of these simulations can be found in Amin et al., (1998a).

Figures 6.1 and 6.2 show the sequential unsteady events captured with Kiva-3 computations. The captured flow events such as transition from laminar to turbulent flow, vortex pairing and breakdown, and shear layer instability are in good agreement with Frankel et al.'s (1993) computations.

The round jet simulations show that the difference schemes might have an important influence over the ability of the computed flow instabilities to persist. The use of the flux limiting scheme known as Quasi Second Order Upwinding (QSOU), although it approaches

second order accuracy, may lead to disappearance of the diffusive wiggles. Thus the flow instabilities will not be able to persist. Higher grid resolution may require introduction of artificial eddy viscosity or changes in the properties of the advection scheme in order to maintain computational stability.

6.3 Probability Density Function Model Development

In mixing limited combustion the rate of reaction is determined by the mixing frequency between the fuel and oxidizer eddies. The use of conventional RANS techniques fails to directly capture the dynamics of mixing-controlling eddies. With the use of Large Eddy Simulation (LES) technique we are able to describe accurately the large scale mixing process while the small scales are left to be modeled. Extension of LES techniques devised for isothermal turbulence to combustion problems is not trivial. This is because of the fact that chemical reactions occur within thin zones much smaller than the grid scale. Therefore knowledge of the reactants distribution in the grid cell is an important perquisite. One strategy to account for the strong non-linear reactant distribution within the grid cell is to employ a probability density function (pdf) for the mixing process.

In this section we will present the development of a pdf model for combustion of direct injection diesel engines which are characterized by mixing limited reactions.

6.3.1 Filtered mixture fraction and concentration fluctuations

The transport of a filtered mixture fraction, ξ, field can be described by the following equation.

$$\frac{\partial(\rho\xi)}{\partial t}+\frac{\partial(\rho v_\alpha \xi)}{\partial x_j}-\frac{\partial}{\partial x_j}\left[\frac{\mu_t}{\sigma_\xi}\frac{\partial \xi}{\partial x_j}\right]=0 \qquad (6.1)$$

Where v and x are the velocity and position in α space coordinate direction (α=1,2,3), μ_t is the turbulent eddy viscosity and σ_ξ is the turbulent Schmidt number for ξ. To be able to describe the statistics of the subgrid-scale scalar fluctuations a model for the Probability Density Function (pdf) of the scalar has to be found. One of the most commonly used approaches is to assume the shape of the pdf and then determine the first two statistical moments of the

distribution from modeled transport equations (e.g. Bilger, 1976, Amin and Celik (1999b). The transport equation of the second statistical moment can determined from a modeled SGS concentration fluctuations can be written as (Spalding, 1971);

$$\frac{\partial(\rho g)}{\partial t}+\frac{\partial(\rho v_j g)}{\partial x_j}-\frac{\partial}{\partial x_j}\left[\frac{\mu_t}{\sigma_g}\frac{\partial g}{\partial x_j}\right]=C_{g1}\mu_t\left[\frac{\partial \xi}{\partial x_j}\right]^2-C_{g2}\rho g\varepsilon/k \qquad (6.2)$$

The numerical values of the constants in the above equations are listed in Table 6.1. In the subsequent analysis we follow a one-equation model approach in which k is determined form a modeled equation and ε is determined form a prescribed grid dependent length scale.

Table 6.1 Values of constants in the k-ε-g model of turbulence.

C_{g1}	C_{g2}	σ_ξ	σ_g
2.8	1.84	0.7	0.7

6.3.2 The large eddy probability density function

The large eddy probability density function (pdf) gives a distribution of mixing frequencies and therefore we are not restricted to a single mixing frequency as in the case of conventional time averaging techniques. In the past many experimental studies have been conducted to determine the most appropriate pdf shape to represent the grid cell mixing process. Various pdf shapes that can be found in typical flows are discussed by (Bilger, 1989). The most commonly used pdf forms are the Gaussian (Lockwood and Naguib, 1975), the Beta function (Jancika and Kollman, 1978) and the Dirac-Delta functions (Khalil, et al, 1975). The use of the Clipped Gaussian pdf is justified on the bases of experimental observations and Direct Numerical Simulation (DNS) data. These studies indicate that the passive scalar pdf at the final stages of mixing is relaxed to a Gaussian distribution. However, the initial stages of mixing, which can be approximated by a Double Delta function, cannot be well represented by assuming a fixed Gaussian form for the pdf throughout the mixing process. Beta function seems to be able to better represent the different mixing stages including the bimodal distribution. In addition, it has the potential for extension to multiple scalar mixing (Girimaji, 1991). It has been also used

in many previous LES studies (e.g. Cook and Riley, 1994). The p (ξ) is assumed here to follow a Beta function distribution which is given by;

$$p(\xi, x) = \frac{\xi^{(\alpha-1)}(1-\xi)^{(\beta-1)}}{\int_0^1 \xi^{(\alpha-1)}(1-\xi)^{(\beta-1)} d\xi} \tag{6.3}$$

The exponents α and β are related to the Favre filtered mixture fraction and the subgrid-scale variance of the turbulent part of the composite pdf.

$$\alpha = \tilde{\xi}\left[\frac{\tilde{\xi}(1-\tilde{\xi})}{g} - 1\right] \tag{6.4}$$

$$\beta = \alpha(1-\tilde{\xi})/\tilde{\xi} \tag{6.5}$$

Thus, the filtered density can be determined from;

$$\overline{\rho}(x) = \int_0^1 \rho(\xi) P(\xi, x) d\xi \tag{6.6}$$

6.3.3 Large eddy species mass fraction and reaction rate

Two of the main objectives of LES of reacting flows are the determination of Large Eddy Mass Fraction (LEMF) and Large Eddy Reaction Rate (LERR). The LEMF can be determined from

$$\tilde{Y}_i = \frac{1}{\overline{\rho}} \int_0^1 Y_i(\xi) P(\xi) d\xi \tag{6.7}$$

Similarly the LERR can be obtained from

$$\tilde{w}_i = \frac{1}{\overline{\rho}} \int_0^1 w_i(\xi) P(\xi) d\xi \tag{6.8}$$

In the above equations the relationships Y_i (ξ) and w_i (ξ) are thermo-chemical state-relationships obtained from the fuel/oxidizer reaction chemistry.

Because of the inherent difficulty in obtaining the thermo-chemical state-relationships as a function of local mixing intensity and other external factors (e.g. varying pressure conditions,

radiative heat loss, turbulence/radiation interaction) integration of expressions 6.7 and 6.8 could represent a demanding computational effort. Therefore a more simplified, yet accurate approach seems to be in favor for the 3-D modeling of engines combustion chambers. In the next section we present the development and application of a simplified model to determine the large eddy reaction rate which is originated from the commonly used Eddy Breakup Model (EBU). This model is widely used by the combustion modeling community in general and the Kiva code users in particular.

6.4 A Modified Eddy Breakup Model For Turbulent Combustion Modeling in Diesel Engines

In this section we present an application of a modified form of the Eddy Breakup (EBU) turbulent combustion model originally developed by Brian Spalding of the Imperial College more than two decades ago. The later modifications allows the EBU model coefficient to be dynamically linked to the flame surface. This link is achieved through the use of a Conditional Probability Density Function (CPDF). The application of the model is not computationally intensive and can be easily incorporated in multidimensional CFD codes like Kiva-3. This makes it suitable to be used as a subgrid-scale turbulence/chemistry interaction model for large eddy simulation of turbulent combustion in diesel engines. The application of the modified EBU model to the case a D. I. diesel engine using KIVA III has shown the importance of this modification in modeling of chemistry/turbulence interaction for I.C. engines (Amin et al., 1998b).

In the present analysis we will follow the approach of Bilger and coworkers in modifying the EBU coefficient. Consider the case of a single step overall heat releasing reaction of the form;

$$\nu_F F + \nu_O O \rightarrow \nu_p P \tag{6.9}$$

Where F, O, and P denote fuel, oxidizer and product, respectively. The coefficient ν_i is the stoichiometric coefficient for species i. The stoichiometric oxidizer/fuel ratio, r, can be then computed from the following relation;

$$r = \frac{\nu_O W_O}{\nu_F W_F} \tag{6.10}$$

In the above expression W_i is the molecular weight of species i.

The average rate of diffusion flame burning in the EBU model is expressed as;

$$\tilde{\dot{\omega}} = A\bar{\rho}\tilde{Y}_{min}\tilde{\varepsilon}/\tilde{k} \tag{6.11}$$

The over-bars indicate ensemble averaging, and tilde indicates a density-weighted filtered reaction rates. The symbols ρ, k, and ε, are the filtered mixture-density, the kinetic energy of turbulence, and its dissipation rate respectively. In the above formulation Y_{min} stands for the minimum of the reactant concentrations;

$$Y_{min} = \min(Y_F, Y_O/r) \tag{6.12}$$

In expression 6.11 A is the model coefficient and is taken here to be 5.0. It should be noted however that a wide range of values exists for this coefficient (typically in the range 1.0 to 7.0). This can be helpful sometimes to tune the computed results to that observed experimentally. However, in the present investigation we are following Bilger's approach to determine the value of this coefficient as a function of the mixing characteristic in the engine. We define the mixture fraction (ξ) which is related to the stoichiometry of the reaction by;

$$\xi = \frac{1}{r+1} \tag{6.13}$$

In the detailed analysis shown by Bilger (1976a&b) the mean reaction rate can be written as;

$$\tilde{\dot{\omega}} = -\frac{1}{2}\rho_{st}\tilde{Y}_B\tilde{\chi}_{st}P_\xi(\xi_{st}) \tag{6.14}$$

In the above expression

$$\tilde{Y}_B = Y_{f,1}/(1-\xi_{st}) = Y_{o,2}/r\xi_{st} \tag{6.15}$$

Where ξ_{st} is the stoichiometric mixture fraction, $Y_{f,1}$ is the fuel mass fraction in the fuel stream (in our case it is equal to unity), $Y_{o,2}$ is the oxidizer mass fraction in the air stream (=

0.232 for O_2 in air), and ρ_{st} is the mixture density of the stoichiometric composition. The quantity χ_{st} is the mean scalar dissipation rate evaluated at the flame sheet and is equal to (e.g. Bilger, 1976a&b);

$$\tilde{\chi}_{st} = 2\frac{\mu_{eff}}{Pr_g}\left(\nabla\tilde{\xi}\right)^2 \tag{6.16}$$

Where μ_{eff} is the effective viscosity, Pr_g is the Prandtl number of the concentration fluctuations (≈ 0.7) and $\nabla\xi$ is the spatial gradient of the filtered mixture fraction. The mean scalar dissipation rate is an important quantity that is related to the degree of species mixing in the flowfield and determines the status of combustion completeness in the combustor (Peters, 1984). The final quantity in the previous expression for mean reaction rate (P_ξ), is the probability density function (pdf) for the mixture fraction ξ. The assumed shape of the pdf has been defined previously in expression 6.3-6.5.

In order to evaluate the filtered square of the concentration fluctuations, g; A transport equation can be solved for this quantity (Spalding, 1971), however we chose here to simplify the analysis by assuming that the local value of filtered g can be evaluated by the equilibrium between production and dissipation of the concentration fluctuations. Thus the local value of g can be computed from the following algebraic expression;

$$\tilde{g} = C_g\frac{\tilde{k}^3.\left(\nabla\tilde{\xi}\right)^2}{\tilde{\varepsilon}^2} \tag{6.17}$$

Where C_g is a constant of order 0.1. Computing g this way will give a good approximation to the level of concentration fluctuations without having to solve a separate transport equation. This simplification reduces the computational cost especially in demanding applications of LES modeling of turbulent reacting flows. To evaluate k and ε; a transport equation can be solved for k while ε can be computed using a prescribed length scale. The large eddy reaction rates computed by the above expressions were coded and linked to the Kiva-3 code.

The coefficient A is computed dynamically during the solution procedure by equating the large eddy rate expression 6.11 and 6.14. The dynamical value of this coefficient is termed here

as A_d. The large eddy reaction rates computed from Expression 6.3 and 6.6 will be called here $\tilde{\dot{\omega}}_{pdf}$ and $\tilde{\dot{\omega}}_{EBU}$ respectively.

$$A_d = A\frac{\tilde{\dot{\omega}}_{pdf}}{\tilde{\dot{\omega}}_{EBU}} \tag{6.18}$$

Thus the coefficient A_d is equal to;

$$A_d = \frac{1}{2}\rho_{st}\frac{\tilde{Y}_B\tilde{\chi}_{st}}{\tilde{\rho}\tilde{Y}_{min}\,\varepsilon/k}\tilde{g}P_\xi(\xi_{st}) \tag{6.19}$$

Where the ratio between the large eddy mass fractions $\frac{\tilde{Y}_{min}}{\tilde{Y}_B}$ can be expressed as (Bilger; 1989);

$$\frac{\tilde{Y}_{min}}{\tilde{Y}_B} = J_1(z_{st})\sqrt{\tilde{g}} \tag{6.20}$$

Here we make an assumption based on the experimental data given by Mudford & Bilger (1987), for the function J_1 as;

$$J_1(Z_{st}) = 0.45\exp(|-z_{st}|) \tag{6.21}$$

And Z_{st} is defined as;

$$Z_{st} = \frac{\xi_{st} - \tilde{\xi}}{\tilde{g}} \tag{6.22}$$

After some manipulation this leads to the following expression for the dynamic coefficient A_d;

$$A_d = \frac{\rho_{st}}{\tilde{\rho}}\frac{P_\xi(\xi_s)}{J_1(Z_{st})} \tag{6.23}$$

The above value of A_d is used in the present subgrid-scale modeling of turbulent combustion in a diesel engine configuration.

6.5 Validation of the PDF model in RANS jet mixing studies

Before we use the developed pdf model in LES of reacting flow in diesel engine geometry we conducted some validation numerical experiments and compared the computations with some published measurements of the pdf in free jet mixing of propane and air. This test case was studied experimentally at SANDIA National Lab. The key parameters are listed in Table 6.2. The comparison between the predictions of the assumed pdf shape is shown in Figs. 6.4-6.7. The variation in calculated pdf along the jet centerline (i.e. Y/D = 0.0) in the initial mixing region (X/D =3.08) is shown in Fig. 6.4. The measured pdf is more biased towards the fuel side and the computed pdf at this location is flatter and wider than measurements. This indicates that some degree of mixing is achieved at this location (i.e. a faster jet decay is predicted). Further downstream, (at X/D = 24.78) the experimental pdf shows a clear Gaussian-like distribution and slightly over-predicting the propane/air mixing (Fig. 6.5). Figures 6.6 and 6.7 compare the evolution of the pdf at two different axial locations (X/D=15, X/D=50) and the same radial location of Y/D = 0.55. Again the predicted pdf seems to overestimate the mixing at small axial distances while further downstream the comparison between the predicted and measured pdf is satisfactory. In the mixing region the distribution is bimodal and consists of a contribution from both the unmixed air and mixed propane and air. Outside the mixing region the assumed pdf could not simulate the spiked nature of mixing profile and severely underestimates the fluctuations level (pdf width).

Table 6.2 Test section dimensions and inlet conditions for propane/air jet mixing case of SANDIA.

Test Section	.30 m x .30 m
Jet Tube Exit Diameter	0.052 m (I.D.), 0.09 m (O.D.)
Jet velocity (Bulk)	53 m/s
Co-flow Air Velocity	9.2 m/s
Reynolds Number (based on jet exit diameter)	68,000
Co-flow Air Turbulence	0.4%
Axial Pressure Gradient	6 Pa/m

6.6 Application of the developed pdf model in combustion simulation in diesel engines

In this section we will present an application of the developed pdf in LES of the diesel engine case of Aoyagi (1980) et al., the simulated cylinder and piston configuration listed in Table 6.3. A two-dimensional fine grid computational mesh composed of 80 nodes in x direction and 250 nodes in z direction is used. The advection scheme accuracy and time accuracy is similar to the ones used for the free jet simulation in section 6.2. The k-ε sgs turbulence model was used in this simulation.

To start with suitable initial condition for the engine flow simulation, a complete isothermal (motored) engine cycle have been simulated first

The computations show the development of turbulence in the compression and expansion strokes (Figures 6.8-6.9). These figures indicate the chaotic nature of the turbulent flow with various eddy sizes distributed non-homogeneously throughout the cylinder and show great variations with time. The turbulence generation did not die out as a result of compression near TDC. As the piston moves upward the maximum length scale reduced from 1.5 mm at –44 deg. ATDC to 0.1 mm at –13 deg. ATDC. The velocity vector contours show that eddies of different recirculation strength is found near the edge and corner of the piston walls. During expansion the strength of the recirculating eddies did not die-out and disappear. In fact, the velocity magnitudes show extensive localized recirculation in different parts of the computational domain. During the expansion stroke the turbulence intensity is sustained and vorticial strength increases. At the BDC position (i.e. 180 deg.) the contours of the subgrid kinetic energy of turbulence shows the different eddies swept by the expansion down to the BDC. The velocity contours at 315 deg, which is just before the onset of injection starts indicated that the flow is quite turbulent and a random initial flow field could be successfully established. Figure 6.10 shows the instantaneous radial velocity at a point near the cylinder head. The temperature variation at the same point is depicted in Figure 6.11. Near the TDC the mean Radial velocity increased but the fluctuations did not die out. In fact the turbulent fluctuations intensity seemed to be sustained after compression even without the presence of the initial turbulence introduced by the valve motion in the conventional engine geometry. The increase in mean temperature near the onset of ignition is observed also in these figures. Figure 6.10 shows large-scale variations in

temperature as an indication of unsteady flame propagation. At about 355° CA the flame edge sweeps through this particular point, then at about 15° CA the main flame front arrives. The increase in velocity fluctuations as a result of combustion is noteworthy.

Table 6.3 Specification of the simulated engine, Aoyagi et al. (1980)

Bore (mm)	95
Stroke (mm)	110
Compression ratio	14.6
Squish (mm)	0.9
Diameter of piston bowl (mm)	72
Height of piston bowl (mm)	11.5
Fuel	Gas oil
Fuel density (at 15 de. C.)	0.849
Fuel cetane number	57
Number of injector nozzle holes	4
Hole diameter (mm)	2
Injection angle (deg.)	150
Nozzle opening pressure (MPa)	17
Injection starts (°ATDC)	-15
Fueling rate (mm3/cycle/cylinder)	39
RPM	1250
Swirl Ratio	0

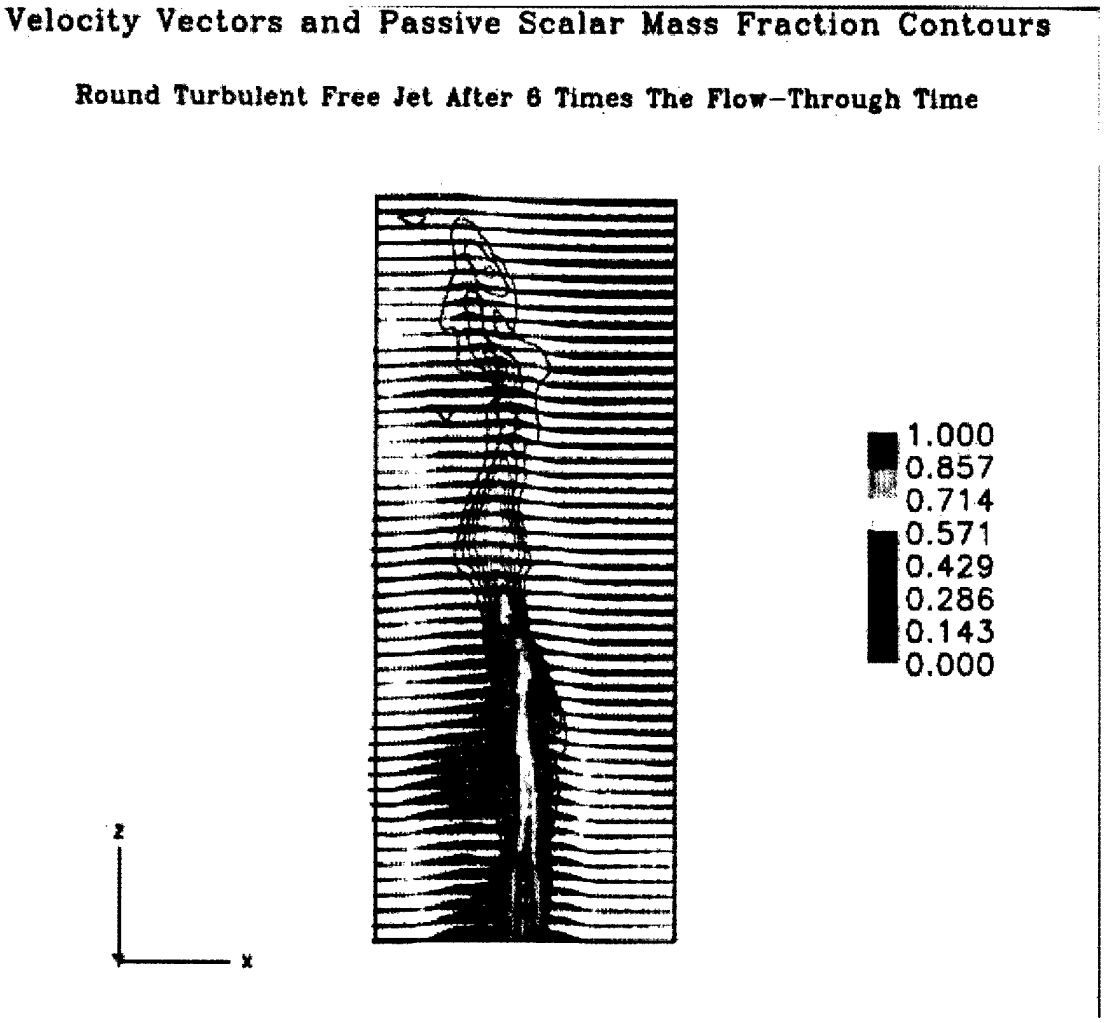

Figure 6.1 Intantaneous contours of passive scalar mass fraction in a round turbulent free jet.

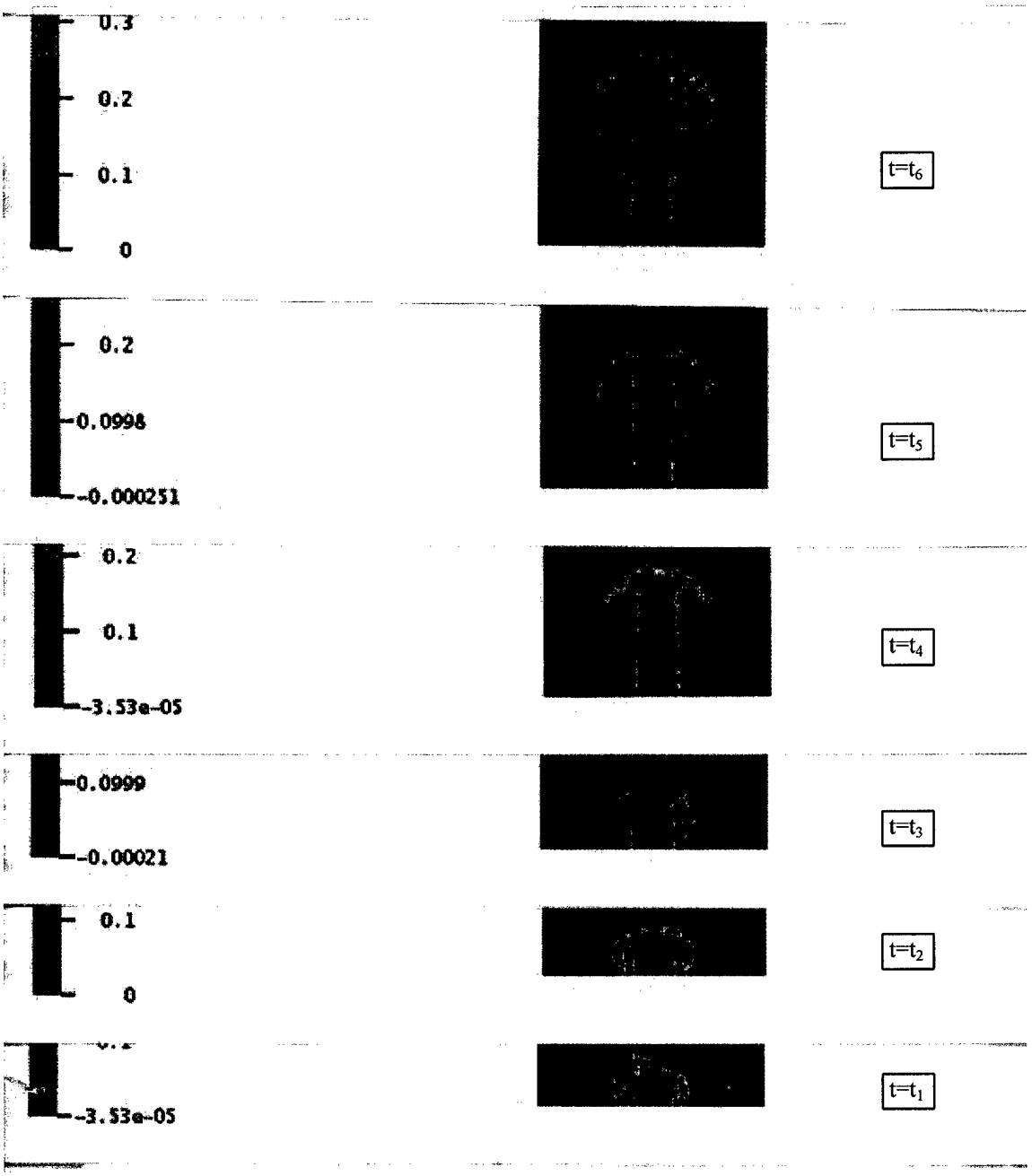

Figure 6.2 Initial development of the low Mach number free jet; $0 < t_1 < t_2 < \ldots < t_6$

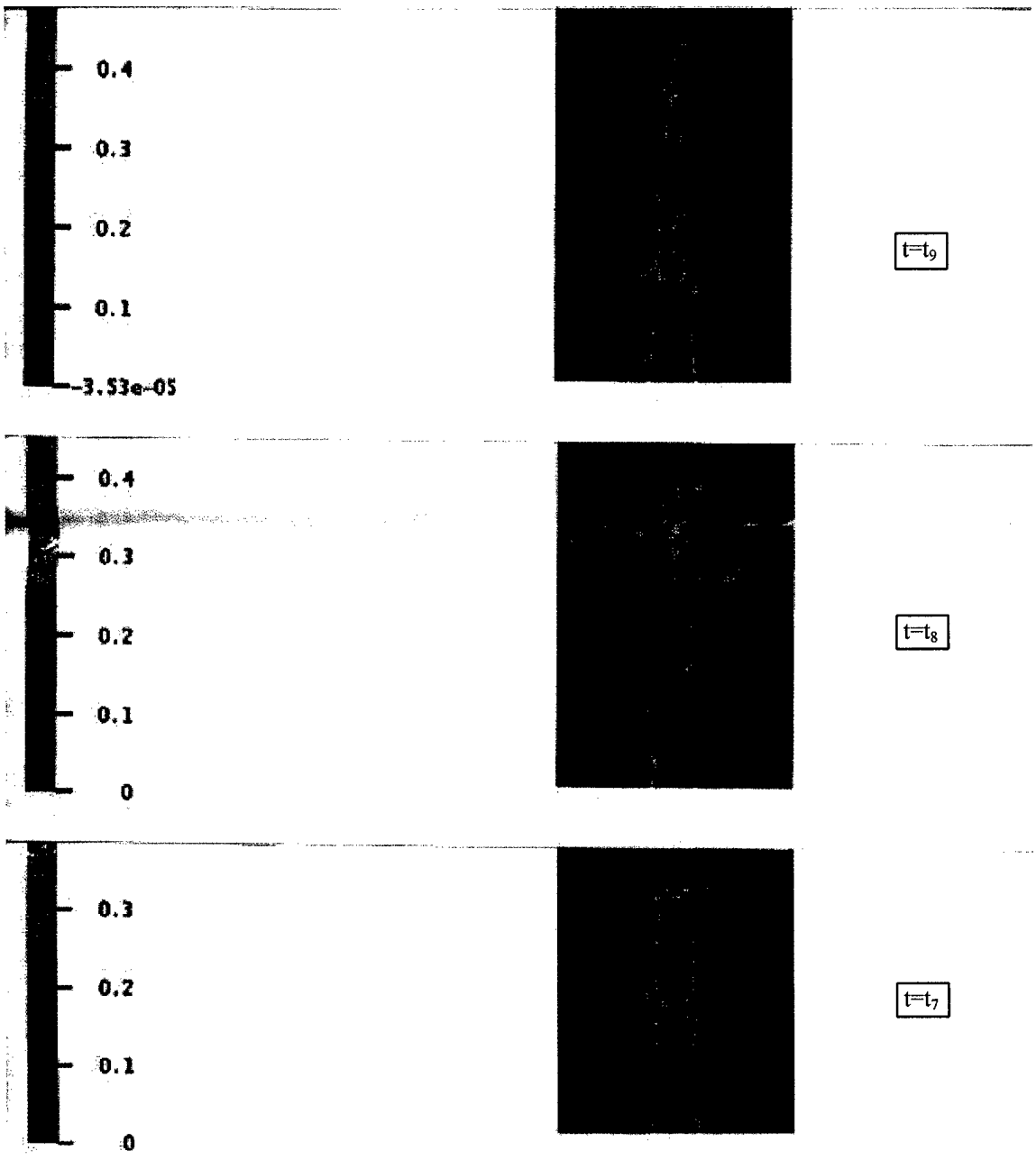

Figure 6.3 Intermediate development of the low Mach number free jet and initial development of the jet asymmetry; $0 < t_1 < \ldots < t_7 < t_8 < t_9$

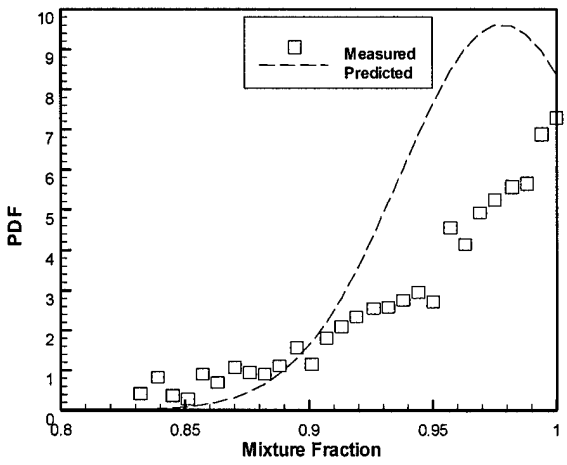

Figure 6.4 Measured and predicted mixture fraction pdf in the jet (X/D=3.08, Y/D=0.0).

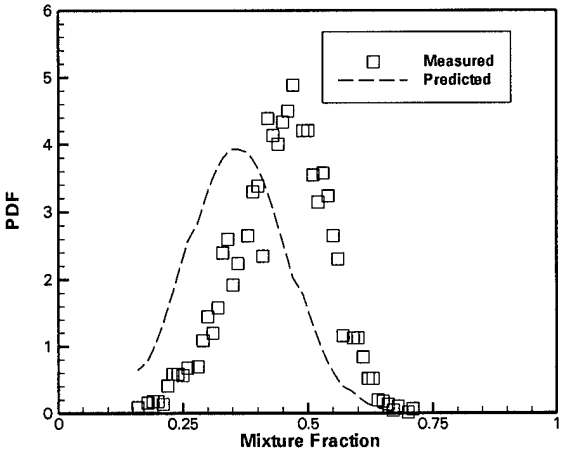

Figure 6.6 Measured and predicted mixture fraction pdf in the jet (X/D=15, Y/D=0.55).

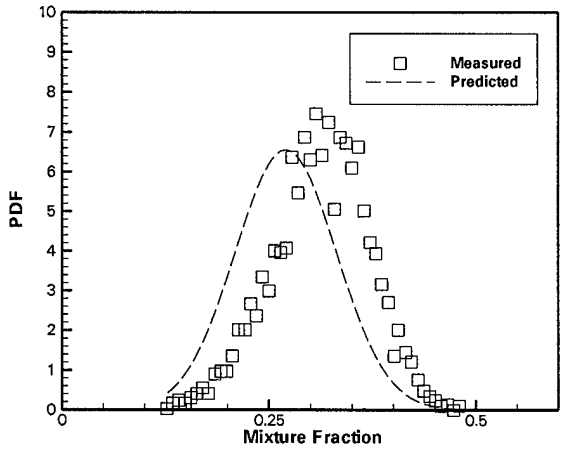

Figure 6.5 Measured and predicted mixture fraction pdf in the jet (X/D=24.78, Y/D=0.0).

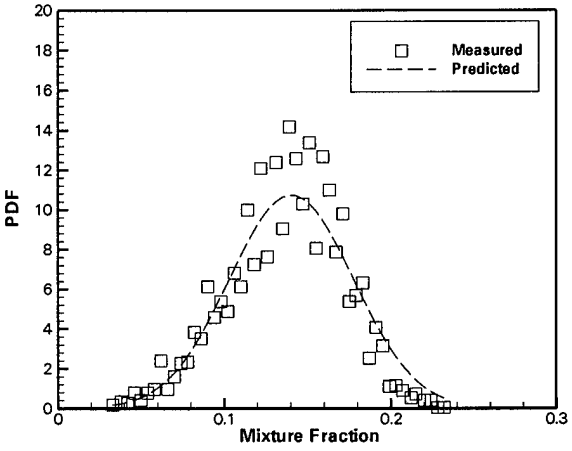

Figure 6.7 Measured and predicted mixture fraction pdf in the jet (X/D=50, Y/D=0.55).

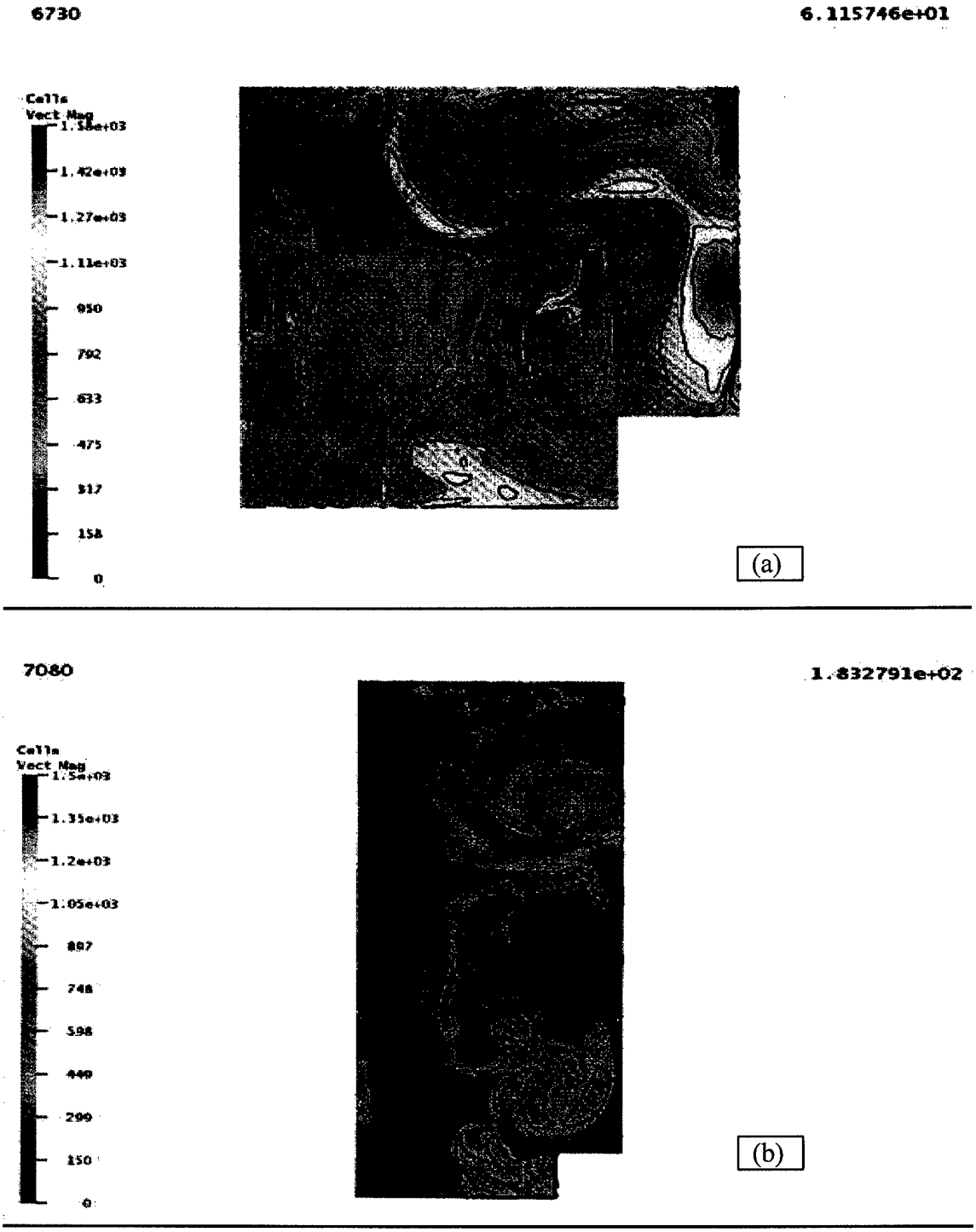

Figure 6.8 Velocity magnitude contours; (a) 61° CA, (b) 183° CA

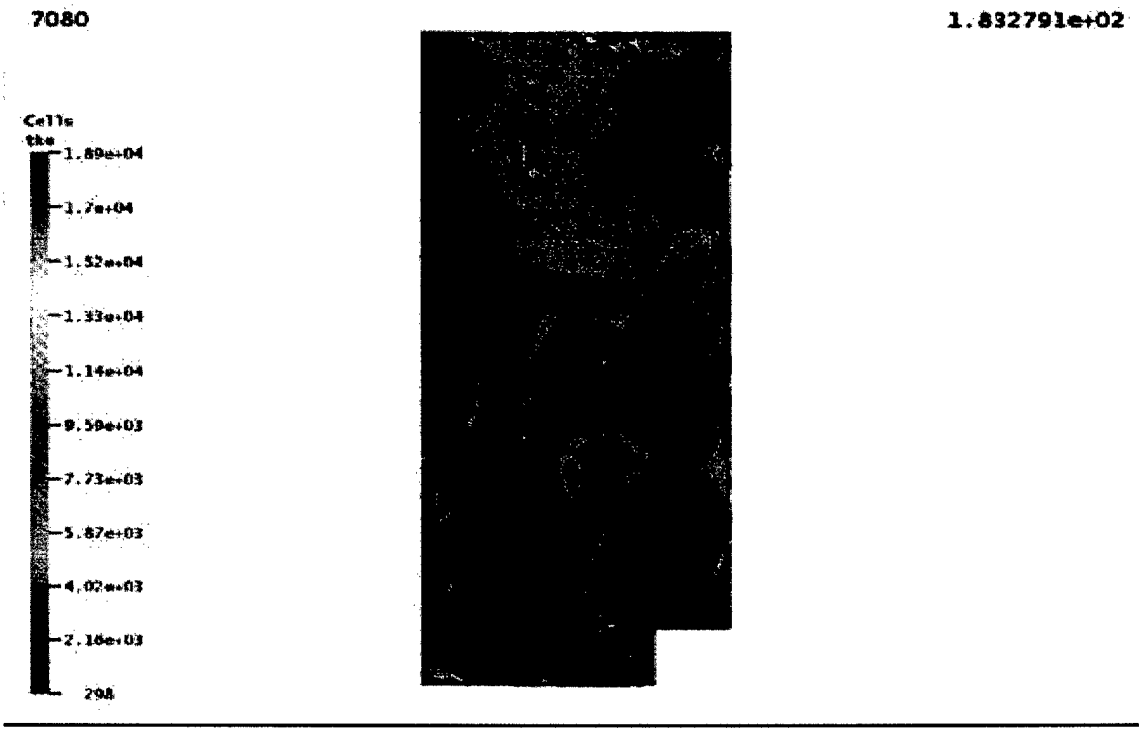

Figure 6.9 Turbulent kinetic energy contours near BDC (183° CA)

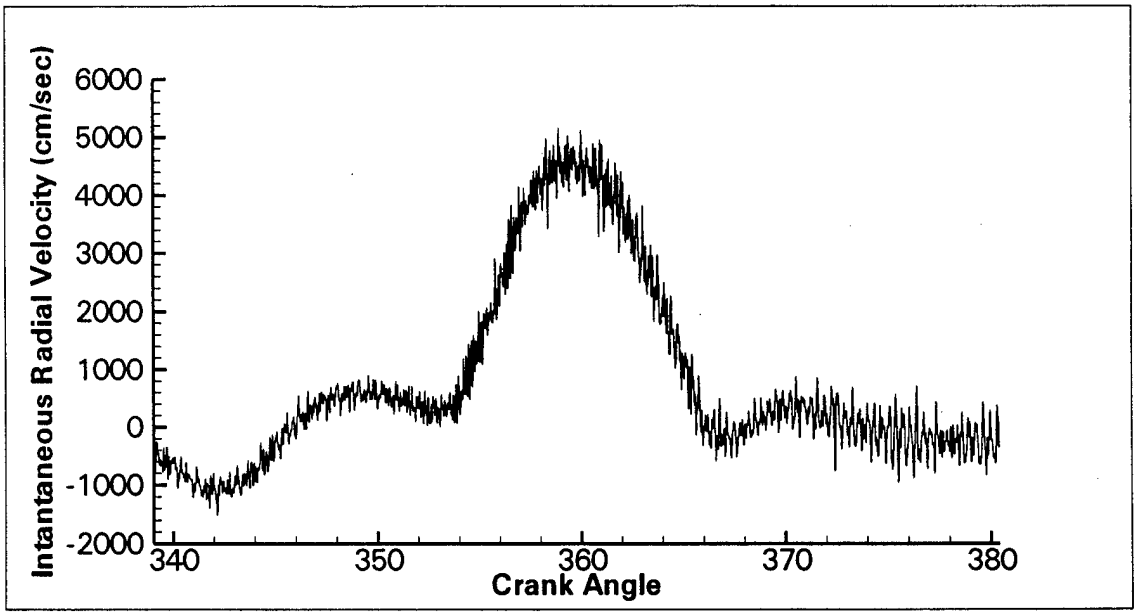

Figure 6.10 Instantaneous radial velocity with Crank Angle in combustion simulation at point (x, y, z': 29, 0, 117), 5.4 mm below the cylinder head

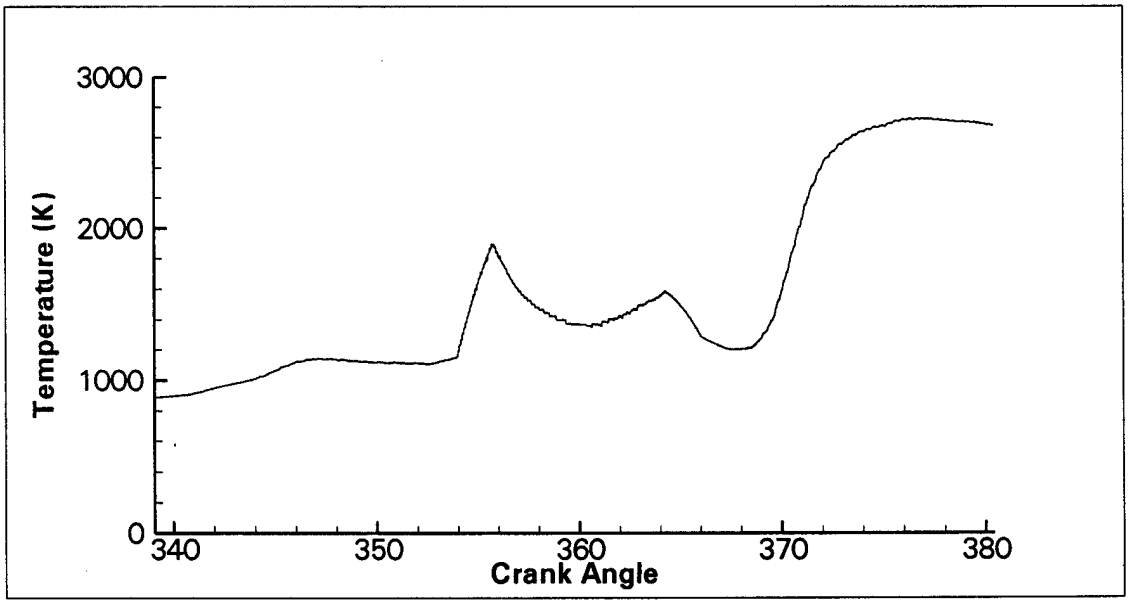

Figure 6.11 Instantaneous temperature with Crank Angle in combustion simulation, at same point as in Figure 6.10

Chapter 7 Development of Turbulent Flow Measurement Technique

Several different non-intrusive whole field velocimetry techniques are currently under development which provide velocity data in a plane, which can thus reduce the time required to map out a complex flow field. This project is exploring the accuracy of Doppler Global Velocimetry (DGV), a nonintrusive, planar imaging, Doppler-based velocimetry technique, as well as the accuracy of related Point Doppler Velocimetry (PDV). Both of these techniques use an iodine vapor cell to determine the Doppler shift, and hence the velocity, of small seed particles in a flow field, as these particles pass through a two-dimensional sheet of laser light. The same portion of the light sheet is viewed through a beamsplitter, either by a pair of video cameras (for DGV), or a pair of photodetectors (for PDV), with the iodine cell placed in the optical path of one of the cameras or photodetectors. Laser wavelength and cell absorption band are matched such that flow velocities of interest yield Doppler shifted frequencies in the linear portion of the absorption band of the cell. As a result, the ratio of the light intensities seen by the two detectors at a point in the flow yields a signal that is proportional to the particle velocity.

A two-channel non-scanned point PDV system has been developed (Kuhlman, et al., 1997), along with a two-channel planar imaging DGV system (Naylor and Kuhlman, 1998, 1999). The accuracy limits of both systems are being systematically explored, through a series of measurements in relatively simple, unheated flows such as fully-developed turbulent pipe flow, a circular jet, and the flow over an airfoil. A rotating wheel is also being used as a velocity standard. While current DGV systems lack the accuracy or resolution of conventional Laser Velocimetry or Particle Image Velocimetry (accuracy of mean velocity typically on the order of 5% of full scale, versus 1% for LV), DGV has proven in a short time to be a very flexible whole-field velocimetry technique.

7.1 Apparatus and Procedure

The present point PDV system closely follows the basic DGV system that was originally developed by Meyers et al. (1991), except that photodiodes have been used, along with front lenses and pinholes, to collect scattered light from a single point in a seeded flow. Kuhlman, et al. (1997) and James (1997) have described the PDV system in detail. A reference iodine cell

has been used to compensate for laser frequency drift. Calibration of the iodine cells has been accomplished using a continuous scan of the mode structure of the cw Argon ion laser, by mechanically altering the tilt of the etalon through about 10-20 mode hops (James, 1997).

DGV system hardware and have been described in Naylor and Kuhlman (1998, 1999), and in more detail in Naylor (1998). Most of this hardware is similar to that used for the PDV system. Eight-bit Hitachi KP-M1 CCD cameras and a Matrox Genesis frame grabber have been used to capture images for the DGV system. All four cameras are read simultaneously using horizontal and vertical sync pulses from the Genesis board. Nikon 35-135mm, f3.5-4.5 zoom lenses have been used with the CCD cameras, because of their versatility in imaging different sized areas over a wide range of distances. Polarizing filters have been placed in front of the beam splitters to minimize effects due to polarization sensitivity of the beam splitters. Image processing software has been developed, as described by Naylor (1998), which closely follows the image processing methods developed at NASA Langley by Meyers (1992, 1996). Flow seeding for DGV and PDV measurements is provided by a commercial fog machine, which feeds a large plenum to damp out pulsations in smoke output.

Most recent results include 2-component PDV data for the flow over a nominally 11.8 inch chord NACA 0012 airfoil model at zero degrees angle of attack, as described in Kuhlman and Webb (1999). The airfoil has been mounted at the exit of a 2.25x3.25 inch flow channel, fed by a blower capable of exit velocities of 40-45 m/sec. The present results have been obtained at an exit velocity of 21 m/sec, due to limitations on removing the smoke-seeded flow from the laboratory. Several series of 2-component PDV data and single component hot wire data have been obtained at eleven chordwise stations along the airfoil, from x/c=0.13 to x/c=0.98. All data have been obtained at a fixed z location of 0.5" above the airfoil shoulder (z/c=0.04). At each location data have been obtained at a sampling rate of 10 kHz, in 1k 4k or 16 k blocks. The present results are for 1 k data records, corresponding to 0.1 sec time records. This has been done to minimize the time required to obtain a PDV data set, in order to minimize time for iodine cell stem temperatures to drift. Such drift of the temperatures of the iodine cell stems has been identified as the key source of the apparently randomly varying offset errors in mean velocity results. From these 1 k time series, mean and RMS velocities, as well as time autocorrelation coefficients and power spectra have been computed for both the PDV and hot wire data, to assess the accuracy of the PDV system for turbulence measurements. Also, similar data are presently

being acquired in a series of one inch diameter jets: a uniform jet, an annular jet, and a swirling jet.

7.2 Results

Early PDV data repeatability, as documented in the thesis by Ramanath (1997), was poor. However, improved cell calibration procedures (James, 1997) have significantly increased PDV and DGV system accuracy. Both single and 2-component PDV data measured on a rotating wheel have been presented by James (1997), and by Kuhlman, et al. (1997). Total wheel velocity range for these measurements was 57 m/sec, so the observed velocity error magnitudes of approximately ±0.6-1.2 m/sec, correspond to 1-2 % errors, which is quite good. Also, the standard deviations of the actual PDV wheel velocity data points from the least squares linear curve fits have been found to be 0.5-0.7 %.

Two-component PDV data obtained from a traverse across the exit of the fully-developed pipe flow at a nominal Reynolds number of 76,000, have been previously presented by Kuhlman (1998). The axial mean velocities agree well with results from a pitot-static probe survey, but circumferential mean velocities display an offset error on the order of 2-5 m/sec. Turbulent velocity levels agree with hot wire data of Laufer (1954). Significant difficulties occur near the pipe walls, both due to reduced signal-to-noise levels due to less smoke, and to secondary scattering and reflections of the scattered light off of the pipe walls. However, the greatest difficulty was in obtaining accurate, reliable zero velocity values.

Recent PDV data has been compared with hot wire data by Kuhlman and Webb (1999) for flow over an NACA 0012 airfoil model at zero degrees angle of attack. PDV streamwise mean velocities show a total variability of about 5 to 6 m/sec for the 4 runs; this variability is consistent with earlier PDV data (Kuhlman, 1998) and DGV data (Naylor and Kuhlman, 1999). PDV RMS velocities agree with corresponding hot wire data to within about 0.5m/sec, and display a similar level of repeatability from run to run. The computed PDV correlation coefficients agree well with hot wire correlation coefficients; both autocorrelations decay in less than 10 msec. However, PDV power spectra show a larger amount of noise at frequencies above about 1000 Hz.

Recent 2-component PDV data in a circular jet are shown in Figs. 7.1 and 7.2. Mean and RMS data at the jet exit (x/D=0.25, where D=exit diameter) are shown in Fig. 7.1, while similar results are shown in Fig. 7.2 for x/D=6. Mean streamwise velocities at the exit (Fig. 7.1) again show about 5 m/sec of offset from preliminary pitot probe results on the centerline at the exit. Measured PDV mean circumferential velocity varies by about 2 m/sec from the correct value of zero m/sec. RMS velocities are between 1 and 2 m/sec on the centerline (Fig. 7.1). At x/D=6, the PDV mean streamwise velocity profile (Fig. 7.2) appears Gaussian in shape, as expected. Both the mean streamwise and circumferential velocities display offset errors of 4-5 m/sec from the correct values. RMS velocities have risen to 4-10 m/sec. Detailed comparisons are now being made between PDV and hot wire data for this turbulent circular jet flow field. Also, the same jet flow facility has been modified to allow PDV and hot wire data to be obtained for a swirling jet as well as for an annular jet.

Recent analysis of the offset error has indicated that it is largely due to the random, uncorrelated variations in iodine cell stem temperatures. This stem temperature variation has been observed to vary with a short term RMS of 0.1 degrees C (Naylor, 1998). This has been found to correspond to an error in the computed Doppler shift frequency of 7 MHz, which then corresponds to a mean velocity error of from 2 to 10 m/sec, depending on the geometry and viewing direction of the PDV system. This level of velocity error is consistent with the observed mean velocity offset error.

A recent upgrade has been performed of the iodine cells and beamsplitters used in the present system. Vapor-limited iodine cells have recently been installed, along with polarization-insensitive beamsplitters. Now, both PDV and DGV data are being taken in the one-inch diameter circular jet facility, for comparison with pitot-static and hot wire data that has recently been obtained. It is expected that the new, vapor-limited cells will largely eliminate the mean velocity offset error that has been observed in all point and DGV data taken to date. Also, a DGV system using line scan cameras is under development, and a higher power, pulsed YAG laser will be added to the existing system. All of these efforts are aimed at both improving measurement accuracy and allowing turbulence measurements to be made with the improved DGV and PDV systems.

a.)

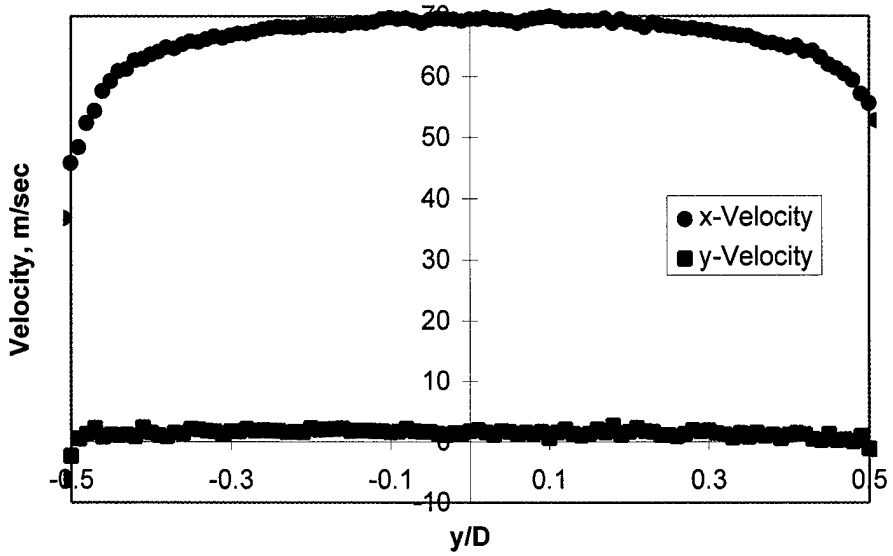

b.)

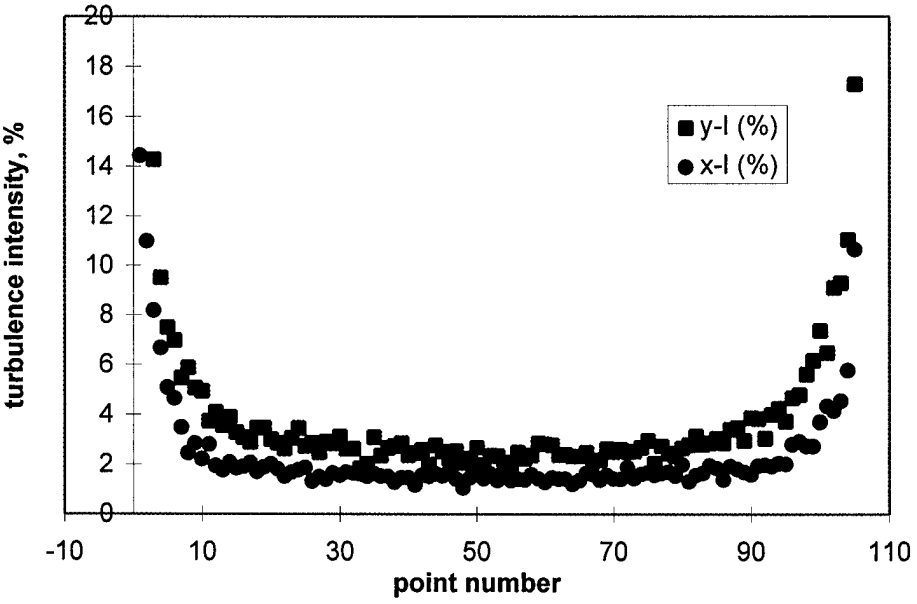

Figure 7.1 Two-component PDV data at exit of uniform circular jet

a.) Mean velocities

b.) Turbulence intensities

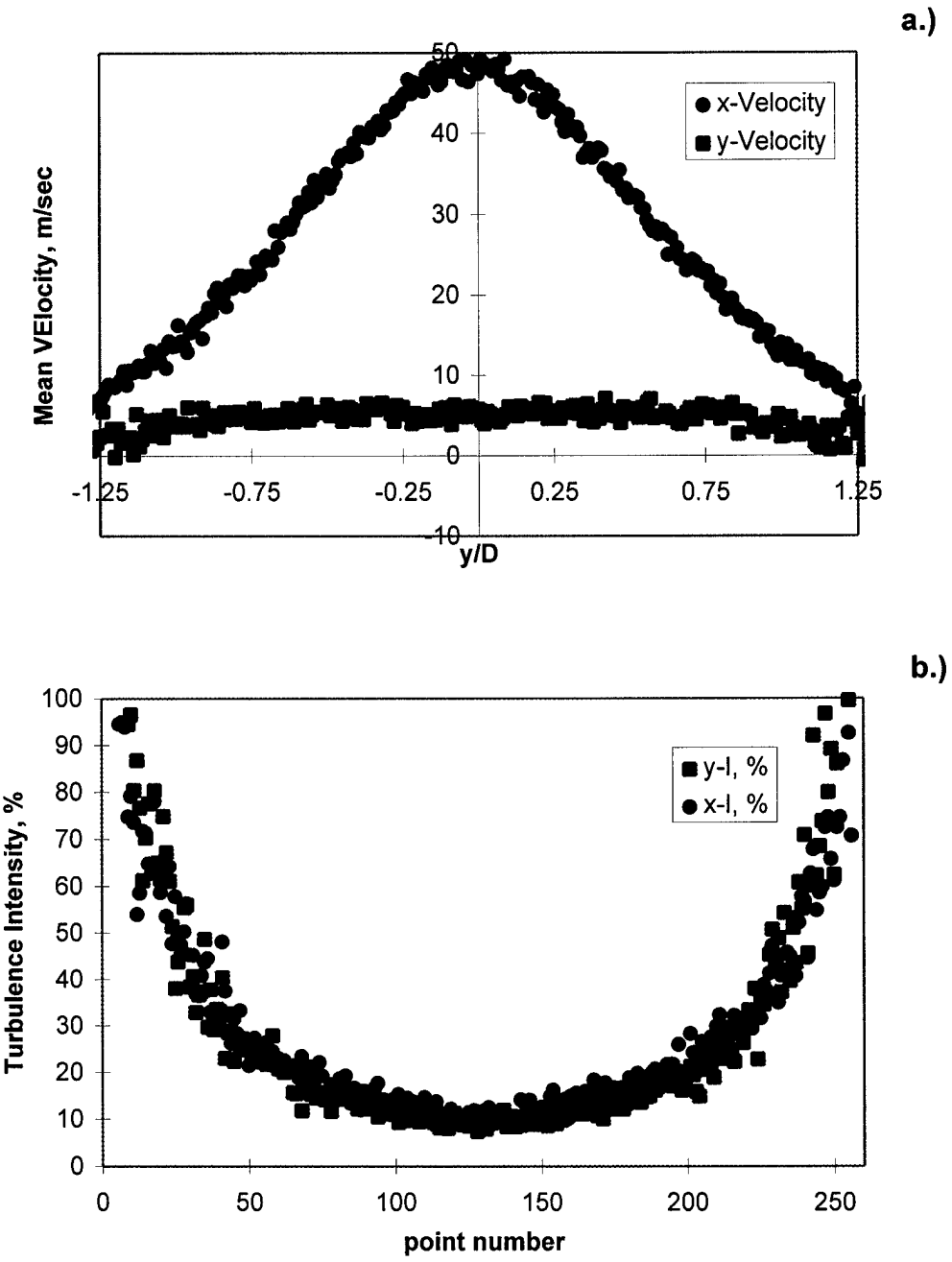

Figure 7.2 Two-component PDV data at x/D = 6 for uniform circular jet

a.) Mean velocities

b.) Turbulence intensities

Chapter 8 Turbulence Predictions in IC Engines

In this section we present our most important findings from application of the LES technique to typical engine cylinder geometries. First, the flow dynamics due to piston motion during the compression and expansion strokes is studied. Here the primary instability is induced by the presence of a bowl, and the squish flow combined with an imposed swirl component. The initial conditions for these simulations were only approximate and are not reminiscent to the intake stroke. Next, the flow inside the cylinder during the intake stroke and compression strokes without combustion was simulated including the valve dynamics. Here, the objective was to investigate the generation of turbulence during the intake and subsequently its decay during compression in addition to demonstrating the predictive capability of the LES technique when applied to in-cylinder turbulence. Finally, two cases were simulated with combustion (1) was the continuation of the intake flow case with spray injection and subsequent combustion, (2) combustion with a piston bowl, again without the influence of the turbulence generated during the intake stroke. The results are compared to available experiments whenever possible.

8.1 Bowl Induced Flow Instability

This study (Yavuz et al., 1998) focuses on capturing flow instability, and possibly turbulence, induced by a typical piston bowl geometry by simulating the flow dynamics using the KIVA-3 code. Both two- and three-dimensional simulations were performed using relatively fine grid resolution in a piston-bowl assembly with various wedge angles in the circumferential direction. The differences in solutions using a subgrid scale (SGS) model are elucidated. Simulations with no turbulence model seem to capture a high frequency of the instabilities with significant amplitudes. The r.m.s. (root mean square) values of the fluctuations have been calculated at selected points inside the cylinder. An assessment of the influence of numerical parameters on the predictions is made.

The results are not compared with any experimental work directly because such a comparison requires strict matching of the intake flow situation, which is not done in the present study. Moreover, the experiments most of the time present ensemble averages which include cycle-to-cycle variations, and they can not be easily isolated. However, the experiments by

Catania et al., (1995), and Valentino et al., (1998) are used as a guide to make qualitative assessment of the predictions. The simulations are enlightening in that the turbulence inside an engine cylinder can be predicted, and further the influence of cylinder bowl geometry can be isolated from that of the turbulence generated by other mechanisms such as shear layers and the swirl induced during the intake stroke.

8.1.1 Application

The flow field inside a typical piston-cylinder assembly (Figure 8.1, 2-D, axisymmetric) was simulated under motored conditions (i.e., without combustion) at two speeds, namely 600 RPM and 1500 RPM. Only the compression and expansion strokes are simulated; cycle-to-cycle variations are not considered. These simulations were performed using a maximum time step of 0.15 μs over a compression and expansion stroke repeated twice. The focus is on the prediction of flow instabilities induced by the bowl geometry and the squish flow, which may contribute significantly to the overall turbulence generation. The numerical mesh used in the simulations is depicted in Figure 8.2. Two numerical meshes of 20,000 and 130,000 vertices were used with a wedge angle of 0.5 and 180 degrees in the circumferential direction, respectively. The maximum cell size for the wedge calculations was 0.5x0.9 mm in the radial and axial direction. The 3-D simulation with 180-degree wedge angle span was investigated with 18 cells in the cirumferential direction to see the influence of the domain size. For this case the median cell size in the tangential direction was 3.0 mm. As reported by Celik and Yavuz (1997), the minimum integral length scale occurs at the end of the compression stroke and is in the order of a few millimeters for automotive size engines.

Early calculations have revealed that it was possible to capture flow instability with the present grid resolution even at the lower engine speed of 600 RPM. However, the selection of the time step played a crucial role in the resulting amplitude and the frequency of oscillations. It was possible to totally destroy the flow instability (most probably induced by the flow separation at the corner where the bowl meets the piston head) either by increasing the time step, or by simply using the standard k-ε turbulence model, which is known to be overly diffusive. The time steps used in the results presented in this paper were selected carefully after much experimentation.

Figure 8.1 2-D Streamlines at CA 210° ATDC (with mirror image)

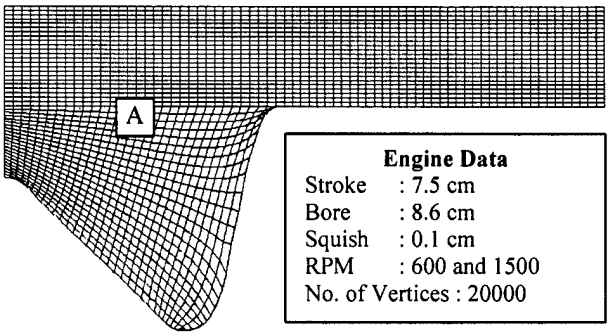

Figure 8.2 Computational mesh for 2-D simulation and specific engine data

As it was mentioned above the quasi-second order upwind (QSOU) scheme was used for the convective terms, and central differencing for the diffusion terms. Normally the central differencing (CD) scheme should be used for the momentum equations. However, CD is usually an unstable scheme when used for convection. The stability can be secured by adding some diffusion, via either SGS model or artificially. Therefore, prediction of turbulent fluctuations via the QSOU scheme, which is strictly monotonic, was preferred at the expense of some loss of formal accuracy near sharp gradients that may be present in the flow field.

The simulations were started at CA 90° BTDC. As an initial condition the radial velocity was taken as zero and the axial velocity varied linearly from piston velocity at the piston face to zero at the cylinder head. The tangential velocity was defined by the Bessel function dependent

on engine speed as provided in the code. Moreover, periodic boundary conditions were applied on the front and back face of the wedge, whereas the law of the wall was applied on the walls. And in the case the SGS model was applied, an initial turbulence intensity of 10% and L_{SGS} = 0.4 cm was used, whereas without the SGS model no turbulence quantities were initiated at all.

Cycle resolved phase averaging was applied to the calculated data to separate the mean and fluctuating components of the instantaneous velocity as explained in Yavuz et al. (1998).

8.1.2 Results

An example of the complexity of the flow field as predicted with the present model is shown in Figure 8.1. This figure is indicative of the level of details, which can be captured by the present simulations. The variation of the instantaneous velocity components with time at location A (see Fig. 8.2), which is fixed with respect to the bowl, 1.0 mm below the piston face and 10.6 mm from the axis, are depicted along with the time averaged values in Figure 8.3 for the compression-expansion stroke. Here, the two indicated TDC's (Figure 8.3 and 8.4) are repetitions of the compression/expansion stroke.

As it was expected, the fluctuations in the tangential direction are much smaller compared to the other two directions. This is a direct consequence of the pseudo two-dimensional nature of the present calculations with 0.5 degree wedge angle. Both the large-scale time variations of the velocity components induced by the piston motion, as well as the random "turbulent" fluctuations are captured. Figure 8.4 shows these random velocity fluctuations as a function of the crank angle. It is seen that the turbulence intensity is somewhat reduced during the second compression/expansion stroke; however, it persists at a considerable level indicating that the numerical diffusion is sufficiently small not to render turbulent dynamics of the flow. Whether these fluctuations will continue to persist over several cycles remains to be seen. Figure 8.4 and 8.5 indicate that there are significant changes occurring near the TDC both in the magnitude and frequency of the velocity fluctuations. As it is shown in Figures 8.5 and 8.6 the time averaging interval, as well as the time step used for the numerical simulation has significant influence on the intensity of the fluctuations.

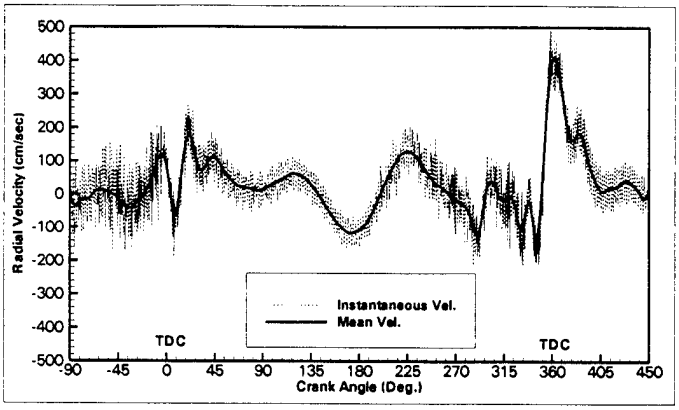

Figure 8.3 Instantaneous velocity components at point A (without SGS model) : pseudo 2-D calculations for a motored engine at 1500 RPM

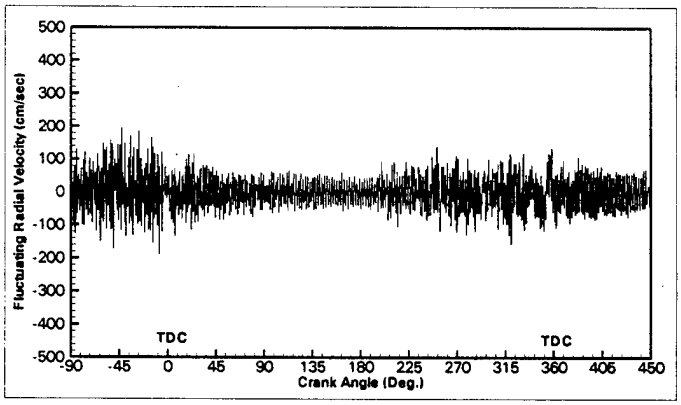

Figure 8.4 Instantaneous fluctuating velocity components at point A (without SGS model): pseudo 2-D calculations for a motored engine at 1500 RPM

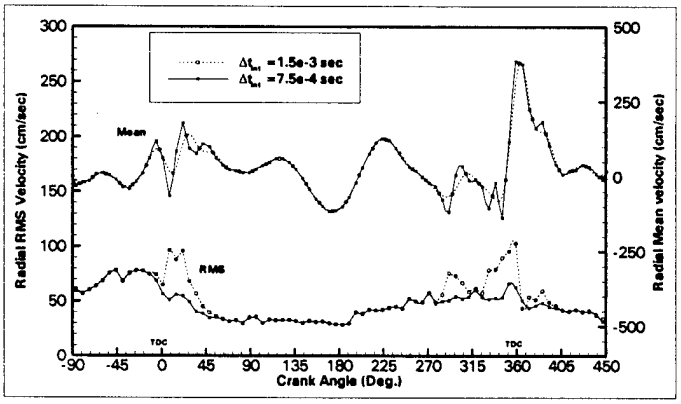

Figure 8.5 Influence of time averaging interval on various flow quantities: pseudo 2-D calculations for a motored engine at 1500 RPM

It should be pointed out that the predicted "turbulent" fluctuations are significantly affected by the time step (Figure 8.6a). The smaller the time steps, the better is the resolution of turbulence scale, and the higher is the turbulent intensity. Figure 8.6b shows the influence of SGS turbulence model, which essentially has a damping effect. At this grid resolution, which is relatively coarse for LES simulations we believe that the results without the SGS model should be better than the ones with a SGS model.

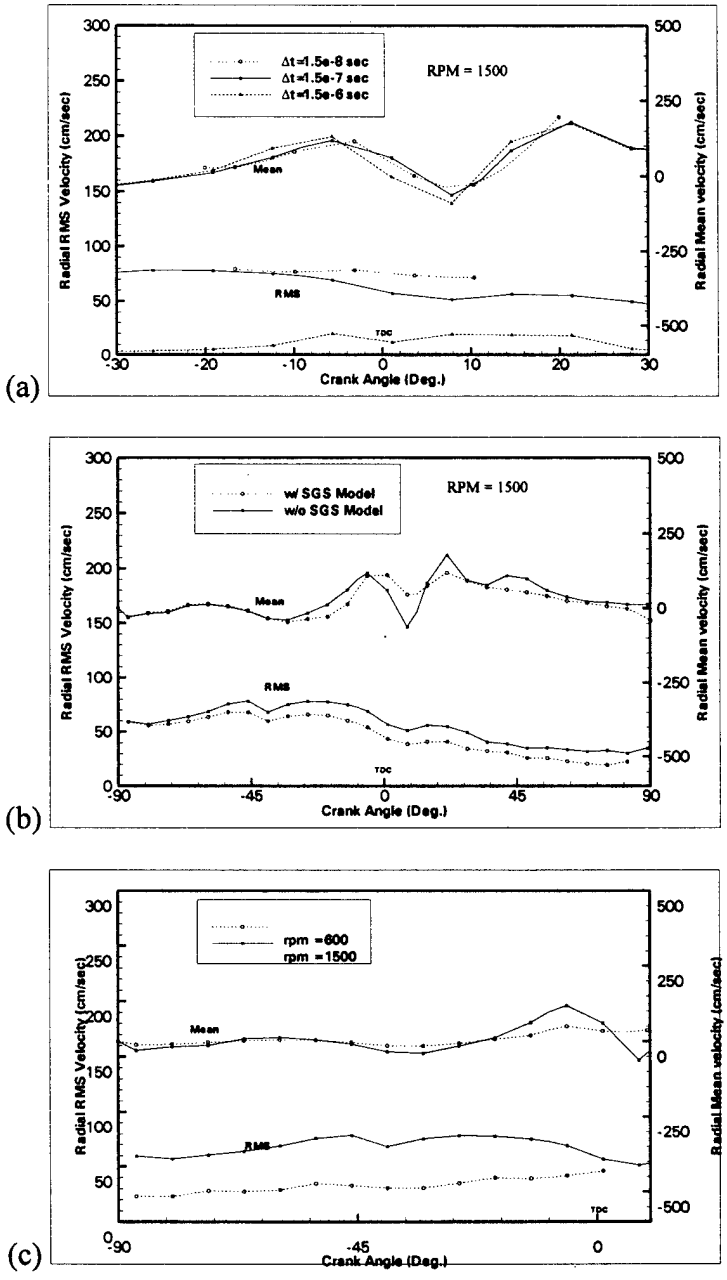

Figure 8.6 Influence of various parameters on calculated quantities: pseudo 2-D calculations

The predicted fluctuations are anisotropic (Fig. 8.6) even very near the TDC. The magnitudes of the fluctuations are in the range 0.5-1.0 m/sec in radial, 1.0-2.0 m/sec in the axial and 0.5-1.5 m/sec in the tangential directions, respectively. For a similar engine configuration, Catania and Spessa (1996) measured velocity fluctuations in the order of 10 m/s for the cycle-resolved turbulence intensities, and about 5m/s for the r.m.s. fluctuations of the in-cyclinder mean velocity. According to Catania (1998), the present computations should be compared to their cycle-resolved turbulence intensities. In another experimental study Auriemma et al., (1998) reported measured rms velocity fluctuations during the compression/expansion stroke of a motored engine at 1500 RPM. These indicated maximum values of 2 m/s for the radial and 3.5 m/s for the tangential directions respectively. The measured values included both cycle-to-cycle fluctuations and in-cycle fluctuations. Valentino et al., (1998) presented a method to reduce the effect of cycle-to-cycle variations of mean motion on turbulence. Their results seem to indicate that the cycle-resolved turbulence can be augmented by as much as 30% due to cycle-to-cycle-variations. In any case, the experimental data indicate that the predicted turbulence intensities are much lower compared to those measured, although direct comparison is not possible at this stage. This may be mainly due to the fact that reminiscent turbulence generated during the intake stroke was not accounted for.

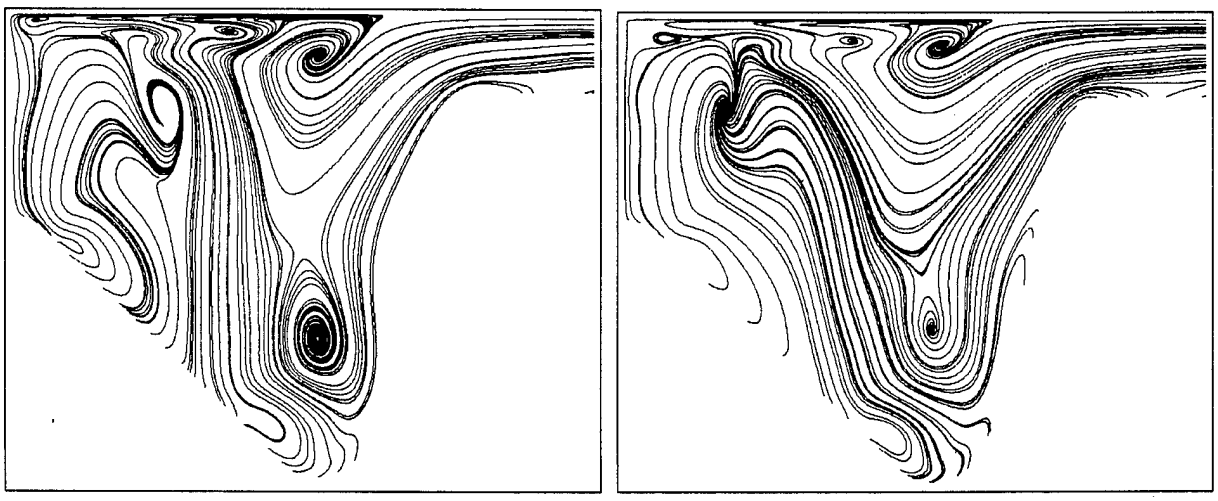

Figure 8.7 Streamlines to show the influence of three-dimesionality on the flow field at CA 18° ATDC at a) 0° and b) 90° wedge angles

In Figure 8.6c, the influence of engine speed is depicted. There is a significant increase in predicted turbulent intensity with increasing engine speed as has been observed in experiments (see e.g., Corcione and Valentino, 1994; Catania and Spessa, 1996).

The 3-D, 180° wedge calculations with 130000 vertices did not show any significant change in the predicted rms fluctuations. This could be due to the stabilizing effect of the arbitrarily imposed swirl velocity profile in addition to the coarse grid used in the tangential direction. However, the streamlines shown on two perpendicular planes of the 3-D geometry (in Figures 8.7a and b), reveals some expected 3-D effects.

8.1.3 Discussions

Three dimensional, and pseudo-two dimensional (i.e., a small wedge angle), time accurate calculations have been performed to predict the flow field inside a typical diesel engine piston-bowl assembly. The engine was run under motored conditions at 600 and 1500 RPM, spanning only the compression and expansion strokes. The objective was to capture the flow instabilities, and possibly turbulence induced by the bowl geometry alone, i.e. without the influence of residual turbulence generated during the intake stroke. It was shown that this was possible by using the KIVA-3 code with a fine grid resolution and relatively small time steps. The bowl induced "turbulence" seems to be persistent over a few cycles without recharging induced by the intake stroke. The small scale flow instabilities and unsteadiness observed in the computer simulations seem to be the results of unsteady flow separation that occurs at the sharp corner of the piston bowl and the flat piston head. This is in accordance with the combustion improvements that are observed experimentally when re-entrant type bowl geometry is used. The magnitude of the calculated r.m.s. velocity fluctuations seem to be much lower than measured ones under similar geometry and operating conditions. But the calculations do not include the significant contribution that arises from the turbulence generated during the intake stroke, nor do they include the significant cycle-to-cycle variations. Although the grid resolution used in the present study may be considered as relatively coarse for LES, this study demonstrated that there is a potential to predict in-cylinder turbulence for IC engines using large eddy simulations with relatively modest computational resources at the workstation level.

8.2 Prediction of In-Cylinder Turbulence for IC Engines

Results of under-resolved large eddy simulations of an intake and a compression stroke in a typical IC engine geometry are presented. A modified KIVA-3V program is used with a special precaution to keep the time accuracy at a level acceptable for LES. A Smagorinsky sub-grid scale model is used with improved spatial discretization scheme. The simulations could achieve a spatial resolution of turbulent eddies on the order of several millimeters and temporal resolution of velocity fluctuations on the scale of 10^{-4}s. The predicted growth and the subsequent decay of turbulence during the intake phase agree well with experiments. Statistics of turbulent velocity fluctuations is analyzed and compared with experimental studies. Combustion of n-Tetradecane is modeled using a 7-reaction Arrhenius mechanism and Magnussen eddy-dissipation combustion model. A standard KIVA spray model is used to model injection and evaporation of the fuel. Auto-ignition of the gaseous phase of the fuel occurs close to 10^{o} CA BTDC. The influence of combustion on turbulence is analyzed.

8.2.1 Numerics

Modifications were made to the KIVA code to allow a fairly simple Smagorinsky SGS model where the eddy viscosity is calculated from the algebraic relation (Eqn. 1.6). The model constant C_s was set equal to 0.2, a typical value used in the literature (see e.g. Rodi et al., 1997). The sub-grid length-scale was estimated as an average computational cell dimension (see Smith et al., 1998).

In some of the cases presented "no SGS turbulence model" was used. This requires, in most instances, some numerical diffusion for stability, which is accomplished via the use of QSOU (Quasi Second Order Upwind) scheme instead of the central differencing (CD) which has no diffusion error, or by using a combination of CD and upwind differencing heavily biased towards CD.

The above turbulence models were employed in conjunction with the commonly used law-of-the-wall boundary condition which is implemented in KIVA-3. The basic assumption here is that the interaction between the modeled near wall region and the outer region is weak as observed experimentally by Brooke and Hanratty, (1993).

Convective terms are advanced explicitly in time and the diffusion terms are advanced explicitly, implicitly, or semi-implicitly. The degree to which the diffusion terms are implicitly discretized is based on a combination of stability and efficiency considerations. Sub-time steps (referred to as sub-cycles) are taken to advance the convective terms. The time step in each sub-cycle is based on Courant stability considerations. The convective terms are advanced with time steps that are the same or smaller than what is used for the diffusion terms. Though the overall time accuracy for convection terms is only of the first-order, the global time step is based on several considerations including stability and several accuracy constraints. To increase the time accuracy even further the time step was confined to the interval [$1.5 \cdot 10^{-7}$ - $5 \cdot 10^{-7}$ sec] far below the Kolmogorov time scale, which is in the order of 10^{-4} -10^{-5} seconds for a typical automotive size engine (Celik and Yavuz, 1997). This precaution compensates for the first order time accuracy of convective terms and guarantees the time resolution required for LES.

8.2.2 Engine Application

The computational procedure described above was applied to a typical engine geometry. The cylinder assembly was prototyped after the Diesel engine used in the experiments of Catania et al. (1996) with the following dimensions: bore - 79.5mm, stroke - 86mm, compression ratio - 18, inlet valve opening - 5 deg BTDC, inlet valve closure - 55 deg ATDC, exhaust valve opening - 55 deg BTDC, exhaust valve closure 5 deg ATDC. Piston speed was set to 1600 rpm. A realistic valve geometry with the swirling intake configuration was used (Figure 8.8). The computations were performed on two grids consisting of 220,000 and 440,000 nodes including the intake/exhaust ducts. The average grid size was in the order of one millimeter. A curvilinear block-structured coordinate system was used in preference to the cylindrical coordinate system because the former avoids high grid distortions at the cylinder axis. The first set of computations on both the coarse and the fine grids was carried out without any turbulence model and with the QSOU numerical scheme. Later the computations on the fine grid were repeated with the Smagorinsky sub-grid-scale turbulence model and the second order discretization scheme for the convective terms (as described by Smith et al., 1999). The exhaust duct pressure was set equal to the atmospheric pressure and the intake pressure was set 40% above the former, to prevent the in-cylinder gas from entering the intake duct during the first phase of intake. No random forcing was used at the inlet. It should be noted that the simulated engine configuration and the one

studied experimentally by Catania et al. are not exactly the same. The simulated engine has a flat piston head, whereas the experimental one had a specifically designed piston bowl, which is off-centered with respect to the cylinder axis. These differences were due to the limitations of the computer code and the currently available computational resources. The intake valve geometry and movement were modeled in accordance with the real engine parameters, but a generic profile was used to describe the shape of the upper portions of the valves (Figure 8.8b).

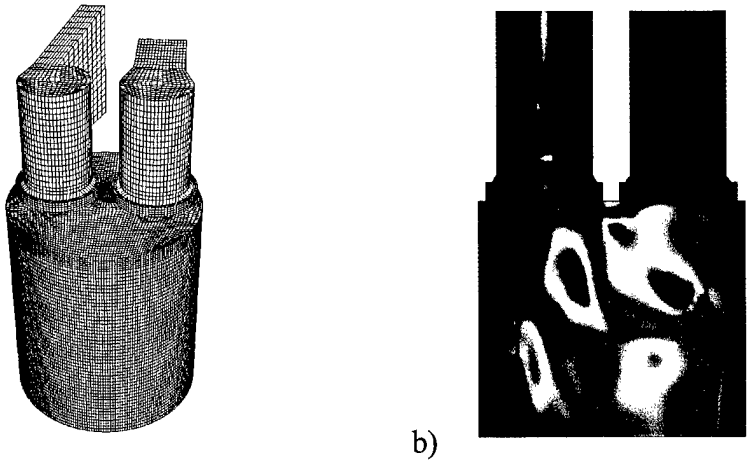

a) b)

Figure 8.8 (a) Geometry of the simulated engine; (b) Velocity distribution in the valve region

The Smagorinsky sub-grid-scale model and the Magnussen Eddy-Dissipation model (Magnussen, 1976) were used to account for the effects of turbulence and combustion respectively. Time step was varied depending on the time-scale of the limiting process. Thus, in the evaporation phase (285-360 CA) the time scale could reach the order of 10^{-9}s, which was due to the limits imposed by the evaporation process of smallest droplets. A standard KIVA spray model is used in all the simulations to account for injection, initial droplet size distribution and evaporation of the fuel. The initial gas and wall temperatures of 450°K were used. The average droplet diameter of the spray was set equal to 10^{-4}cm and $3 \cdot 10^{-4}$cm for the case with a bowl and two-valve assembly respectively.

8.2.3 Statistical Data Processing

The fluctuating component u(t) was obtained by subtracting the mean value, $\overline{U}(t)$, from the instantaneous velocity

$$u(t) = U(t) - \overline{U}(t) \tag{8.1}$$

The mean velocity was computed by continuous time averaging (phase averaging) over the interval T corresponding to the crank angle interval Φ by discrete integration corresponding to.

$$\overline{U}(t) = \frac{1}{T}\int_{-T/2}^{T/2} U(t+\tau)d\tau = \frac{1}{\Phi}\int_{-\Phi/2}^{\Phi/2} U(\theta(t)+\vartheta)d\vartheta \tag{8.2}$$

The auto correlation function R^*_{uu} and the power spectral density were computed according to the following formulae

$$R^*_{uu}(\tau) = \frac{1}{u^2 T}\int_{T_0-T/2}^{T_0+T/2} u\ (t-\tau/2)u(t+\tau/2)dt \tag{8.3}$$

$$E^*_{uu}(f) = 4\int_0^{T/2} R^*_{uu}(\tau)w(\tau)\cos(2\pi f\tau)d\tau \tag{8.4}$$

where T_0 corresponds to the crank angle of Φ_0, which is the middle of the integration interval. The Hanning window function $w(\tau)$ was applied to decrease the variance in the spectrum. A similar technique was applied in the experimental study of Catania et al (1996), which was used for comparison. The difference between our definitions of E^*_{uu}, R^*_{uu} and those used by Catania et al., E_{uu}, R_{uu} is that in the latter case the ensemble averaging over cycles is also applied in addition to phase averaging.

8.2.4 Results of Intake Turbulence Predictions:

The contours of the magnitude of the velocity vector depicted in Figure 8.9 illustrate the details of the three-dimensional flow structures at two different crank angles that are captured by the simulations. The figure shows a largely asymmetric annular intake jet with significant number of eddies forming in the shear layers surrounding the main body of the jet. The sizes of the smallest eddies captured are proportional to the grid size (~1 mm). The integral length scale is estimated (Celik and Yavuz, 1997) to attain a minimum value of a few millimeters at the TDC proportional to the squish/clearance height. The details of the flow inside the intake duct were smeared (filtered) out by the relatively coarse grid in that region.

Figure 8.10 shows the fluctuating velocity components and its fluctuating part located at a point approximately 5 mm below the cylinder head in the middle between the centerlines of the intake and exhaust ducts. As such this particular point can be compared with one measurement point of Catania and Spessa (1996) which is 5 mm below the cylinder head, and close to the cylinder axis. The reader is reminded that the geometry of Catania's experiment is different from the computational model in that there is no cylinder bowl in the latter case. Because of that and a slight difference in special locations where the measured and computed velocities were retrieved it was not possible to predict the mean flow-field exactly. But our main concern was to reproduce the trend in the fluctuating component, which is seen to agree well with experimental data (Figure 8.10b). The predicted cycle resolved mean velocity (not depicted here) showed roughly the same trend as in experiments but with a slightly lower magnitude. It is noteworthy to see that the velocity fluctuations decrease significantly towards the BDC (~180 CA degree) as observed in the measurements.

105^0 crank angle.

120^0 crank angle.

Figure 8.9 Absolute value of the velocity vectors (440000 node case).

One of the early experimental study demonstrating the decay of turbulence during the expansion stroke is that of Semenov and Sokolik, (1958). In these experiments the piston head was flat which corresponds to the computational setup, but the intake valve was located co-axially relative to the cylinder. The hot wire anemometer used was insensitive to the direction of velocity thus only the instantaneous magnitude of velocity was measured. According to the authors their measurements underestimate the amplitude of velocity fluctuations by 15-20%. In Figure 8.11 the measured and computed time dependence of the absolute value of velocity in the plane normal to the cylinder axis is shown. The general trend of decreasing velocity variations (both in the mean and fluctuating components) can be observed in both cases. As our grid dependence study showed doubling the number of nodes in the grid revealed more fine structures in the flow and led to higher amplitudes of velocity fluctuations. Nevertheless, the general trend of turbulence decay was unchanged in both cases (Figure 8.12). It is important to note that these particular measurements (both Catania et al.'s and Semenov's data) show cycle-resolved turbulence rather than ensemble averages.

Finally we present the normalized autospectral density function (i.e. energy spectra) in comparison with experiments in Figure 8.13 at a representative point which roughly corresponds to the measurement point. The agreement of both the energy content and the frequency ranges captured in the present simulations are good in spite of the differences in the cylinder configurations as explained above. The calculated spectra looks wavy as compared to the experiments, but this is most probably due to the smoothing effect of the double averaging (including ensemble averages) applied to measure data (see Equation 11, Catania et al (1996)). Indeed when the average of the wavy autocorrelation function is used to compute the energy spectra the wiggles seen in the computed curve reduced drastically. Figure 8.13 is seen as a confirmation of the fact that the present methodology is capable of resolving a significant portion of the inertial sub-range in the energy spectra.

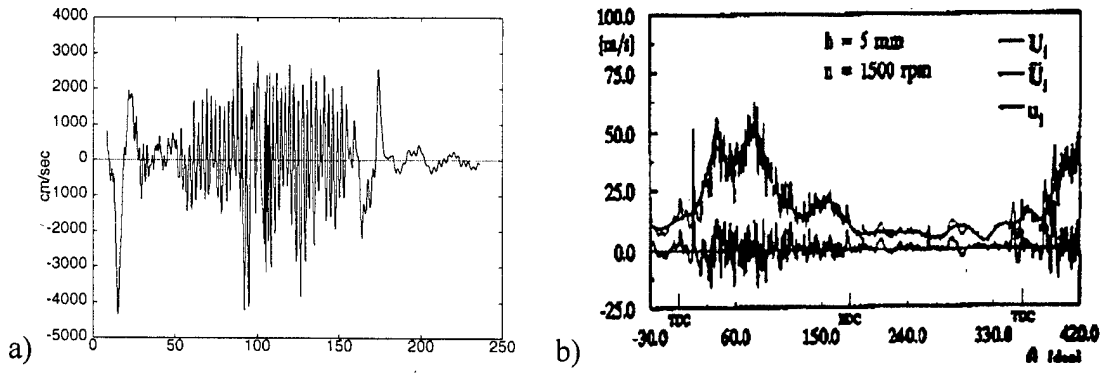

Figure 8.10 Fluctuating velocity: (a) computed (440000 node case), (b) Catania and Spessa (1996)

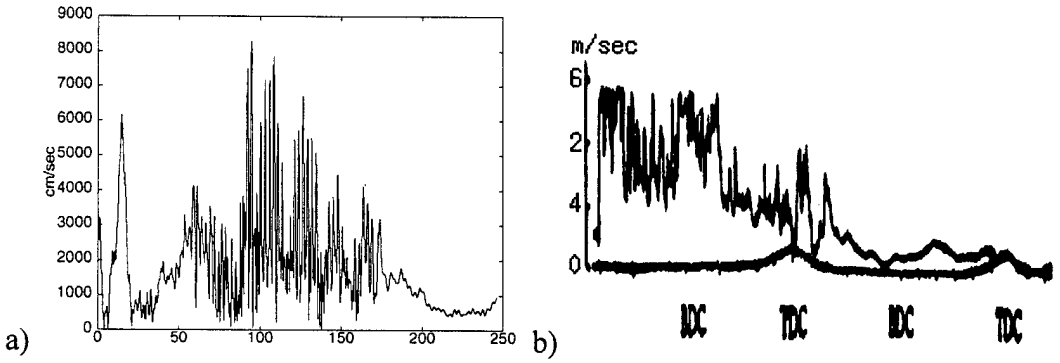

Figure 8.11 The magnitude of velocity: (a) computed (440000 node case), (b) Semenov's data

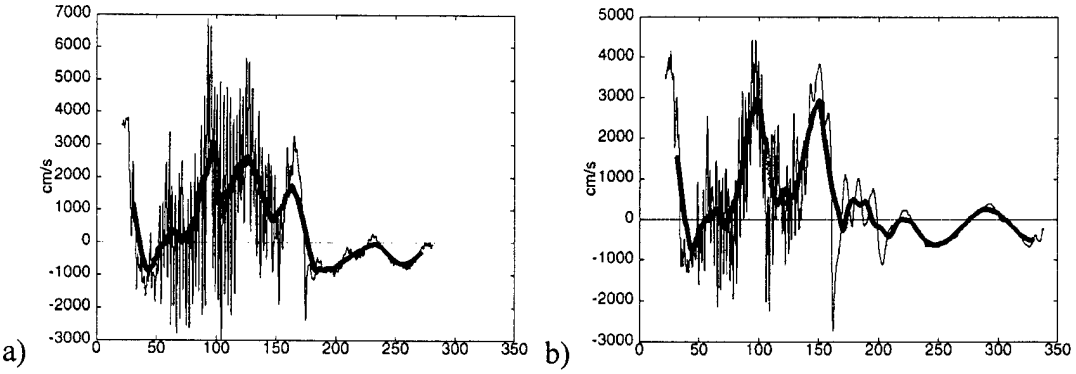

Figure 8.12 Grid dependency of computed instantaneous velocity: (a) 440,000 grid, (b) 220,000 grid

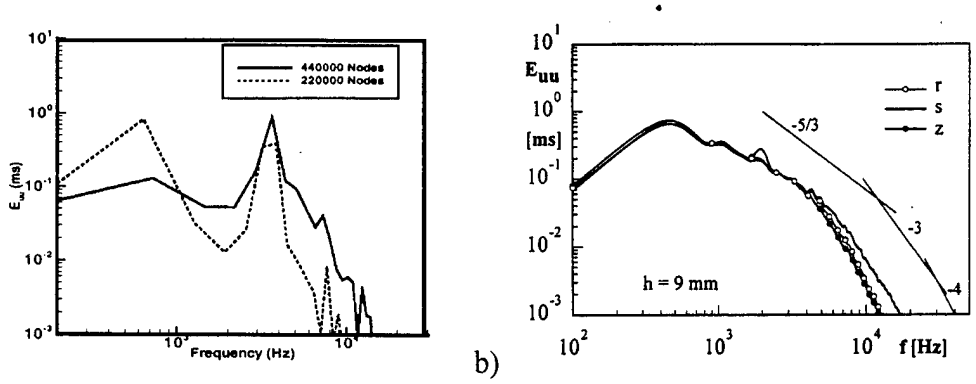

Figure 8.13 Power density spectra: a) computed (engine without a bowl), b) measured (engine with a bowl): r = radial, s = tangential, z = axial wire

8.2.5 Combustion Results:

Two types of simulations were performed to approach a realistic case of three-dimensional fine-grid combustion simulation. At the first stage a 2D grid with 71x75 nodes in the cylinder region and 31x23 nodes in the bowl region was used. In 3D simulations this grid was extended to 150,000 nodes by a simple revolution of the 2D grid. A 7-reaction reduced mechanism for n-Tetradecane with Arrhenius rate expressions was used at this stage. A standard KIVA spray model is used in all the simulations to account for injection, initial droplet size distribution and evaporation of the fuel. The initial gas and wall temperatures of 450° K were used. The average droplet diameter of the spray was set equal to $1 \cdot 10^{-4}$ cm and $3 \cdot 10^{-4}$ cm for the case with a bowl and two-valve assembly, respectively. No SGS model was used for the auto-ignition of the fuel in its gaseous phase, which occurs near TDC approximately at 352° CA. Figure 8.14 shows the temperature contours of this case on a vertical cross-section just after TDC. The perfectly symmetric initial conditions were broken during the three-dimensional transient calculations, and resulted in a three dimensional skewed flame structure. In the later case with flat piston, the asymmetry was already in the flow due to valve arrangements. Here the combustion mostly occurs near the wall. The predicted flame front is rather smooth. Due to the very simple combustion model used, the wrinkled laminar flamelet structure could not be captured. Nevertheless these calculations showed that it is feasible to do engineering LES combustion in IC engines using the widely used engine code KIVA. Work is underway to refine

the combustion sub-grid scale models via employment of PDF (Probability Density Function) approach (see Amin and Celik, 1999).

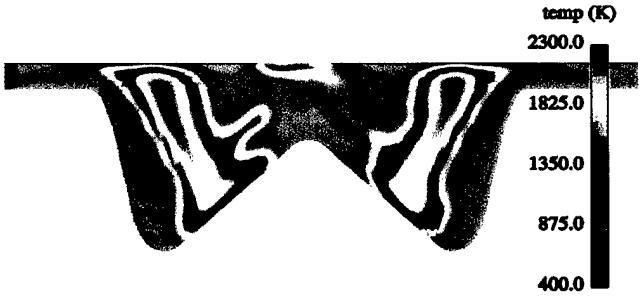

Figure 8.14 Temperature contours at 15° CA atdc for 3D case with piston bowl

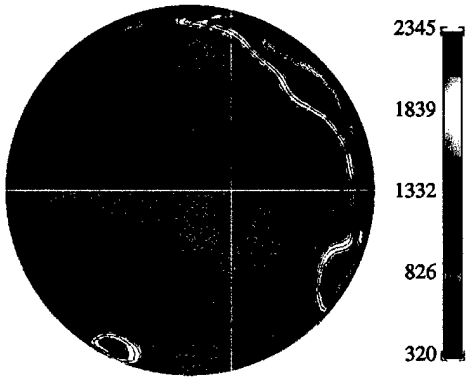

Figure 8.15 Temperature contours at 24° CA btdc of the 3D case with 2 valves

At the second stage a Cartesian block-structured grid with 220,000 nodes was applied to a two-valve flat-piston geometry. The Smagorinsky subgrid-scale model and the Magnussen eddy-dissipation model were used to account for the effects of turbulence and combustion respectively. Figure 8.15 presents the temperature contours of this case on a horizontal cross-section just before TDC. Spray distribution and dynamics was found to be grid-sensitive. A finer grid leads usually to a slower spray penetration and higher breakup frequencies. Autoignition of the fuel was modeled by a standard Arrhenius reaction mechanism. Time step was varied depending on the time-scale of the limiting process. Thus, in the evaporation phase (285°-360° CA) the time steps could be as small as 10^{-9} seconds which was due to the limits imposed by the

evaporation process of smallest droplets. In this case the geometry is essentially asymmetric with two valves located off the symmetry plane of the cylinder, but the jet spray was axe-symmetric at the inlet of the nozzle. As a result the ignition starts asymmetrically with multiple ignition regions (Fig.8.15). These regions are confined to the peripheral part of the cylinder. Both turbulent dynamics and the geometry may contribute to the symmetry breaking in this case.

The onset of combustion in both cases was marked by an increase in turbulent intensity, which was more pronounced in the case when the piston bowl was present (Fig. 8.16). This result is supported by experimental studies by Driscoll et al (Driscoll et al., 1986), where the turbulence intensity increase associated with combustion was demonstrated for swirling flows of various swirl intensity. This finding is also consistent with the results of Rapid Distortion theory (Hoult and Wong, 1980). A more visual understanding of the three-dimensional nature of combustion the iso-contours of temperature during combustion are presented in Figure 8.17.

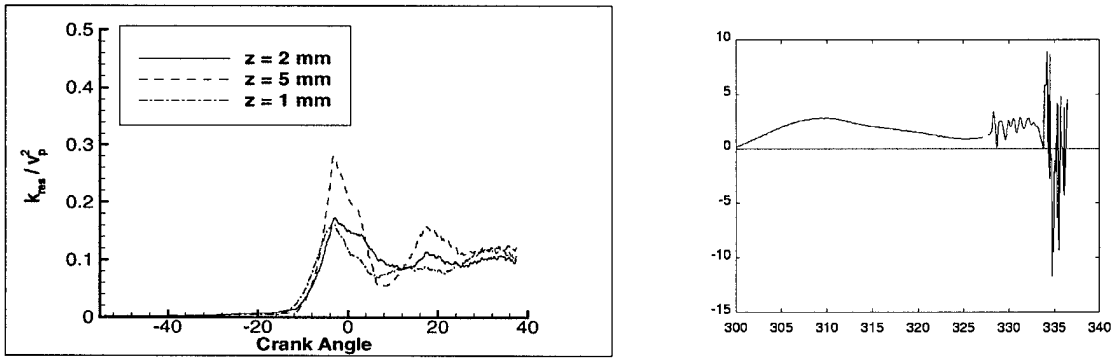

a) Bowl Geometry

b) Two-valve assembly

Figure 8.16 Velocity fluctuations at the auto-ignition point

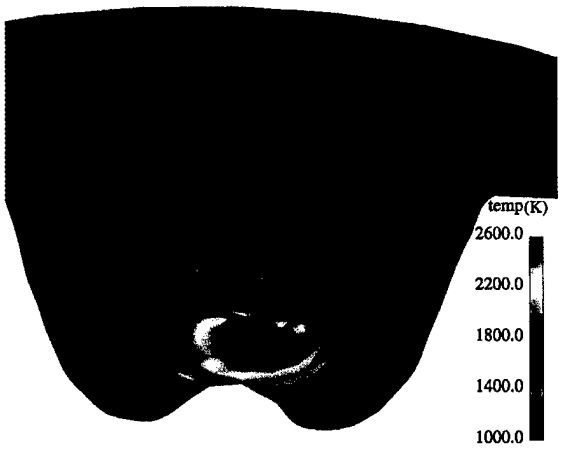

Figure 8.17 Temperature Iso-Contours during Combustion in Bowl Geometry

CONCLUSIONS

A systematic investigation of numerical prediction of in-cylinder turbulence (i.e. instantaneous random fluctuating components of flow variables) in internal combustion engines is performed. For this purpose, the well-known KIVA code has been utilized. The results of the simulated benchmark cases have revealed that, though KIVA is not the most suitable code for LES, nevertheless, by carefully controlling the numerical errors and using relatively fine grid resolution and a very small time step the unsteady dynamics of turbulent flows can be captured reasonably well. Particularly the time averaged predictions for the free swirling annular jet are in reasonable agreement with measurements and with results obtained from another well tested LES code, which gives confidence that the in-cylinder turbulence inside engine cylinders can be studied with this code.

The present engine applications show that the instantaneous large scale flow structures (i.e. coherent large eddies) can be captured, and the predicted turbulence statistics are in good qualitative agreement with the experimental data in a similar engine. In particular, the good correspondence of normalized spectra to that obtained from measurements by other authors is encouraging. It can be said that a significant portion of the energy spectra can be resolved within the range of 100 to 10,000 Hz. However, the reader should be cautioned that the cycle-to-cycle variations, which are usually significant, could not be accounted for in the present calculations. The predicted trends of velocity fluctuations during the intake as a function of crank angle as well as its magnitude are also in good agreement with experimentally observed trends. Close agreement of fluctuating velocity component produced on different grids and a good comparison with experimental data indicate that the numerical diffusion errors can not be a dominant factor in the defining the dynamics of the resolved flow-field.

This study has also shown that contrary to some arguments, significant turbulence is likely to be generated by a carefully designed bowl, and that the intake turbulence decays rapidly towards the TDC during compression stroke. Instability seems to be induced by the unsteady flow separation at the edge of the bowl and the squish region.

It has been further demonstrated that the statistics of coherent large flow structures can be studied using the widely used engine code KIVA on a workstation level. This opens a whole new avenue in simulation of in-cylinder turbulence for IC-engines. Extension of this study to cases

with combustion and many cycles is currently underway. The preliminary results from spray combustion are encouraging in this regard.

Simulations of the combustion stroke show that the intensity of velocity fluctuations increases at the onset of combustion, though at a level considerably lower than observed during the intake stroke. Temperature distributions captured at a single point show a considerable intermittency at least at the initial stage of combustion.

Because of the general decay of turbulence after the intake stroke, shown in experiments and confirmed by the present calculations, turbulence generated at the onset of combustion is not greatly affected by the intake turbulence. This may provide some justification for setting up approximate initial conditions at the intake stroke, i.e. without modeling a complicated valve assembly, and still reproduce the main dynamics of the combustion process. Spray evaporation time constants may significantly reduce the execution speed by limiting the iteration time-step. Spray distribution and dynamics show some grid-dependence. An improvement of the spray model would be desirable.

The case studies have shown that the intake turbulence generation and decay can be predicted in good agreement with experiments. Turbulence generated during the intake decays rapidly, and the turbulence generated by the bowl is relatively small. Turbulence generation increases with the onset of combustion.

The accuracy and efficiency of the primary simulation code KIVA-3 was improved in many ways, as the time accuracy, spatial accuracy, and the efficiency of the pressure solver was improved. The overall computational performance was improved significantly with the distributed-memory implementation of KIVA-3 (KIVA-3/MPI). Moreover, a beowulf cluster of 20 alpha processors has been developed for complex computations. Twelve nodes are made operational with the MPI (Message Passing Interface) library, and successful KIVA-3 runs have been performed on this cluster. Although it was completed rather late to have a major impact on the current simulations reported on here, it should be an important asset for future simulations.

Turbulence measurement capabilities with non-intrusive Doppler Global velocimetry were also developed which should have an impact in future validation studies.

RECOMMENDATIONS

This study has demonstrated that much can be learned from large eddy simulations of turbulent flow dynamics and combustion in diesel combustion chambers. There still remain, however, some obstacles to be overcome. First of all in order to ensure practicality in engineering applications, the turnaround time for the computations should be decreased drastically. This can be accomplished by resorting to parallel programming with the appropriate numerical algorithms and the use of parallel computers. A parallel implementation of the KIVA code on work station clusters with distributed memory seems to be a viable alternative and cost effective for research institutions as well as industry. To accomplish this, the preliminary KIVA-3/MPI parallel version needs to be extended to more general domains, and sub-models, such as combustion and spray dynamics need to be included.

Since the laminar flame thickness is very thin and beyond the realm of LES resolutions, a robust, well tested, and validated sub-grid scale combustion model is essential for accurate prediction of diffusion flames. The computations of Lagrangian spray dynamics with droplet evaporation consume most of the CPU time. Again, this can be improved by implementing a parallel particle-tracking algorithm, but it is also crucial to improve the stability limits of spray calculations especially when the spray impinges at the cylinder walls.

It is also highly desirable to obtain a good set of experimental data specifically for validation of large eddy simulations. The experiments need to be performed in conjunction with the computations, and cover a range of engine speeds with and without combustion, while keeping the valve and cylinder geometry relatively simple.

ACKNOWLEDGMENTS

This work is sponsored by the US DOD Army Research Office (ARO) through the DEPSCoR Program under Grant No.: DAAH04-96-1-0196. The technical monitor for this project was Dr. David M. Mann.

Computations on SGI Origin 2000 were performed at U.S. Army Engineer Waterways Experiment Station (ERDC MSRC), Naval Oceanographic Office (NAVOCEANO MSRC), U.S. Army Research Laboratory, (ARL MSRC).

San Diego Supercomputer Center's (SDSC) and Pittsburgh Supercomputing Center's Cray T3-E is also acknowledged for the use during the initial development of the distributed-memory implementation of KIVA-3.

The authors would like to thank Dr. David M. Mann for his continuos support and guidance throughout the duration of this project.

LIST OF PUBLICATIONS

Amin, E. M., Celik, I. (1999a) "A Computational Study of Strain Rate Effects on Thermal NOx Formation", ASME-ICED Spring Technical Conference April 25-28, 1999, Columbus, Indiana.

Amin, E. M., Celik, I. (1999b) "A Validation Study for a Turbulent Mixing Model Based on the Probability Density Function Approach" Paper no. 1999-01-0231, SAE International Congress and Exposition Detroit, MI.

Amin, E. M., Celik, I. (1999d) "Validation of Sub-Grid Scale Finite-Rate Chemistry Models for Turbulent Diffusion Flames", AIAA Computational Fluid Dynamics Conference, June 1999, Norfolk, Virginia.

Amin, E. M., Celik, I., and Yavuz, I., (1998a) "Towards LES of A Round Turbulent Free Jet Using Kiva-III Code", Proceedings of ASME Fluids Engineering Division Summer Meeting. - Paper no. 4970., June 21-25, Washington, D.C.

Amin, E. M., Celik, I., Yavuz, I., and Smith, J. (1998b) "Application of A Variable EBU Coefficient For Turbulent Combustion Modeling in a Direct Injection Diesel", Proceedings of ASME-ICE Spring Technical Conf., April 26-29, Fort Lauderdale, FL.

Amin, E. M., Celik, I. (2000) "Finite-Rate Chemistry Modeling of Bluff-Body Stabilized Gas Turbine Engine Combustion", Submitted to ASME ICE Division Spring Meeting, April, 2000, San Antonio, TX

Celik, I., Yavuz, I., Smirnov, A., Smith, J., Amin, E., Gel. A. (2000) "Prediction of In-Cylinder Turbulence For IC Engines" Combustion Science and Technology, Vol. 150, pp. 1-30

Celik, I., Yavuz, I., Smirnov, A., Smith, J., Amin, E., Gel. A. (1999) "Prediction of In-Cylinder Turbulence For IC Engines" Mediterranean Combustion Symposium, June 14-17, Antalya, Turkey

Celik, I., Smirnov, A., Yavuz, I., (1999) "Prediction of Turbulence Generated during the Intake Stroke of an IC Engine", KIVA Users Group Newsletter #16

Celik I, Yavuz, I., Amin, E., Smith, J., Gel, A., (1998) "Flow Instability Induced By a Typical Diesel Engine Bowl" KIVA Users Group Newsletter #15

Celik, I., Amin, E., Smith, J., Yavuz, I., and Gel, A. (1998), "Towards Large Eddy Simulation using the KIVA-Code", Proceedings of Combustion Multi-dimensional Modeling Conference, at the SAE Congress, Feb. 22, Detroit, Michigan.

Celik, I. and Yavuz, I. (1997) "Turbulence Scales in IC Engines Implied by the k-ε Model," Kiva Users Meeting, at SAE Congress, Feb.13, Detroit, Michigan

Celik, I. and Yavuz, I. (1997) "An Assessment of Turbulence Length Scales Relevant to IC Engines," Proceedings of the ASME-ICE Division, Spring Technical Conference, Fort Collins, CO, April 27-30.

Gel, A. and Celik, I., (1999a) "Parallel Implementation of a Commonly Used Internal Combustion Engine Code", in: Ecer and Emerson, eds., *Prcoeedings of the Parallel Computational Fluid Dynamics'99 Conference*, Elsevier, (To be published).

Gel, A. and Celik, I., (1999b) "Parallel Implementation of a Commonly Used Internal Combustion Engine Code, KIVA-3" DoD High Performance Computing Modernization Program, 1999 Users Group Conference, Monteray, CA. (http://www.hpcmo.hpc.mil)

Gel, A. and Celik, I., (1999c) "Distributed-Memory Implementation of a Commonly Used Internal Combustion Engine Code, KIVA-3 with Preliminary Results on a Beowulf Cluster", Annual Conference for Vendor-Independent High Performance Computing Users (HPCU) Group, Stony Brook, NY. (http://www.hpcu.org)

Gel, A. and Celik, I., (1999d) "Parallel Implementation of a Commonly Used Internal Combustion Engine Code on a Cluster of High Performance Workstations", Parallel CFD Workshop: Experiences in Implementation, Istanbul Technical University

Gel, A., (1999) "Distributed-memory Implementation of KIVA-3 with Refinements for Large Eddy Simulation Applications", Ph.D. Dissertation, Mechanical & Aerospace Eng. Dept., West Virginia University.

Gel, A., Smith, J. and Celik, I., (1998) "Assessment of Spatial Accuracy and Computational Performance of KIVA-3", Proceedings of the Fall Technical Conference of ASME ICE Div., FEDSM98-ICE-136, Irwin, PA, pp. 75-82.

Kuhlman, J. M., Naylor, S., James, K., and Ramanath, S., (1997) "Accuracy Study of a 2-Component Point Doppler Velocimeter (PDV)", AIAA-97-1916, presented at AIAA 28th Fluid Dynamics Conference, June 29-July 2, Snowmass, CO

Kuhlman, J. M. and Webb, D. L. (1999) "2-Component Point Doppler Velocimetry (PDV) Measurements of Turbulent Flow over an Airfoil," paper AAIAA-99-3517, presented at AIAA 30th Fluid Dynamics Conference, June 28-July 1, Norfolk, VA.

Kuhlman, J. (1998), "Development of Doppler Global Velocimeter," Final Report for AFOSR/DEPSCoR Grant F49620-94-1-0434

Lewellen, D. C., Lewellen, W. S. and Xia, J. (1999), "The Influence of a Local Swirl Ratio on Tornado Intensification near the Surface", (In press, *J. Atmos. Sci.*).

Lewellen, D., Lewellen, S., and Xia, J. (1998) "Simulation of Turbulence in a Swirling Jet," Submitted to Physics of Fluids.

Naylor, S. and Kuhlman, J. (1998), "Accuracy Studies of a Two-Component Doppler Global Velocimeter (DGV)," paper AIAA-98-0508, AIAA 36th Aerospace Sciences Meeting, Jan. 12-15, 1998, Reno, NV.

Naylor, S. and Kuhlman, J. (1999), "Results for a Two-Component Doppler Global Velocimeter (DGV)," paper AIAA-99-0268, AIAA 37th Aerospace Sciences Meeting, Jan. 11-14, 1999, Reno, NV.

Naylor, S. (1998), "Development and Accuracy Determination of a Two-Component Doppler Global Velocimeter (DGV)," Ph.D. Dissertation, West Virginia University, MAE Department

Smirnov, A., Celik, I., Yavuz, I. and Smith, J. (1999), "Preliminary Results from LES of In-Cylinder Turbulence for IC-Engines", SAE International Congress and Exposition, March 1-4, Detroit, Michigan

Smirnov, A. and Yavuz, I. and Celik, I. (1999) "Diesel Combustion and LES of In-Cylinder Turbulence for IC-Engines", In-Cylinder Flows and Combustion Processes, ASME Fall Technical Conferece, October 16-20, Ann Arbor, Michigan

Smith, J., Celik, I. and Yavuz, I., (1999) "Investigation of the LES Capabilities of An Arbitrary Lagrangian-Eulerian (ALE) Method", AIAA-99-0421, pp. 1--11.

Smith, J., Smirnov, A., Yavuz, I. and Celik, I. (1998), "Simulation of swirling flows related to an intake stroke of a Diesel engine", ASME ICE-Division Fall Conf., Clymer, N.Y., Sept. 27-30, 1998

Smith, J., Celik, I., Amin, E. and Yavuz, I., (1998) "Investigation of a Swirling Jet Using KIVA-3", Proceedings of the Fall Technical Conference of ASME ICE Div., FEDSM98-5247, Irwin, PA.

Smith, J., Celik, I., Amin, E., Yavuz, I., and Gel, A. (1997) "Modeling Rotational Effects Via Subgrid-Scale Turbulence Models Using the KIVA Code," ASME-ICE Fall Technical Conference, Madison, Wis.

Smith, J., Celik, I., Yavuz, I., Gel, A., and Amin, E. (1998), "Investigation of a Swirling Jet using KIVA-3", Proceeding of ASME-FEDSM, June 21-25, Washington, D.C.

Smith, J., Gel, A. and Celik, I., (1999b) "Improvement of the Pressure Solver in KIVA", Proceedings of 1999 SAE International Congress under Multi-Dimensional Engine Modeling, SAE 99-011187, Detroit, MI.

Yavuz, I. (2000), "Refined Turbulence Models for Simulation of IC Engine Cylinder Flows", Ph.D. Dissertation in preparation, Mechanical & Aerospace Eng. Dept., West Virginia University.

Yavuz, I. and Celik, I. (1999), "Applicability of the k-ε Model for IC-Engine Simulations", ASME-FEDSM99-7318, July 18-23, 1999, San Francisco, California

Yavuz, I. and Celik, I. (1999) "Assessment of Various Turbulence Models for IC-Engine Applications", ASME ICE Division 1999 fall technical conference, October 16-20, 1999, Ann Arbor, Michigan

Yavuz, I., Smirnov, A., Gel, A., and Celik, I. (1999) "Predicting Turbulence", ASME ICE Summer 1999 Newsletter

Yavuz, I., Celik, I., Smith, J., Gel, A., and Amin, E. (1998), "Bowl Induced Flow Instability in a Typical Engine Cylinder", ASME ICE-Division Fall Conf., Sept. 27-30, Clymer, NY

LIST OF PARTICIPANTS

(a) Senior Personnel

I. B. CELIK, Professor (Principal Investigator – PI)

W. S. LEWELLEN, Research Professor (Co-PI)

J. M. KUHLMAN, Professor (Co-PI)

E. AMIN, Research Assistant Professor

D. LEWELLEN, Research Assistant Professor

A. SMIRNOV, Research Assistant Professor

J. SMITH, Research Assistant Professor

A. GEL, Research Assistant Professor

(b) Graduate Students

A. GEL, Ph.D. (Graduated Feb. 1999)

S. NAYLOR, Ph.D. (Graduated 1998)

I. YAVUZ, Ph.D. (Graduation expected in Feb. 2000)

T. WALTON, MSME

J. XIA, Ph.D. (Graduation expected in Summer 2000)

(c) Undergraduate Students

A. KENNEDY

S. ROWAN

BIBLIOGRAPHY

Abou-Ellail, M. M. M. and Salem, H. (1990) A Skewed PDF Combustion Model for Jet Diffusion Flames, Trans ASME, Jour of Heat Trans. 112:1002-1007.

Amin, E. M., Celik, I. (1999a) "A Computational Study of Strain Rate Effects on Thermal NOx Formation", ASME-ICED Spring Technical Conference April 25-28, 1999, Columbus, Indiana.

Amin, E. M., Celik, I. (1999b) "A Validation Study for a Turbulent Mixing Model Based on the Probability Density Function Approach" Paper no. 1999-01-0231, SAE International Congress and Exposition Detroit, MI.

Amin, E. M., Celik, I. (1999c) "Validation of Sub-Grid Scale Finite-Rate Chemistry Models for Turbulent Diffusion Flames", AIAA Computational Fluid Dynamics Conference, June 1999, Norfolk, Virginia.

Amin, E. M., Celik, I., and Yavuz, I., (1998a) "Towards LES of A Round Turbulent Free Jet Using Kiva-III Code", Proceedings of ASME Fluids Engineering Division Summer Meeting. - Paper no. 4970., June 21-25, Washington, D.C.

Amin, E. M., Celik, I., Yavuz, I., and Smith, J. (1998b) "Application of A Variable EBU Coefficient For Turbulent Combustion Modeling in A Direct Injection Diesel", Proceedings of ASME-ICE Spring Technical Conference, April 26-29, Fort Lauderdale, FL.

Amsden, A. A. (1993), "KIVA-3: A KIVA Program with Block-Structured Mesh for Complex Geometries," Los Alamos National Laboratory, Los Alamos National Laboratory Report LA-12503-MS, UC-361, Los Alamos, New Mexico 87545.

Amsden, A. A. (1997), "KIVA-3V: A Block-Structured KIVA Program for Engines with Vertical or Canted Valves," Los Alamos National Laboratory, Los Alamos National Laboratory Report LA-13313-MS, UC-1412, Los Alamos, New Mexico 87545.

Amsden, A. A., O'Rourke, P. J., and Butler, T. D. (1989) "KIVA-II: A Computer Program for Chemically Reactive Flows with Sprays," Los Alamos National Laboratory Report LA-11560-MS, Los Alamos, New Mexico 87545. Also US DOE Report DE89 012805.

Amsden, A. A., T. D. Butler, P. J. O'Rourke and J. D. Ramshaw (1985), "KIVA - A Comprehensive Model for 2-D and 3-D Engine Simulations," SAE Paper 850554.

Amsden, A. A., Ramshaw, J.D., Cloutman, L.D. and O'Rourke, P.J., (1985) "Improvements and Extensions to the KIVA Computer Program", Los Alamos National Laboratory, Technical Report, LA-10534-MS, Los Alamos, NM 87545.

Aoyagi, Y., Kamimoto, T., Matsui, Y., and Matsuoka, S., (1980) A Gas Sampling Study on the Formation process of Soot and No in a D. I. Diesel Engine, SAE paper 800254.

Arcoumanis, C., Whitelaw, J.H., Hentschel, W. and Schindler, K-P (1994) "Flow and Combustion in a transparent 1.9 liter direct injection diesel engine," IMechE 1994, Part D: Journal of Automobile Engineering, Proc. Instn Mech Engrs, Vol. 208, pp. 191-205.

Auriemma, M., Corcione, F.E., Macchioni, R., and Valentino, G. (1998) "Interpretation of Air Motion in Reentrant Bowl in-Piston Engine by Estimating Reynolds Stresses," SAE Technical Paper Series #980482

Bardina, J., Ferziger, J., and Rogallo, R. (1985) "Effect of Rotation on Isotropic Turbulence: Computation and Modeling," Journal of Fluid Mechanics, Vol. 154, pp. 321-336.

Bilger, R. W. (1976a). The Structure of Diffusion Flames. *Combust. Sci. Technol.* 13, 155-70

Bilger, R. W. (1976b). Turbulent Jet Diffusion Flames. *Prog. Energy Combust. Sci.* 1, 87-109.

Bilger, R. W. (1980). Turbulent flows with Non-Premixed Reactants. In turbulent reacting flows ed. P. A. Libby, F. A. Williams, pp. 65-113. Berlin: Springer-Verlag.

Bilger, R. W. (1989) Turbulent Diffusion Flames, Ann. Rev. Fluid Mech., 21:101-35

Bilger, R. W. and Stårner, S. H. (1983). A Simple Model for Carbon Monoxide in Laminar and Turbulent Hydrocarbon Diffusion Flames. *Combust. Flame*. 51, 155-176.

Brizuela, E. A., and Bilger, R. W., (1996) On the Eddy Break-up Coefficient, Brief Communication, Combust Flame 104:208-212.

Brooke, J. W. and Hanratty, T. J., Phys. Fluids A 5,1011 (1993)

Buriko, Y.Y., and Kuznestov, V. R. (1978). *Combust. Explos. Shockwaves* 14(3):296-303.

Catania, A.E (1998) Private communication

Catania, A.E. and Spessa, E. (1996) "Speed Dependence of Turbulence Properties in a High-Squish Automotive Engine Combustion System," SAE Technical Paper Series #960268

Catania, A.E., Dongiovanni, C., Mittica, A., Molina, G., and Spessa, E. (1995) "A New Test Bench for HWA Fluid-Dynamic Characterization of a Two-Valved In-Piston-Bowl Production Engine," SAE Technical Paper Series #952467

Catania, A.E., Dongiovanni, C., Mittica, A., Negri, C. and Spessa, E., (1997), "Study of Turbulent Flow Components and Their Statistical Properties in a DI Automotive Diesel Engine", Proc. of SAE Int. Pacific Conference, November, Bali, Indonesia

Catania, A.E., Dongiovanni, C., Mittica, A., Negri, C. and Spessa, E., (1996), "Turbulence spectrum investigation in a DI Diesel engine with a reentrant combustion bowl and a helical inlet port", SAE Paper #962019

Celik, I., Yavuz, I., Smirnov, A., Smith, J., Amin, E., Gel. A. (1999) "Prediction of In-Cylinder Turbulence For IC Engines" Mediterranean Combustion Symposium, June 14-17, Antalya, Turkey

Celik, I. and Yavuz, I. (1997) "An Assessment of Turbulence Length Scales Relevant to IC Engines," Proceedings of the ASME-ICE Division, Spring Technical Conference, Fort Collins, CO, April 27-30.

Celik, I. and Yavuz, I. (1997) "Turbulence Scales in IC Engines Implied by the k-ε Model," Kiva Users Meeting, at SAE Congress, Feb.13, Detroit, Michigan

Celik, I., Wang, Y.Z., Crawford, B.G. and Lyons, D.W. (1992) "A Numerical Study of Diesel Engine Emissions from Combustion of Various Fuels," in New Developments in Off-Highway Engines, Edt.: B. Chrisman ASME publications, New York, pp. 73-80.

Choi, H., and Moin, P. (1994) "Effects of the Computational Time Step on Numerical Solutions of Turbulent Flow," J. Comp. Physics, Vol. 113, pp. 1-4.

Colella, P. and Woodward, P. R. (1984) "The Piecewise Parabolic Method (PPM) for Gas-Dynamical Simulations" *J. Comp. Physics*, **54**:174-201

Cook, A. W. and Riley, J. J. (1994) A Subgrid model for equilibrium chemistry in turbulent flows, Phys. Fluids 6, 2868-2870.

Corcione, F.E. and Valentino, G. (1990) "Turbulence Length Scale Measurements by Two-Probe-Volume LDA Technique in a Diesel Engine," SAE Paper # 902080, Society of Automotive Engineers, Int. Fuels and Lubricants Meeting and Exposition, Tulsa, Oklahoma, October 22-25.

Corcione, F.E. and Valentino, G. (1994a) "Analysis of In-Cylinder Turbulent Air Motion Dependence on Engine Speed," SAE Technical Paper Series # 940284

Corcione, F.E. and Valentino, G. (1994b) "Analysis of In-Cylinder Flow Processes by LDA," Combustion and Flame, Vol. 99, pp. 387-394

Dimotakis P.E., Brown, G. L., (1976) The Mixing Layer at High Reynolds Number: Large Structure Dynamics and Entrainment, *Jnl. Fluid Mech.*, 79:535-560.

Driscoll, J., Tangirale, V., and Kezerle, J.: 1986, "Effects of chemistry and swirl on the production of turbulence in a flame", Technical Report 5083-260-0875, Gas Research Institute

Erlebacher, G., and Hussaini, M.Y. (1993) "Direct Numerical Simulation and Large Eddy Simulation of Compressible Turbulence," in Large Eddy Simulation of Complex Engineering and Geophysical Flows, Editors: B. Galperin, and S. A. Orszag, Cambridge University Press

Ferziger, J (1993) "Subgrid-Scale Modeling," Large Eddy Simulation of Complex Engineering and Geophysical Flows, edited by Galperin, B. and Orszag, S., Cambridge University Press.

Frankel, S. H., Adumitroaie, V., Madina, C. K. and Givi, P. (1993) "Large Eddy Simulation of Turbulent Reacting Flows by Assumed PDF Methods", in Engineering Applications of Large Eddy Simulations, Ragab, S. A. and Piomelli, U. ed., pp. 81-101, New York, NY

Galperin, B. and Orszag, S. A. (1993) editors, Large Eddy Simulation of Complex Engineering and Geophysical Flows, Cambridge Univesity Press.

Garrick, S.C. (1995) "Large Eddy Simulations of a Turbulent Reacting Mixing Layer," AIAA-95-0010, 33rd Aerospace Sciences Meeting & Sciences, Reno, NV, January 9-12.

Gel, A. and Celik, I., (1999a) "Parallel Implementation of a Commonly Used Internal Combustion Engine Code", in: Ecer and Emerson, eds., *Prcoeedings of the Parallel Computational Fluid Dynamics'99 Conference*, Elsevier, (To be published).

Gel, A. and Celik, I., (1999b) "Parallel Implementation of a Commonly Used Internal Combustion Engine Code, KIVA-3" DoD High Performance Computing Modernization Program, 1999 Users Group Conference, Monteray, CA. (http://www.hpcmo.hpc.mil)

Gel, A. and Celik, I., (1999c) "Distributed-Memory Implementation of a Commonly Used Internal Combustion Engine Code, KIVA-3 with Preliminary Results on a Beowulf Cluster", Annual Conference for Vendor-Independent High Performance Computing Users (HPCU) Group, Stony Brook, NY. (http://www.hpcu.org)

Gel, A. and Celik, I., (1999d) "Parallel Implementation of a Commonly Used Internal Combustion Engine Code on a Cluster of High Performance Workstations", Parallel CFD Workshop: Experiences in Implementation, Istanbul Technical University, (http://www3.itu.edu.tr/~parcfdws).

Gel, A., (1999) "Distributed-memory Implementation of KIVA-3 with Refinements for Large Eddy Simulation Applications", Ph.D. Dissertation, Mechanical & Aerospace Eng. Dept., West Virginia University.

Gel, A., Smith, J. and Celik, I., (1998) "Assessment of Spatial Accuracy and Computational Performance of KIVA-3", Proceedings of the Fall Technical Conference of ASME ICE Div., FEDSM98-ICE-136, Irwin, PA, pp. 75-82.

Ghia U., Ghia, K., and Shin, C. (1982) "High-Re Solutions for Incompressible Flow Using the Navier-Stokes Equations and a Multigrid Method", Journal of Computational Physics, Vol. 48, pp. 387-411.

Girimaji, S S (1991). Assumed β-pdf Model for Turbulent Mixing: Validation and Extension to Multiple Scalar Mixing *Combust. Sci. Technol.* 78:177-196.

Givi, P., (1989) Model Free Simulations of Turbulent Reactive Flows, Prog. Energy Combust. Sci, Vol. 15, pp. 1-107.

Gladnick, P. G., Enotiadis, A. C., LaRue J. C. and Samuelsen G. S. (1990) "Near-Field Characteristics of a Turbulent Coflowing Jet", AIAA J., 28, 1405-1414.

Golub, H.G., Van Loan, C.F., (1996) Matrix Computations, The John Hopkins University Press, Baltimore, MD.

Goludin F. C., Schefer R. W., Johnson S. C. and Kollmann W. (1986) Non reacting Turbulent Mixing Flows, *Prog. Energy Combust. Sci.* 12:257-303.

Gosman, A. D. (1985) "Multidimensional Modeling of Cold Flows and Turbulence in Reciprocating Engines," SAE Paper # 850344, Int. Congress & Exposition, Detroit, Michigan, Feb. 25-March 1.

Grinstein, F. F., Oran, E. S., and Boris, J. P. (1987) "Direct Numerical Simulation of Axisymmetric Jets", AIAA J., 25, 1-98.

Hardenberg, H. O., and Hase, F. W., (1979) An Empirical Formula for Computing the Pressure Rise Delay of a Fuel From Its Cetane Number and From The relevant Parameters of Direct Injection Diesel Engines. SAE paper 790493.

Haworth, D. (1998), "Large Eddy Simulation of In-Cylinder Flows", International Conference on Multi-dimensional Simulation of Engine Internal Flows, IFP, Rueil-Malmaison, France, Dec. 3-4

Hessel, R.P. and Ruthland, C. J. (1995) "Intake flow modeling in a four-stroke diesel using KIVA-3," AIAA Journal of Propulsion and Power, 11(2): 378-384, March-April.

Heywood, J.B. (1987), "Fluid Motion within the Cylinder of Internal Combustion Engines," The 1986 Freeman Scholar Lecture, ASME Journal of Fluids Engineering, Vol. 109, pp. 3-35.

Hirt, C., Amsden, A., and Cook, J. (1997) "An Arbitrary Lagrangian-Eulerian Computing method for All Flow Speeds," J. Comp. Physics, Vol. 35, pp. 203-216.

Holzapfel, F., (1996) Zur Turbulenzstruktur Freier Und Eingeschlossener Drehstromungen, Ph.D. Dissertation, University of Karlsruhe, Germany.

Hossain, M.S. and Rodi, W. (1982), "A Turbulence Model for Buoyant Flows and its Application to Vertical Buoyant Jets", in Turbulent Jets and Plumes, editor: W. Rodi, Pergamon Press, New York, pp.121-178

Hoult, D. and Wong, V.: 1980, "The generation of turbulence in an internal-combustion engine", *Combustion Modeling in Reciprocating Engines*, J. Mattavi and C. Amann (eds.), pp 131--155, Plenum Press

James, K., "Determination of the Accuracy of a Two-Component Point Doppler Velocimetry System," MS Thesis, West Virginia University, MAE Department, 1997.

Jancika, J., and Kollman, W., (1978) 17th Symposium (International) on Combustion, The Combustion Institute, Pittsburgh, PA, pp. 421-429.

Jancika, J., Kolbe, W. and Kollman, W. (1978). Closure of the Transport Equation for the Probability Density Function of Turbulent Scalar Fields. Journal of Non-equilibrium Thermo-Dynamics 4, 47.

Jones, W. P. and Whitelaw, J. H. (1982). Combust. Flame, 48, 1.

Khalil, E. E., Splading, D. B., and Whitelaw, J. H., (1975) The Calculation of local flow properties in Two-dimensional Furnaces International Journal of Heat and Mass Transfer, 24, pp. 109-124.

Kuhlman, J. M., Naylor, S., James, K., and Ramanath, S., (1997) "Accuracy Study of a 2-Component Point Doppler Velocimeter (PDV)", AIAA-97-1916, presented at AIAA 28th Fluid Dynamics Conference, June 29-July 2, Snowmass, CO

Kuhlman, J. M. and Webb, D. L. (1999) "2-Component Point Doppler Velocimetry (PDV) Measurements of Turbulent Flow over an Airfoil," paper AAIAA-99-3517, presented at AIAA 30th Fluid Dynamics Conference, June 28-July 1, Norfolk, VA.

Kuhlman, J. (1998), "Development of Doppler Global Velocimeter," Final Report for AFOSR/DEPSCoR Grant F49620-94-1-0434.

Laufer, J., "The Structure of Turbulence in Fully Developed Pipe Flow," NACA TR 1174, 1954.

Launder, B., Piddin, C., and Sharma, O. (1977) "The Calculation of Turbulent Boundary Layers on Spinning and Curved Surfaces," ASME, J. Fluids Engr., Vol. 99, pp. 231-239.

Lee, J. and Farell, P.V.(1992) "Particle Image Velocimetry Measurements of IC Engine Valve Flows," Sixth Int. Symp. on Applications of Laser Techniques to Fluid Mechanics and Workshop on Computers in Flow Measurements. Lizbon, Portugal.

Lewellen, D. C., Lewellen, W. S. and Xia, J. (1999), "The Influence of a Local Swirl Ratio on Tornado Intensification near the Surface", (In press, *J. Atmos. Sci.*).

Lewellen, D. C., Lewellen, W. S. and Yoh, S. (1996) "Influence of Bowen Ratio on boundary layer cloud structure," *J. Atmos. Sci.*, **53**, 175 (1996).

Lewellen, D., and Lewellen, S. (1996) "Large-Eddy Simulations of the Vortex-pair Breakup in Aircraft Wakes," AIAA J., Vol. 34, No. 11, pp. 2337-2345.

Lewellen, D., Lewellen, S., and Xia, J. (1998) "Simulation of Turbulence in a Swirling Jet," Submitted to Physics of Fluids.

Lockwood, F. C., and Naguib, A. S. (1975). *Combust. Flame*, 24, 109-124.

Magnussen, B.: 1976, On mathematical modeling of turbulent combustion with special emphasis on soot formation and combustion, in *16-th International Symposium on Combustion,* The Combustion Institute, Pittsburgh

Margolin, L. (1997) "An Introduction to "An Arbitrary Lagrangian-Eulerian Computing Method for All Flow Speeds," J. Comp. Physics, Vol. 135, pp. 198-202.

Masri, A. R., Subramaniam, S. and Pope, S. B. (1998) A Mixing Model to improve the PDF Simulation of Turbulent Diffusion Flames *Twenty-Six Symposium (International) on Combustion*, The Combustion Institute, Pittsburgh, PA.

Menon, S. and Jou W-H (1991) "Large-Eddy Simulations of Combustion Instability in an Axisymmetric Ramjet Combustor," Combust. Sci. and Tech. Vol. 75, pp. 53-72.

Meyers, J. F., "Doppler Global Velocimetry, The Next Generation?," paper AIAA-92-3897, presented at AIAA 17th Ground Testing Conference, July 6-8, 1992, Nashville TN.

Meyers, J. F., "Evolution of Doppler Global Velocimetry Data Processing," 8th Int'l. Symp. On Applications of Laser Techniques to Fluid Mechanics, July 8-11, 1996, Lisbon, Portugal.

Meyers, J. F., Lee, J. W., and Cavone, A. A., "Signal Processing Schemes for Doppler Global Velocimetry," 14th International Congress on Instrumentation in Aerospace Simulation Facilities, Rockville, MD, Oct. 27-31, 1991.

Mittal, R. and Moin, P. (1997) "Suitability of Upwind-Biased Finite Difference Schemes for Large-Eddy Simulation of Turbulent flows," AIAA J., Vol. 35, No. 8, pp. 1415-1417.

Mudford, N. R., and Bilger, R. W., (1987) "Examination of Closure Models for Mean Chemical Reaction Rate using Experimental Results for an Isothermal Turbulent Reacting Flow", 20th Symposium (International) on Combustion, The Combustion Institute, Pittsburgh, PA, pp. 387-94.

Naitoh, K., Itoh, T., Takagi, Y. (1992), "Large Eddy Simulation of Premixed-Flame in Engine Based on the Multi-Level Formulation and the Renormalization Group Theory," SAE Tech. Paper No. 920590. International Congress & Exposition, Detroit, MI, Feb. 24-28.

Naylor, S. and Kuhlman, J. (1998), "Accuracy Studies of a Two-Component Doppler Global Velocimeter (DGV)," paper AIAA-98-0508, AIAA 36th Aerospace Sciences Meeting, Jan. 12-15, 1998, Reno, NV.

Naylor, S. and Kuhlman, J. (1999), "Results for a Two-Component Doppler Global Velocimeter (DGV)," paper AIAA-99-0268, AIAA 37th Aerospace Sciences Meeting, Jan. 11-14, 1999, Reno, NV.

Naylor, S. (1998), "Development and Accuracy Determination of a Two-Component Doppler Global Velocimeter (DGV)," Ph.D. Dissertation, West Virginia University, MAE Department

O'Rourke, P.J. and Amsden, A.A. (1987) "Three Dimensional Numerical Simulation of the UPS-292 Stratified Charge Engine, SAE paper # 870597.

Oppenheim, A. V. and Schafer, R. W., (1975) Digital Signal Processing, Prentice-Hall, Englewood Cliffs, NJ

Patankar, S. (1980) Numerical Heat Transfer and Fluid Flow, Hemisphere, Washington, D.C.

Peters, N. (1984) Laminar Diffusion Flamelet Models in Non-Premixed Turbulent Combustion, Prog. Energy Combust. Sci. 10:319-339.

Piomelli, U. (1998) "Large Eddy Simulations: Present State and Future Directions," AIAA Paper 98-0534.

Pope, S. B. (1985). Pdf Methods for Turbulent Reactive Flows. *Prog. Enrg. Combust. Sci.* 11:119-192.

Pope, S. B. (1990). Computations of Turbulent Combustion: Progress and Challenges. *Twenty-Third Symposium (International) on Combustion*, The Combustion Institute, Pittsburgh, PA, p. 591.

Press, W. H. et al., "Numerical Recipes in Fortran", Cambridge University Press, 1992.

Prinkey, M. (1999) Private communication.

Ragab, S.A. and Piomelli, U. (1993) Engineering Applications of Large Eddy Simulations, ASME Publication No. FED-Vol. 162.

Ramanath, S., "Development of a Point Doppler Global Velocimeter (DGV)," MS Thesis, West Virginia University, MAE Department, 1997.

Reitz, R.D., and Rutland, C.J. (1991) "3-D Modeling of Diesel Engine Intake Flow, Combustion and Emissions," SAE paper # 911789 (SAE Trans. Vol. 10, Sec. 3).

Reynolds, W.C. (1980) "Modeling of Fluid Motions in Engines- An Introductory Overview," in Combustion Modeling in Reciprocating Engines, Editors: J.N. Mattavi and C.A. Amann, Plenum Press, New York.

Reynolds, W.C. (1989) "The Potential and Limitations of Direct and Large Eddy Simulations," in Whither Turbulence, Turbulence at Crossroads, Edt.: J.L. Lumley, Springer-Verlag, New York, pp. 313-342.

Rodi, W., Ferziger J. H., Breuer, M. and Pourquie, M. (1997), "Status of Large Eddy Simulation: Results of a Workshop", Trans. of ASME, vol. 119, pp. 248-262.

Saad Y., (1984) " Practical use of some Krylov subspace methods for solving indefinite and nonsymmetric linear systems ", *SIAM J. Sci. Stat. Comput.*, **5**:203--228

Schefer, R. W., Johnston, S. C., Dibble, R. W., Gouldin, F. C. and Kollman, W., (1986) Non reacting turbulent mixing flows: a literature survey and data base. Sandia Rep. SAND86-8217, Sandia National Laboratories, Livermore, CA.

Semenov, E. S. and Sokolik, A. C. (1958), "Investigation of turbulence in a cylinder of a piston engine", Izvestiya Akademii Nauk. Otd. Tekh. Nauk., vol. 8, pp. 130-134

Sloan, D., Smith, P., and Smoot, L. (1986) "Modeling of Swirl in Turbulent Flow Systems," Prog. In Energy Comb. Science, Vol. 12, pp. 163-250.

Smith, J., Celik, I. and Yavuz, I., (1999) "Investigation of the LES Capabilities of An Arbitrary Lagrangian-Eulerian (ALE) Method", AIAA-99-0421, pp. 1--11.

Smith, J., Celik, I., Amin, E. and Yavuz, I., (1998) "Investigation of a Swirling Jet Using KIVA-3", Proceedings of the Fall Technical Conference of ASME ICE Div., FEDSM98-5247, Irwin, PA.

Smith, J., Celik, I., Amin, E., Yavuz, I., and Gel, A. (1997) "Modeling Rotational Effects Via Subgrid-Scale Turbulence Models Using the KIVA Code," ASME-ICE Fall Technical Conference, Madison, Wis.

Smith, J., Celik, I., Yavuz, I., Gel, A., and Amin, E. (1998), "Investigation of a Swirling Jet using KIVA-3", Proceeding of ASME-FEDSM, June 21-25, Washington, D.C.

Smith, J., Gel, A. and Celik, I., (1999b) "Improvement of the Pressure Solver in KIVA", Proceedings of 1999 SAE International Congress under Multi-Dimensional Engine Modeling, SAE 99-011187, Detroit, MI.

Spalding, D. B. (1971). "Concentration fluctuations in a round turbulent free jet", J. Chem. Engng. Sci. 26, pp. 95-107.

Speziale, C. G. (1998) "Turbulence Modeling for Time-Dependent RANS and VLES: A Review", AIAA Journal, Vol. 36 No. 2, pp. 173-184

Sykes, R. I., S.F. Parker, D.S. Henn, and Lewellen, W.S., (1994), "Turbulent mixing with chemical reaction in the planetary boundary layer", Journal of Applied Meteorology, Vol. 33, 825-834

Sykes, R.I., Henn, U.S., Parker, S.F. and Lewellen, W.S. (1990), "Large-Eddy Simulation of a Turbulent Reacting Plume," Atmospheric environment, 26A, 2565-2574.

Valentino, G. Auriemma, M., Corcione, F.E., Macchioni, R., and Seccia, G. (1998) "A LDV Data Refinement Technique to Improve Time Scale Estimation in Reciprocating

Engines," Proceedings of the ASME-ICE Division, Fall Technical Conference, Irvine, PA, Sept. 27-30

Van DerVorst, H., (1992) "BI-CGSTAB: A fast and smoothly converging varient of BI-CG for the solution of nonsymmetric linear systems", *SIAM J.Sci. Stat. Comput.*, **13**:631—644.

Williams, F. A. (1985). Combustion Theory. The Benjamin/Cummigns Publishing Company, Melno Park, CA, 2nd edition.

Xia, J., Smith, B., Benim, A., Schmidlt, J., and Yadigaroglu, G. (1997) "Effect of Inlet and Outflow Boundary Conditions on Swirling Flows," Computers and Fluids, Vol. 26, No. 8, pp. 811-823.

Yang, S. L., Peschke, B. D. and Hanjalic, K. (1998), "IC-Engine Like Flow Study Using a Second-Moment Closure Model," Proceedings of the ASME ICE division fall technical c[illegible]ence. Clymer, New York, September 30, 1998

Yasar, [illegible] Rutland, C.J., (1992) "Parallelization of KIVA-II on the iPSC/860 Su[illegible]mputer", Parallel Computational Fluid Dynamics'92,North Holland, editors R.B. Pe[illegible]al.

Yasar, O[illegible]98) "A scalable model for complex flows", Int. J. Computers & Mathematics with [illegible]ations, **35**:117—128.

Yavuz, I. (2000), "Refined Turbulence Models for Simulation of IC Engine Cylinder Flows", Ph.D. Dissertation in preparation, Mechanical & Aerospace Eng. Dept., West Virginia University.

Yavuz, I. and Celik, I. (1999a), "Applicability of the k-ε Model for IC-Engine Simulations", ASME-FEDSM99-7318, July 18-23, 1999, San Francisco, California

Yavuz, I. and Celik, I. (1999b) "Assessment of Various Turbulence Models for IC-Engine Applications", ASME ICE Division 1999 fall technical conference, October 16-20, 1999, Ann Arbor, Michigan

Yavuz, I., Celik, I., Smith, J., Gel, A., and Amin, E. (1998), "Bowl Induced Flow Instability in a Typical Engine Cylinder", ASME ICE-Division Fall Conf., Sept. 27-30, Clymer, NY